



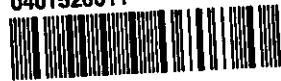
Pilkington Library

Author/Filing Title SCHULZ-UTERMOHL, K

Accession/Copy No. 040152601

Vol. No.	Class Mark	
- 2 NOV 2000	LOAN COPY	

0401526011





Mathematical Modelling of a vector controlled LIM Drive


by

K.Schulz-Utermöhl

Submitted in partial fulfilment
of the requirements for the award of
A Master's Thesis
of the Loughborough University

June 1996

© by K.Schulz-Utermöhl (1996)

 Loughborough University P... ..
Date Ja 98
Class
Acc No. 040152601

79099916

To my parents, who taught me the importance of education ...

ABSTRACT

The linear induction motor is often still considered to be a special-purpose machine that is tailored to meet specific needs, but it is slowly finding more applications with its added advantages over rotary motors.

This thesis is concerned with the development of a mathematical model which provides the transient and steady-state performance of a current-regulated inverter-fed linear induction motor system. The linear induction motor is posed as a one-dimensional electromagnetic field problem, to provide a better understanding of the so called 'end-effect' phenomena, which accounts mainly for the difference in performance between the linear induction motor and its rotary counterpart. An equivalent circuit is described that takes into account these end-effect transients for a single-sided linear induction motor. An accurate model for the inverter switching action is developed and the performance of the complete system under various operating conditions is studied, and compared with experimental results obtained from published literature.

A closed-loop control system is implemented, using conventional field-oriented control and a newer and simpler method known as Natural Field Orientation is investigated, and compared with both the direct and indirect field orientation methods. In Natural Field Orientation, a decoupled control of torque and flux producing components of current is easily achieved by using the machines inherent properties, to establish a correct field-orientation, and this allows the induction motor to provide a performance that combines the control characteristics of the dc motor with the merits of the induction motor.

ACKNOWLEDGEMENTS

I firstly would like to thank my supervisor Mr.G.Kettleborough, who kindly supervised me throughout my research, for his guidance and assistance in completing this work. Thanks must also be extended to my Director of Research, Professor I.R.Smith, for his support and encouragement, and to Dr.K.Gregory for his help on matters mathematical and programming.

I am also very grateful to all my friends whose friendship has kept me going throughout my years at Loughborough University, with special thanks to Steve and Keith who provided useful suggestions and criticisms during the progress of my research.

Last but not least, I would like to thank all my family, above all my mother and father, for their love and support throughout these years.

TABLE OF CONTENTS

Abstract	i
Acknowledgements	ii
Table of Contents	iii
List of Principal Symbols	vii
Chapter 1: INTRODUCTION	1
1.1 Thesis objective	1
1.2 Thesis organisation	2
Chapter 2: THE INDUCTION MOTOR	4
2.1 An analysis of the induction motor	4
2.2 Mathematical model of the induction motor	5
2.2.1 Voltage equation	6
2.2.2 Machine inductance coefficients.....	9
2.2.3 Machine rotational inductance coefficients.....	9
2.2.4 Dynamic equation.....	10
2.3 Numerical solution of the machine equations.....	11
2.4 Simulated and experimental results.....	12
Chapter 3: THE LINEAR MOTOR	19
3.1 Linear induction motor.....	19
3.1.1 Single-sided flat-type	20
3.1.2 Goodness factor.....	21
3.2 Differences between the linear and conventional induction motor	21
3.3 Circuit analysis of a low-speed linear induction motor	22
3.3.1 Equivalent circuit.....	22
3.3.2 Derivation of equivalent circuit parameters	23
3.3.3 Force computation.....	26
3.4 Longitudinal end-effect	28
3.4.1 Principle of the phenomena	28

3.4.2 Modified equivalent circuit.....	29
3.5 Dynamic equation	32
3.6 Simulated results.....	33
Chapter 4: THE INVERTER	36
4.1 The voltage-source inverter.....	36
4.2 Pulse-width-modulated switching schemes	37
4.2.1 Sinusoidal pulse-width-modulation.....	38
4.2.2 Current-regulated pulse-width-modulation	39
4.3 An analysis of the inverter	41
4.3.1 Tensor technique	42
4.3.1.1 Primitive network	44
4.3.1.2 Basic network.....	45
4.3.1.3 Reduced network.....	46
4.3.2 Numerical solution of the inverter equations.....	48
4.4 Simulated and experimental results.....	49
4.4.1 Quasi-square wave inverter	49
4.4.2 Sinusoidal pulse-width-modulated inverter	49
Chapter 5: THE INVERTER-FED INDUCTION MOTOR.....	56
5.1 Mathematical model of the inverter-motor system	56
5.1.1 System tensors.....	58
5.2 Numerical solution of the system equations	61
5.3 Non-regenerative supply	61
5.4 Simulated and experimental results.....	62
5.4.1 Quasi-square wave inverter	62
5.4.2 Sinusoidal pulse-width-modulated inverter.....	63
5.4.3 Linear induction motor drive under constant current excitation	63
Chapter 6: INDUCTION MACHINE CONTROL.....	75
6.1 Vector control	75
6.2 Principle of operation.....	75

6.2.1 Indirect field orientation.....	76
6.2.2 Direct field orientation.....	78
6.2.3 Natural Field Orientation	79
6.3 Vector transformation.....	79
6.4 Implementation of the vector control schemes.....	81
6.4.1 Indirect field orientation.....	81
6.4.1.1 Evaluation of the rotor flux vector.....	84
6.4.2 Direct field orientation.....	86
6.4.3 Natural Field Orientation	88
6.4.3.1 Evaluation of the air-gap voltage	89
6.5 Conclusions	90
Chapter 7: VECTOR CONTROL OF A LINEAR INDUCTION MOTOR.....	91
7.1 Control system design.....	91
7.1.1 Indirect field orientation.....	92
7.1.2 Direct field orientation.....	92
7.2 Simulated results.....	93
7.2.1 Indirect field orientation.....	94
7.2.2 Direct field orientation.....	94
7.3 Conclusions	95
Chapter 8: PROGRAM DESCRIPTION.....	108
8.1 Numerical methods in electrical engineering	108
8.2 Discrete events.....	108
8.2.1 Scheduled	108
8.2.2 Conditional.....	109
8.3 Simulation of switches	109
8.4 Breakpoint detection.....	110
8.4.1 Criteria for device turn-on and turn-off	110
8.4.2 Iterative linear interpolation	110
8.5 Main program description	110
8.5.1 Subroutines.....	114

8.6 Input data file structure	116
8.6.1 Voltage-fed induction motor	116
8.6.2 Quasi-square wave / Sinusoidal PWM inverter with inductive loading	117
8.6.3 Quasi-square wave / Sinusoidal PWM inverter-fed induction motor	118
8.6.4 Current-regulated PWM inverter-fed linear induction motor.....	119
8.6.5 Vector control of a linear induction motor	120
Chapter 9: CONCLUSIONS	122
FURTHER WORK.....	124
REFERENCES	125
BIBLIOGRAPHY.....	132
Appendix A: DERIVATION OF THE PHASE-PARAMETERS FROM THE PER-PHASE EQUIVALENT CIRCUIT	134
Appendix B: FLUX DENSITY CALCULATIONS.....	135
Appendix C: SYSTEM PARAMETERS.....	136
C.1 Induction motor parameters	136
C.2 Linear induction motor parameters.....	136
C.3 Inverter parameters	138
Appendix D: SIMULATION DATA FOR A VECTOR-CONTROLLED LIM DRIVE.....	139
Appendix E: PROGRAM FLOWCHARTS.....	140
E.1 Voltage-fed induction motor.....	141
E.2 Inductively-loaded voltage-source inverter	144
E.3 Linear induction motor drive under constant current excitation.....	149
E.4 Vector-controlled linear induction motor drive	155
Appendix F: MATLAB PROGRAM LISTINGS	161

LIST OF PRINCIPAL SYMBOLS

$2a$	Stack width	(m)
$2a_e$	Equivalent stack width	(m)
B_s	Peak steady-state air-gap flux density	(T)
$2c$	Secondary sheet width	(m)
C_d	Inverter filter branch capacitance	(F)
Q	Instantaneous charge stored in the capacitor.	(C)
d	Secondary sheet thickness	(m)
E	Air-gap voltage	(V)
E_d, E_q	d-q axis air-gap voltages	(V)
f_s	Supply frequency	(Hz)
f_m	Modulation frequency	(Hz)
f_{sw}	Carrier frequency	(Hz)
F_f	Frictional force	(N)
F_l	Load force	(N)
F_n	Normal force	(N)
F_x	Thrust	(N)
g	Nominal air-gap (= $g_m + d$)	(m)
g_e	Effective air-gap	(m)
g_m	Mechanical air-gap	(m)
G_e	Realistic goodness factor	
h_s	Slot depth	(m)
i_s, i_r	Stator and rotor phase current	(A)
i_{mr}	Magnetizing current	(A)
i_{as}, i_{bs}, i_{cs}	Stator phase currents	(A)
i_{ds}, i_{qs}	d-q axis stator currents	(A)
i_{dr}, i_{qr}	d-q axis rotor currents	(A)
i_{α}, i_{β}	d-q axis currents in a stationary reference frame	(A)
l_{ce}	Coil end-connection length	(m)
J	Motor inertia	(kg·m ²)
J_s	Design current density of primary sheet	(A·m ⁻²)
k_c	Carter's coefficient	

List of Principal Symbols

k_e	Longitudinal end-effect factor	
k_f	Rotor friction coefficient	(Nm·rad ⁻¹ ·s ⁻¹)
k_w	Primary winding factor	
k_μ	Secondary friction coefficient	(N·kg ⁻¹)
L	Effective motor length $\{= (2p + 1/3) \tau\}$	(m)
L_f	Inverter supply inductance	(H)
L_{ls}, L_{lr}	Stator and rotor leakage inductance	(H)
L_m	Magnetizing inductance	(H)
L_s, L_r	Stator and rotor phase inductance	(H)
L_{ss}, L_{rr}	Self-inductances of stator and rotor phases	(H)
m	Number of primary phases	
$mass$	Motor weight	(kg)
M_s	Mutual inductance between stator phases	(H)
M_r	Mutual inductance between rotor phases	(H)
M_{sr}	Maximum mutual inductance between stator and rotor phases	(H)
N	Number of primary series turns per phase	
p	Number of pole-pairs	
q	Number of slots per pole per phase	
R_d	Inverter filter branch resistance	(Ω)
R_f	Inverter supply resistance	(Ω)
R_m	Magnetic Reynolds number	
R_s, R_r	Stator and rotor winding resistance	(Ω)
s	Slip	
T_{em}	Electromagnetic torque	(Nm)
T_f	Frictional torque	(Nm)
T_l	Load torque	(Nm)
v	Velocity	(m·s ⁻¹)
v_s	Synchronous velocity	(m·s ⁻¹)
V_{as}, V_{bs}, V_{cs}	Stator phase voltages	(V)
V_{ds}, V_{qs}	d-q axis stator voltages	(V)
V_{dc}	Inverter supply voltage	(V)
V_s	Terminal/dc link voltage	(V)

List of Principal Symbols

V_{α}, V_{β}	d-q axis voltages in a stationary reference frame	(V)
w_s	Slot width	(m)
x	Linear displacement	(m)
X_{ls}, X_{lr}	Stator and rotor per-unit leakage reactance	
X_m	Per-unit magnetizing reactance	
α_i	Ratio of the average to the peak value of magnetic flux density	
θ	Electrical angle between stator and rotor phases	(°)
σ	Conductivity of secondary sheet	(S·m ⁻¹)
σ_c	Conductivity of copper (5.9×10^7)	(S·m ⁻¹)
σ_e	Equivalent secondary conductivity	(S·m ⁻¹)
σ_i	Conductivity of back iron	(S·m ⁻¹)
σ_k	Form factor	
τ	Stator pole-pitch	(m)
τ_e	Pole-pitch of end-effect wave	(m)
τ_r	Rotor time constant ($= L_r/R_r$)	
ρ	Angular position of the rotor flux vector with the stator reference axis(Rad)	
ρ_s	Surface resistivity of secondary sheet	(Ω·m ⁻¹)
μ_0	Permeability of free space ($4\pi \times 10^{-7}$)	(H·m ⁻¹)
ω	Synchronous angular speed	(Rad·s ⁻¹)
ω_r	Rotor angular speed	(Rad·s ⁻¹)
ω_{slip}	Slip speed	(Rad·s ⁻¹)
$\lambda_{dr}, \lambda_{qr}$	d-q axis rotor flux linkages	(Wb)
$\lambda_{\alpha}, \lambda_{\beta}$	d-q axis flux linkages in a stationary reference frame	(Wb)

INTRODUCTION

Although the ac induction motor is used in a variety of applications, its traditional role has been as a fixed-speed machine driven directly from the mains. In recent years the use of an appropriate power electronic controller to produce a variable-speed drive has resulted in a far more versatile system.

An adjustable-frequency supply allows the induction motor to be used for speed control applications, but its transient characteristics are dictated by the control strategy implemented. An open-loop speed control strategy provides satisfactory results, but does not always provide the required stability and precision, since, fluctuations in the supply voltage, and disturbances in the load torque can make the response of the system inadequate.

A closed-loop control technique is therefore essential to provide the induction motor with the fast and precise dynamic performance that is often required in high-performance servo-drive applications. For a dc machine with a constant air-gap flux, the torque is simply proportional to the armature current. However, torque control is not readily implemented with an induction motor, owing to the complex non-linear multivariable nature of the machine and the fact that the rotor currents are not easily sensed.

1.1 Thesis objective

In this thesis, a mathematical model for a single-sided linear induction motor (SLIM) with aluminium-capped solid-steel reaction rail and voltage-source inverter is initially formulated. The performance of the linear induction motor (LIM) is strongly influenced by the end-effects, which are caused by the finite lengths of the primary iron and winding. An equivalent circuit is presented that takes into account the longitudinal end-effects through the use of the usual equivalent circuit components. The transient and steady-state performance of the complete inverter-motor system under various operating conditions is studied, and compared with experimental results obtained from published literature.

Field-oriented, or the so called vector control, aims to provide the induction motor with a decoupled control of torque and flux, similar to that obtained with a dc motor drive. By allowing the torque and flux of the induction motor to be controlled separately, the motor is able to obtain a better torque response than is otherwise possible. Although, the emphasis in this thesis is placed on the development of a mathematical model for the complete inverter-motor system, the concepts of field-oriented control are also highlighted and simulated results provided for both direct and indirect field-oriented control of a LIM.

1.2 Thesis organisation

The first part of the thesis is concerned with the development of a direct-phase parameter model for the induction motor. The electrical and dynamic equations of the machine are evaluated, and then re-arranged to allow them to be solved numerically. This model is adopted in preference to the d-q model as it enables a wider range of operating conditions to be more conveniently studied. The computed results are compared with those obtained experimentally [1], and also with simulation results from a mathematically based software package called *MATLAB*.

Chapter 3 introduces the SLIM, with emphasis placed on the basic differences between the rotary induction machine and its linear counterpart. An equivalent circuit for a low-speed LIM is derived, along with a set of equations to help evaluate the lumped-parameters of the machine from its design parameters. The so called 'end-effects' which mainly account for the difference in performance between linear motors and their rotary counterparts is then taken into account. A one-dimensional model of the induction motor is developed and an equivalent circuit is described which allows for the entry and exit end-effects. Simulated results are obtained for a low-speed voltage-fed SLIM with sheet secondary.

Various ways of creating a mathematical model for a complex system such as an inverter are presented in Chapter 4, and a tensor approach is eventually selected as the most useful technique to analyse an inductively-loaded inverter system. A quasi-square wave and sinusoidal pulse-width-modulated switching scheme are implemented to drive the inverter switches. Once again, simulated results are compared with those obtained experimentally for an inductively-loaded inverter.

The next step is to combine the system equations describing the induction motor with those for the inverter, to create an overall model for a complete inverter-fed induction motor system. Although, there are various ways to obtain the required control signals to drive the inverter switches, tolerance band current control is most suited for the method of vector control, which requires instantaneous control of the phase currents. A transient analysis of the LIM under constant frequency and constant current excitation is performed, and compared with experimental results [2]. The parameters used with the equivalent circuit are those for a LIM propelled rapid transit system using steel wheel on rail suspension, developed by the Canadian Institute for Guided Ground Transport (CIGGT).

Field-oriented control, provides a means of controlling an induction motor in high performance applications. Chapter 6 looks at both direct and indirect field-oriented control, whilst also introducing a new, and much simpler form of field-oriented control, known as Natural Field Orientation (NFO). The advantages and disadvantages of each of the systems are discussed in great detail, and the control circuits to realise the above systems are also presented.

In Chapter 7, simulated results are obtained for both direct and indirect field-oriented control of a LIM.

Chapter 8 gives a description of the *FORTRAN77* programme written to predict the transient and steady-state performance of the overall drive system. Flowcharts outlining the step-by-step execution of the software are also provided.

Chapter 9 presents the conclusions drawn from the thesis, including further work that might be carried out to improve the overall control system.

THE INDUCTION MOTOR

Induction motors have the advantage over both synchronous and dc motors in that they are simpler and cheaper to build and operate. Although, an induction motor operates at nearly constant speed when driven directly from a fixed frequency supply, its speed can easily be varied by the use of a power electronic converter.

2.1 Analysis of the induction motor

To help analyse the performance characteristics of the induction machine, it is necessary to first derive an equivalent circuit [3, 4]. The familiar per-phase equivalent circuit of the induction motor is shown in Fig. 2-1.

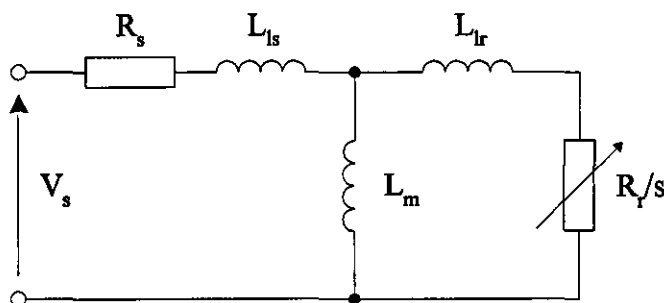


Figure 2-1 *Induction motor per-phase equivalent circuit*

The stator consists of three-phase windings mutually displaced by 120° . When a balanced three-phase voltage is applied to the motor windings, a balanced set of three-phase currents is established that are likewise shifted by 120° . The currents flowing through the stator coils gives rise to a resultant magnetic flux which is rotating. The actual speed of rotation is determined by the number of pole-pairs and the supply frequency, and is termed the synchronous speed ω .

The stator rotating magnetic field induces an emf in the short circuited rotor windings. The rotor tries to rotate at the same speed as the magnetic field of the stator, and as

the rotor accelerates and tries to reduce any speed difference i.e. the slip speed, the motor and load torque eventually reach an equilibrium. The motor then runs at constant speed with a fixed slip speed ω_{slip} .

2.2 Mathematical model of the induction motor

The motor can be modelled in terms of either its d-q equivalent parameters or its direct-phase parameters. Although, the d-q model is used to represent the induction motor in terms of its two-axis equivalent circuit, and as such helps to simplify the resultant system differential equations, the latter approach has been selected because it enables a wider range of operating conditions to be studied [1]. Similarly, for the analysis of the complete inverter-motor system, the direct phase model allows the machine phase variables to be monitored.

A transient analysis is conveniently based on the fundamental Kirchhoff equations, involving emfs caused by the variation of self and mutual flux linkage, and consequently the coefficients in the equations are the self and mutual inductances.

In analysing the motor, it is assumed that

- The motor is star-connected, although a delta connection may be used provided the machine parameters are defined in terms of an equivalent star-connected machine.
- The inductance terms are dependent on the relative position of the rotor with respect to the stator, with the mutual inductance coefficients between two windings being a cosine function of the electrical angle between the axes of both windings.
- The air-gap is assumed to be uniform, with the effects of saturation, hysteresis and eddy currents being neglected. Although, hysteresis and eddy current losses are different in nature, they can ultimately be represented in the same manner, that is by a parallel resistor.

Using the assumptions above, the equivalent 2-pole star-connected machine shown in Fig.2-2 can be represented by the sets of equations developed in the following sections.

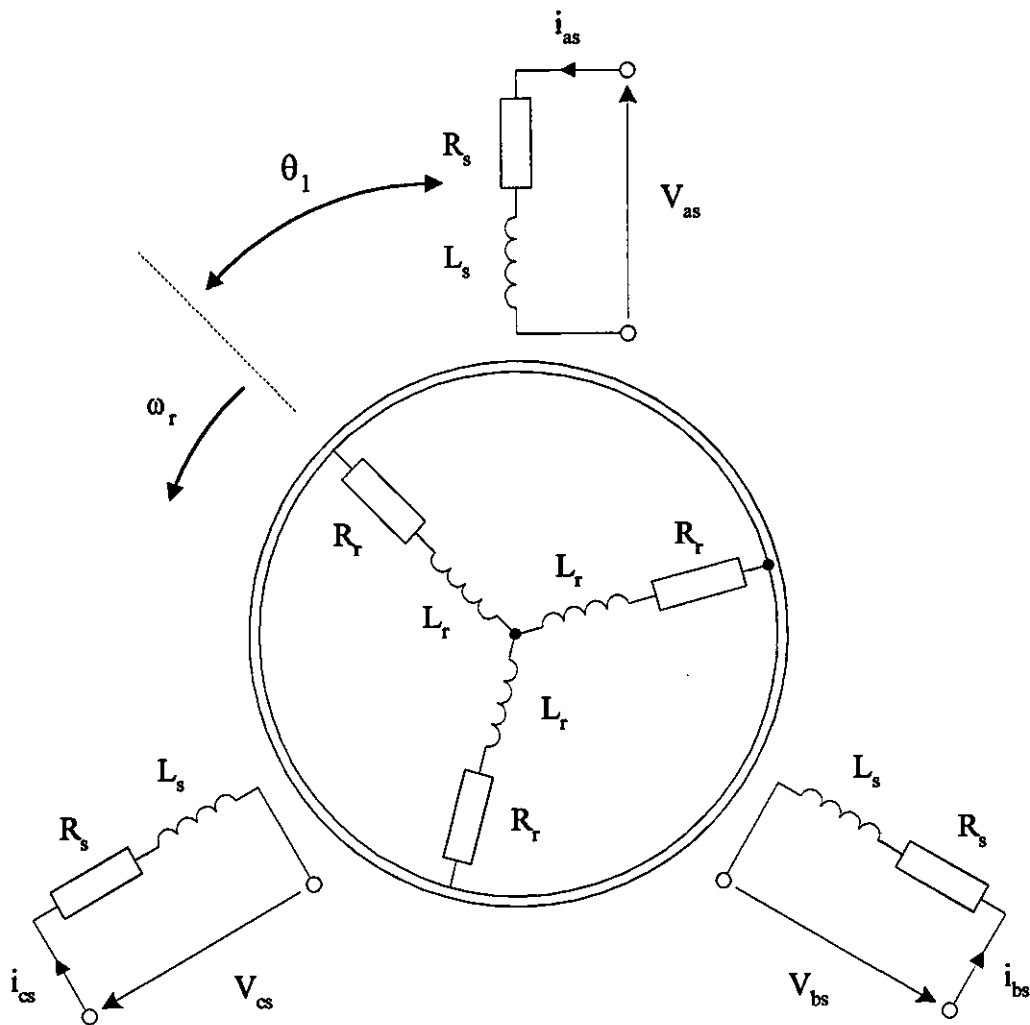


Figure 2-2 Phase model of the induction motor (equivalent 2-pole machine)

2.2.1 The Voltage equation

Using the assumptions above, the voltage equation for a single winding is

$$V_s = Ri + e \quad (2-1)$$

where, e the back emf is given by

$$e = \frac{d\lambda}{dt} = \frac{d}{dt}(Li) \quad (2-2)$$

Hence,

$$V_s = Ri + \frac{dLi}{dt} \quad (2-3)$$

The voltage drop between the terminals consists of two components, the resistance drop Ri , and the voltage drop caused by the variation of the total flux linkage ($d\lambda/dt$). However, a three-phase winding exists on both the stator and rotor of the machine, and this will give rise to mutual coupling between phase a of the stator and the other two phases, with the voltage equation for phase a of the stator being given by

$$V_{as} = R_s i_{as} + \frac{d}{dt} (L_s i_{as} + M_{12} i_{bs} + M_{13} i_{cs} + M_{14} i_{ar} + M_{15} i_{br} + M_{16} i_{cr}) \quad (2-4)$$

where, M_{12}, M_{13} are the stator mutual inductances, and

M_{14}, M_{15}, M_{16} are the mutual inductances between the stator and rotor phases.

As highlighted in Eq.(2-4), the total flux linkage consists of the self and mutual flux linkages. The time derivative (d/dt) applies to both the inductive and the current terms. Due to the relative motion between the stator and rotor, the mutual inductances are a function of the rotor position, so that

$$\begin{aligned} V_{as} = & R_s i_{as} + L_s \frac{di_{as}}{dt} + M_{12} \frac{di_{bs}}{dt} + M_{13} \frac{di_{cs}}{dt} \\ & + M_{14} \frac{di_{ar}}{dt} + M_{15} \frac{di_{br}}{dt} + M_{16} \frac{di_{cr}}{dt} \\ & + i_{ar} \frac{\partial M_{14}}{\partial \theta} \frac{d\theta}{dt} + i_{br} \frac{\partial M_{15}}{\partial \theta} \frac{d\theta}{dt} + i_{cr} \frac{\partial M_{16}}{\partial \theta} \frac{d\theta}{dt} \end{aligned} \quad (2-5)$$

The voltage equations for the remaining two phases can be obtained in a similar manner and the overall machine equations can be written in matrix form as

$$\begin{aligned} [V_m] &= [R_m][i_m] + \frac{d}{dt}[L_m][i_m] \\ \Rightarrow [V_m] &= [R_m][i_m] + [L_m] \frac{d}{dt}[i_m] + [i_m] \frac{d}{dt}[L_m] \\ \Rightarrow [V_m] &= [R_m][i_m] + [L_m] \frac{d}{dt}[i_m] + [i_m][G_m] \frac{d\theta}{dt} \end{aligned} \quad (2-6)$$

where,

$$[V_m] = [V_{as} \quad V_{bs} \quad V_{cs} \quad V_{ar} \quad V_{br} \quad V_{cr}]^T$$

$$[i_m] = [i_{as} \quad i_{bs} \quad i_{cs} \quad i_{ar} \quad i_{br} \quad i_{cr}]^T$$

$$[R_m] = \begin{bmatrix} R_s & & & & & \\ & R_s & & & & \\ & & R_s & & & \\ & & & R_r & & \\ & & & & R_r & \\ & & & & & R_r \end{bmatrix}$$

$$[L_m] = \begin{bmatrix} L_s & M_{12} & M_{13} & M_{14} & M_{15} & M_{16} \\ M_{21} & L_s & M_{23} & M_{24} & M_{25} & M_{26} \\ M_{31} & M_{32} & L_s & M_{34} & M_{35} & M_{36} \\ M_{41} & M_{42} & M_{43} & L_r & M_{45} & M_{46} \\ M_{51} & M_{52} & M_{53} & M_{54} & L_r & M_{56} \\ M_{61} & M_{62} & M_{63} & M_{64} & M_{65} & L_r \end{bmatrix}$$

$$[G_m] = \frac{\partial}{\partial \theta} [L_m] = \begin{bmatrix} G_s & G_{12} & G_{13} & G_{14} & G_{15} & G_{16} \\ G_{21} & G_s & G_{23} & G_{24} & G_{25} & G_{26} \\ G_{31} & G_{32} & G_s & G_{34} & G_{35} & G_{36} \\ G_{41} & G_{42} & G_{43} & G_r & G_{45} & G_{46} \\ G_{51} & G_{52} & G_{53} & G_{54} & G_r & G_{56} \\ G_{61} & G_{62} & G_{63} & G_{64} & G_{65} & G_r \end{bmatrix}$$

$$\frac{d\theta}{dt} = \omega_r$$

Both the inductance and rotational inductance terms are harmonic functions of the rotor electrical angle θ , and the coefficients of the matrix $[L_m]$ and its partial derivative are therefore variable.

2.2.2 Machine inductance coefficients

The mutual inductances between the stator and rotor are the keystone of induction motor performance. Listed below are the coefficients of $[L_m]$ and its partial derivative where the angles θ_1 , θ_2 and θ_3 are electrical angles. Note that an electrical angle is p times the mechanical angle of the actual p pole-pair machine. The angle θ_1 for a 2-pole machine is shown in Fig.2-2, and defines the offset angle between phase a of the stator and the rotor. If the phase windings are mutually displaced by 120° , then

$$\theta_2 = \theta_1 - 120^\circ$$

and $\theta_3 = \theta_1 + 120^\circ$

The inductance coefficients of the machine are

$$\begin{aligned} L_s &= L_{S_s} \quad L_r = L_{R_r} \\ M_{12} &= M_{13} = M_{21} = M_{23} = M_{31} = M_{32} = M_{S_s} \\ M_{45} &= M_{46} = M_{54} = M_{56} = M_{64} = M_{65} = M_{R_r} \\ M_{14} &= M_{25} = M_{36} = M_{41} = M_{52} = M_{63} = M_{SR} \cos \theta_1 \\ M_{15} &= M_{26} = M_{34} = M_{51} = M_{62} = M_{43} = M_{SR} \cos \theta_2 \\ M_{16} &= M_{24} = M_{35} = M_{61} = M_{42} = M_{53} = M_{SR} \cos \theta_3 \end{aligned}$$

where, the coefficients L_{S_s} , L_{R_r} , M_{S_s} , M_{R_r} and M_{SR} of these phase parameters are obtained from the per-phase equivalent circuit parameters of the induction motor. However, the equivalent circuit parameters are usually expressed in per-unit form and as such, it is necessary to transform these parameters into their equivalent quantities in terms of Ohms and Henrys (Refer to Appendix A).

2.2.3 Machine rotational inductance coefficients

The rotational inductance coefficients are the derivative of the inductance coefficients with respect to θ . It follows from the equation for $[L_m]$ that

$$\begin{aligned}
 G_s &= 0, G_r = 0 \\
 G_{12} &= G_{13} = G_{21} = G_{23} = G_{31} = G_{32} = 0 \\
 G_{45} &= G_{46} = G_{54} = G_{56} = G_{64} = G_{65} = 0 \\
 G_{14} &= G_{25} = G_{36} = G_{41} = G_{52} = G_{63} = -M_{SR} \sin \theta_1 \\
 G_{15} &= G_{26} = G_{34} = G_{51} = G_{62} = G_{43} = -M_{SR} \sin \theta_2 \\
 G_{16} &= G_{24} = G_{35} = G_{61} = G_{42} = G_{53} = -M_{SR} \sin \theta_3
 \end{aligned}$$

Several rotational inductance terms are zero, since the stator and rotor self and mutual inductances are constant.

2.2.4 Dynamic equation

The dynamic equation of the machine is

$$T_{em} = T_l + T_f + T_a$$

where, T_{em} is the electromagnetic torque,

T_l is the load torque,

T_f is the frictional torque of the motor/load, and

T_a is the acceleration torque,

Hence,

$$T_{em} = T_l + \frac{k_f}{p} \frac{d\theta}{dt} + \frac{J}{p} \frac{d^2\theta}{dt^2} \quad (2-7)$$

The electromagnetic torque T_{em} is derived from Faradays law, and in matrix form may be written as

$$T_{em} = \left(\frac{p}{2}\right) [i_m]^T [G_m] [i_m] \quad (2-8)$$

The time variation of ω , is obtained by re-arranging equation (2-7) as,

$$\frac{d^2\theta}{dt^2} = \frac{p}{J} \left(T_{em} - T_l - \frac{k_f}{p} \frac{d\theta}{dt} \right) \quad (2-9)$$

2.3 Numerical solution of the machine equations

The transient voltage and dynamic equations cannot be solved in closed form. They have to be solved numerically, and for this purpose equations (2-6) and (2-9) have to be re-arranged in the state-variable form

$$\frac{d}{dt}[i_m] = [L_m]^{-1} \left\{ [V_m] - [R_m][i_m] - [i_m][G_m] \frac{d\theta}{dt} \right\}$$

$$\frac{d\theta}{dt} = \omega_r$$

$$\frac{d\omega_r}{dt} = \frac{p}{J} \left(T_{em} - T_l - \frac{k_f}{p} \omega_r \right)$$

The rotor electrical angle θ can be found, simply by describing the second order system in terms of two first-order differential equations, and solving them simultaneously. At every step of the integration, it is necessary to know θ in order to form $[L_m]$ and its partial derivative. The equations may be written in the abbreviated form

$$\dot{x} = Ax + Bu$$

Hence,

$$\frac{d}{dt}[i_m] = \left[-[L_m]^{-1} \left\{ [R_m] + \frac{\partial [L_m]}{\partial \theta} \omega_r \right\} \right] [i_m] + [L_m]^{-1} [V_m] \quad (2-10)$$

$$\frac{d}{dt} \begin{bmatrix} \theta \\ \omega_r \end{bmatrix} = \begin{bmatrix} 0 & p \\ 0 & -\frac{k_f}{p} \end{bmatrix} \begin{bmatrix} \theta \\ \omega_r \end{bmatrix} + \begin{bmatrix} 0 \\ 1 \end{bmatrix} \left[\frac{p}{J} (T_{em} - T_l) \right] \quad (2-11)$$

In this form, both the above equations can be solved independently using a fourth-order Runge-Kutta numerical integration subroutine in Fortran77, to give a step-by-step time solution for the phase currents, and the rotor position and speed respectively.

2.4 Simulated and experimental results

The transient response of the motor using the direct-phase model was studied and compared with experimental results [1]. The parameters of the motor used to study start-up transients for a sinusoidal input voltage at fixed frequency are given in Appendix C. Figures 2-3 to 2-6 show the results obtained for the motor speed, torque and phase currents following the application of a 380V, 50Hz sinusoidal input voltage.

From the torque waveform, it is evident that the starting torque is oscillatory, causing the initial dips in the speed curve. This arises because of the initially varying nature of the magnetizing current. This has an effect on the air-gap flux and therefore, on the resultant torque produced by the machine.

Eventually, the torque settles to the steady-state value, equal to the sum of the applied load torque and the torque needed to overcome the frictional and windage losses. This is accounted for by the dynamic equation [Eq.(2-7)], where the acceleration term ($d^2\theta/dt^2$) is effectively zero. However, when the motor is unloaded, the steady-state torque will simply equal the torque required to overcome the frictional loss,

$$\text{i.e.} \quad T_{em} = \frac{k_f}{p} \omega_r$$

Although, the induction motor starting current is high, at 6-8 times the rated current it is typical of many induction machines. In this case, the peak amplitude of the initial current drawn by the machine is about 15A, but this eventually decays to a steady-state value of approximately 2A. The rotor phase current on the other hand is initially 14A, but under no load conditions and with only a small frictional torque, it eventually decays to a value close to zero.

The gradual change in the rotor frequency from 50Hz to a value close to zero is noticeable as the motor approaches synchronous speed. This change in both the magnitude and frequency is linked to the motional inductance terms in the electrical equation [Eq.(2-6)], becoming significant as the motor reaches its running speed.

Experimental results for this transient situation are shown in Figures 2-7 and 2-8, and clearly good agreement exists between these results and the computed results. As such, it can be said that the phase model provides a good prediction of the transient characteristics of the motor.

These results were also compared with those obtained using the d-q model. The induction motor is then described by the following state equation in a stationary reference frame,

$$\frac{d}{dt} \begin{bmatrix} i_s \\ \phi_r \end{bmatrix} = \begin{bmatrix} A_{11} & A_{12} \\ A_{21} & A_{22} \end{bmatrix} \begin{bmatrix} i_s \\ \phi_r \end{bmatrix} + \begin{bmatrix} B_1 \\ 0 \end{bmatrix} V_s \quad (2-12)$$

where,

$$i_s = [i_{ds} \quad i_{qs}]^T \quad \phi_r = [\phi_{dr} \quad \phi_{qr}]^T \quad V_s = [V_{ds} \quad V_{qs}]^T$$

$$A_{11} = -\left\{ \frac{R_s}{\sigma L_s} + \frac{(1-\sigma)}{\sigma \tau_r} \right\} I$$

$$A_{12} = \frac{M}{\sigma L_s L_r} \left\{ \left(\frac{1}{\tau_r} \right) I - \omega_r J \right\}$$

$$A_{21} = \left(\frac{M}{\tau_r} \right) I \quad A_{22} = -\left(\frac{1}{\tau_r} \right) I + \omega_r J$$

$$B_1 = \left(\frac{1}{\sigma L_s} \right) I \quad C = [I \quad \theta]$$

$$I = \begin{bmatrix} 1 & 0 \\ 0 & 1 \end{bmatrix} \quad J = \begin{bmatrix} 0 & -1 \\ 1 & 0 \end{bmatrix}$$

The transient response of the system was analysed using the *MATLAB* software package (a listing of the source code can be found in Appendix F). From Figures 2-9 to 2-11, it can be seen that the results obtained are similar to those computed using the phase model.

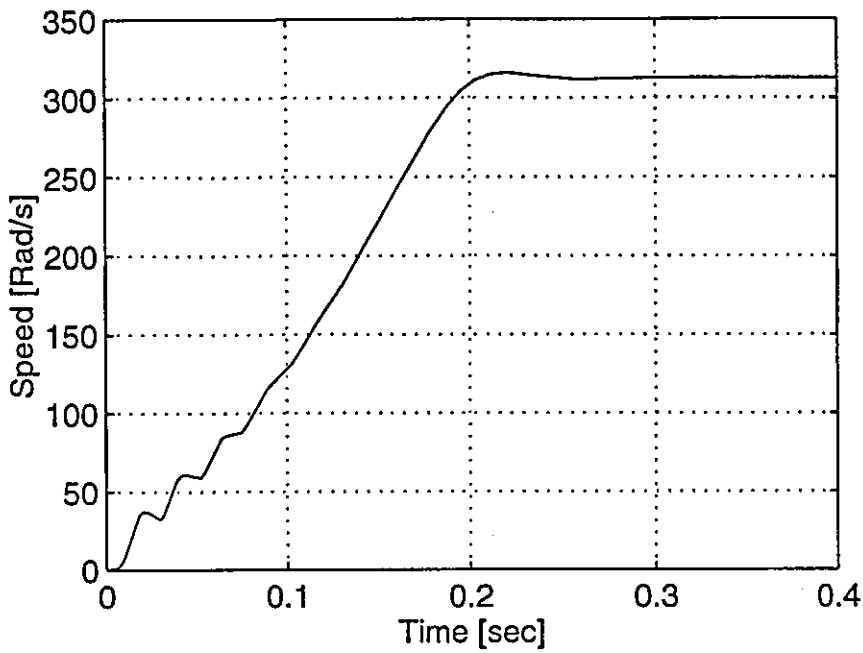


Figure 2-3 Computed results - Speed characteristic for start-up of an Induction Motor - Sine wave input

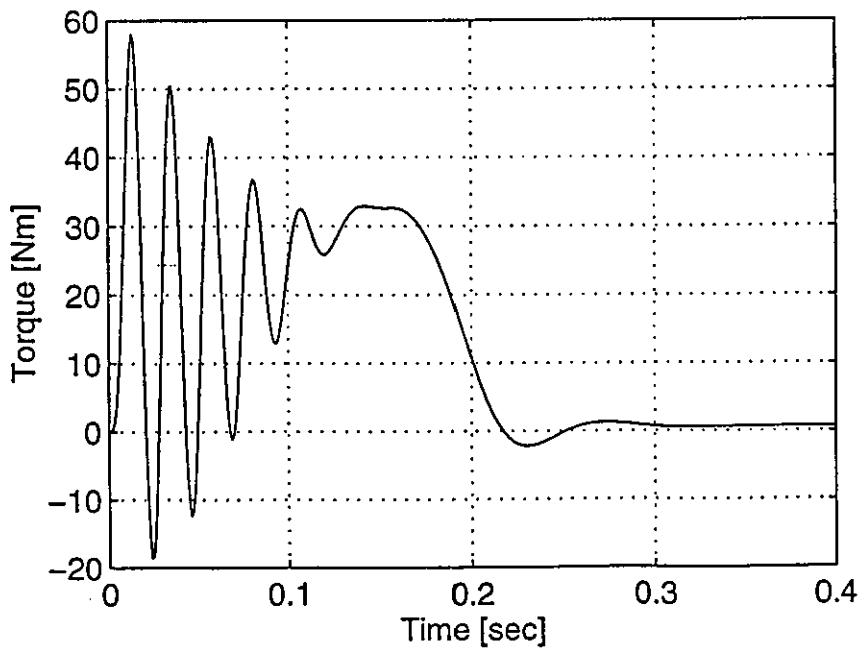


Figure 2-4 Computed results - Torque characteristic for start-up of an Induction Motor - Sine wave input

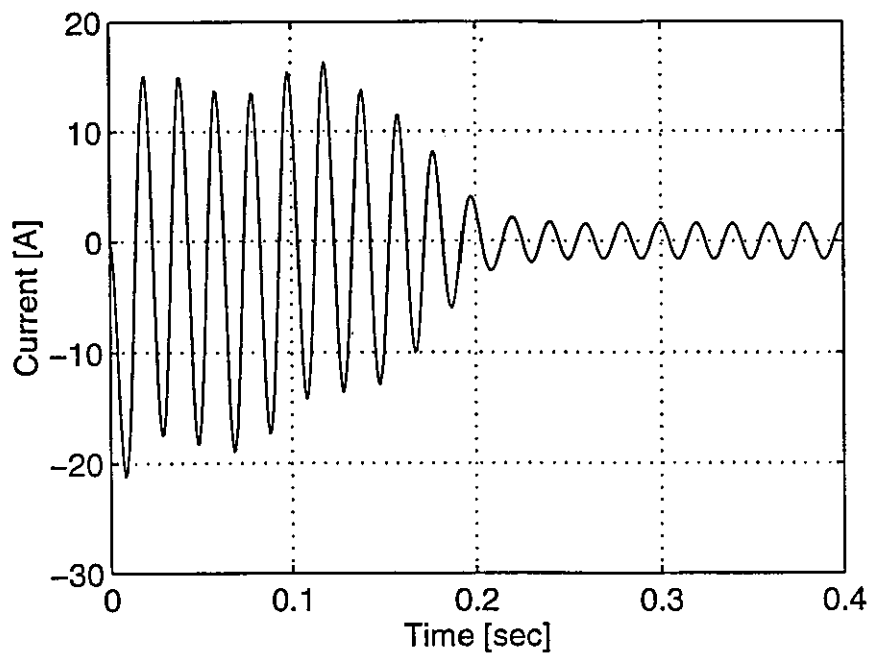


Figure 2-5 Computed results - Stator phase current characteristic for start-up of an Induction Motor - Sine wave input

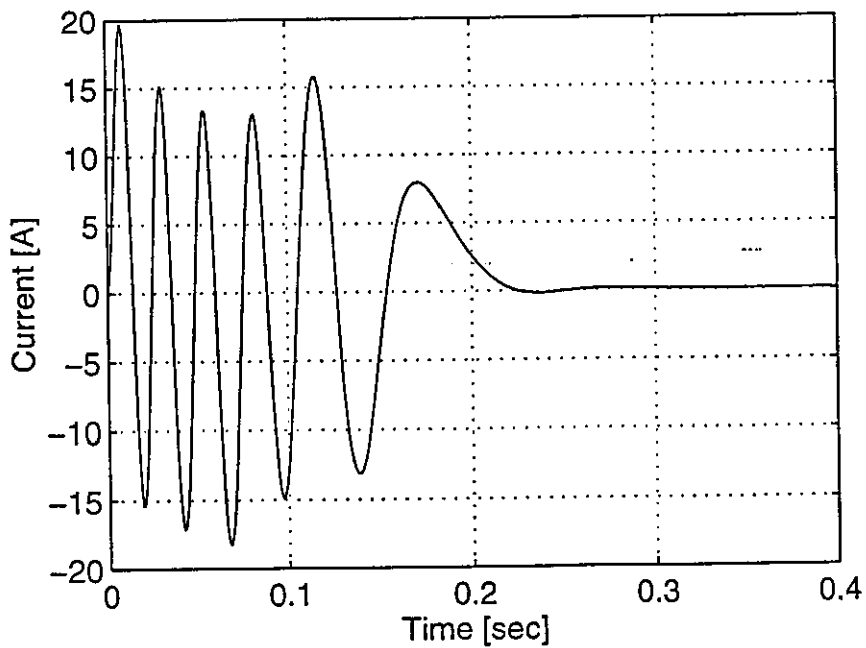


Figure 2-6 Computed results - Rotor phase current characteristic for start-up of an Induction Motor - Sine wave input

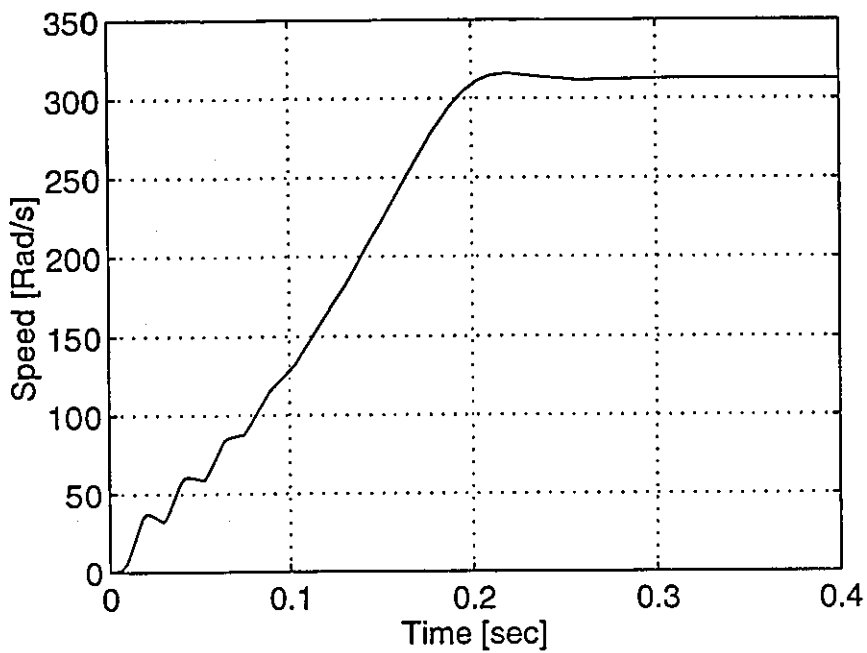


Figure 2-7 Experimental results - Speed characteristic for start-up of an Induction Motor - Sine wave input

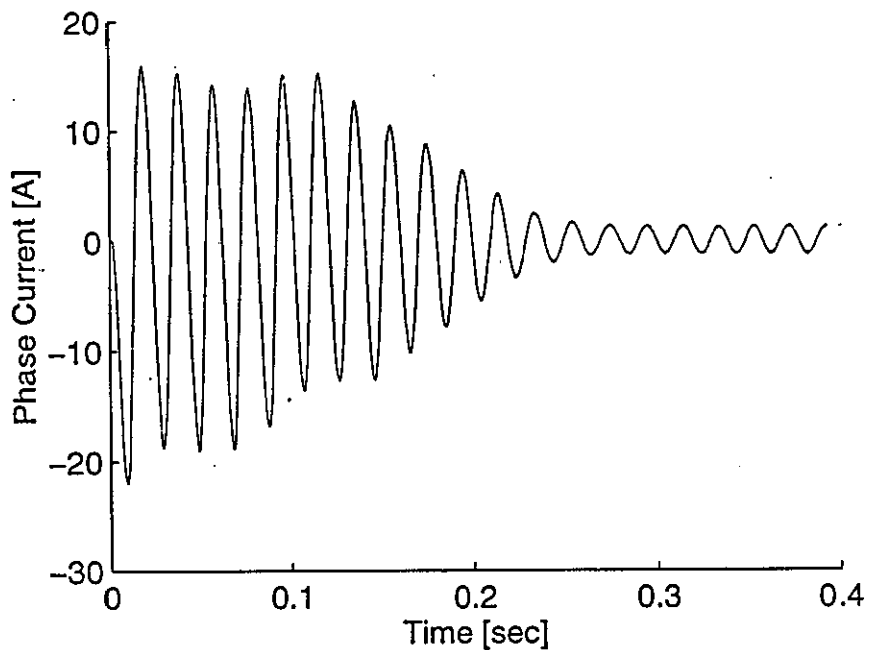


Figure 2-8 Experimental results - Stator phase current characteristic for start-up of an Induction Motor - Sine wave input

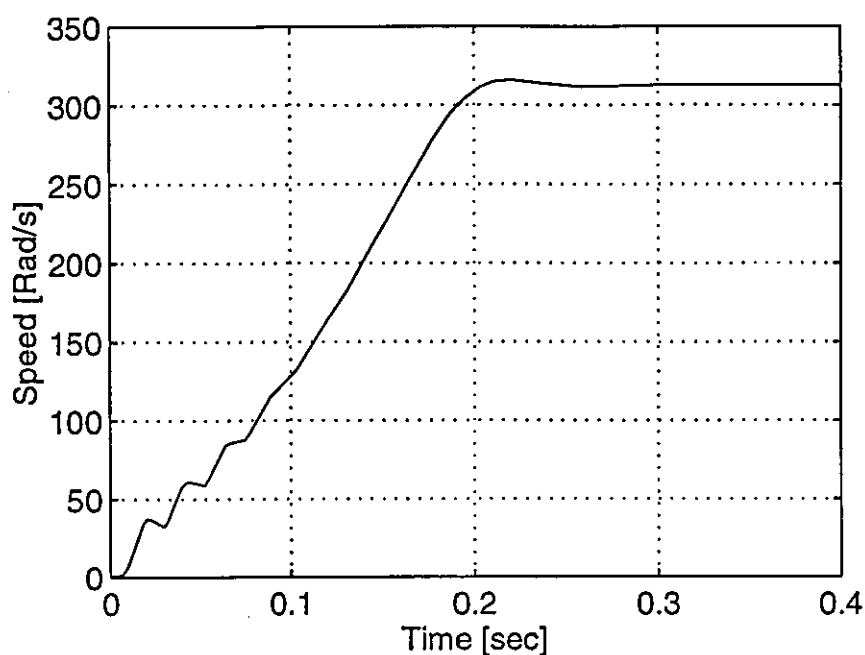


Figure 2-9 Computed results from *MATLAB* - Speed characteristic for start-up of an Induction Motor - Sine wave input

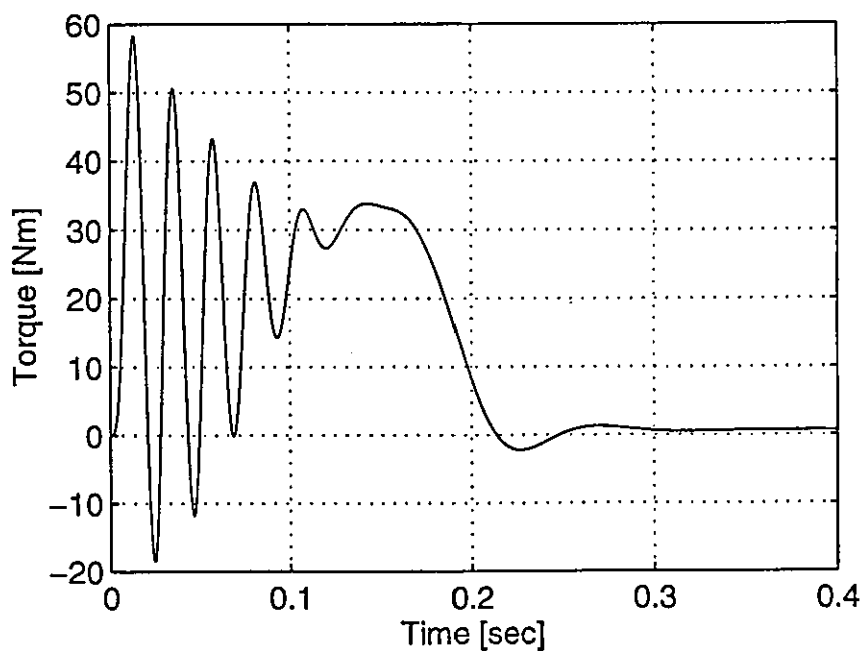


Figure 2-10 Computed results from *MATLAB* - Torque characteristic for start-up of an Induction Motor - Sine wave input

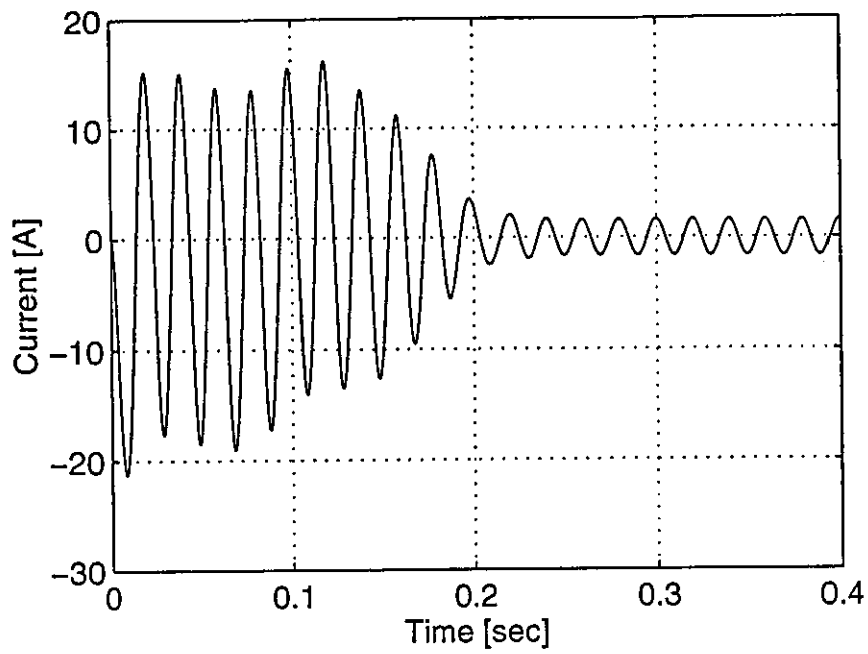


Figure 2-11 Computed results from *MATLAB* - Stator phase current characteristic for start-up of an Induction Motor - Sine wave input

THE LINEAR MOTOR

Linear motors are still in a stage of infancy in development, and one factor contributing to this slow development process is that these large air-gap motors contribute to a low efficiency. Although, linear machines rarely achieve the performance, in terms of either power factor or efficiency, expected from their rotary counterparts, in several applications this reduction in performance is more than compensated for by convenience and robustness.

A linear motor produces a straight line motion, but it is not necessarily the best choice for every application requiring linear motion. In many applications, the conventional rotary motor is used to produce linear motion with the use of gears and other mechanisms that transform rotary into linear motion.

Even though linear motors are not practical for many drives, it seems only natural that they find applications in situations where mechanical gears and rotary-to-linear converters are undesirable whilst at the same time possessing the added advantages of being quieter and more reliable.

3.1 Linear induction motor

By far the most common form of linear motor in industrial use is the single-sided linear induction motor (SLIM). However, because of the inherently large air-gap, there is a practical limitation on its performance and application. The primary applications have been in ground transportation systems ranging from conveyer systems to medium speed trains, and in actuators for automatic equipment [5-7].

The linear induction motor (LIM) is generally of the flat or tubular type. The emphasis in this thesis is placed on the flat-type SLIM because of its suitability for low-speed applications, where in most cases the longitudinal end-effect can be ignored.

3.1.1 Single-sided flat-type

The flat-type SLIM with sheet secondary shown in Fig.3-1 is best introduced by the imaginary process of 'cutting' and 'unrolling' a rotary cage-rotor machine, to produce a linear laminated 'stator' core containing a three-phase primary winding and a linear 'rotor' core containing the secondary cage. The 'rotor' core is formed from ferromagnetic material to provide a return path for the magnetic flux. It is often the stator core and its windings that move, and as such the terms primary and secondary are commonly used to describe the stator and rotor, respectively.

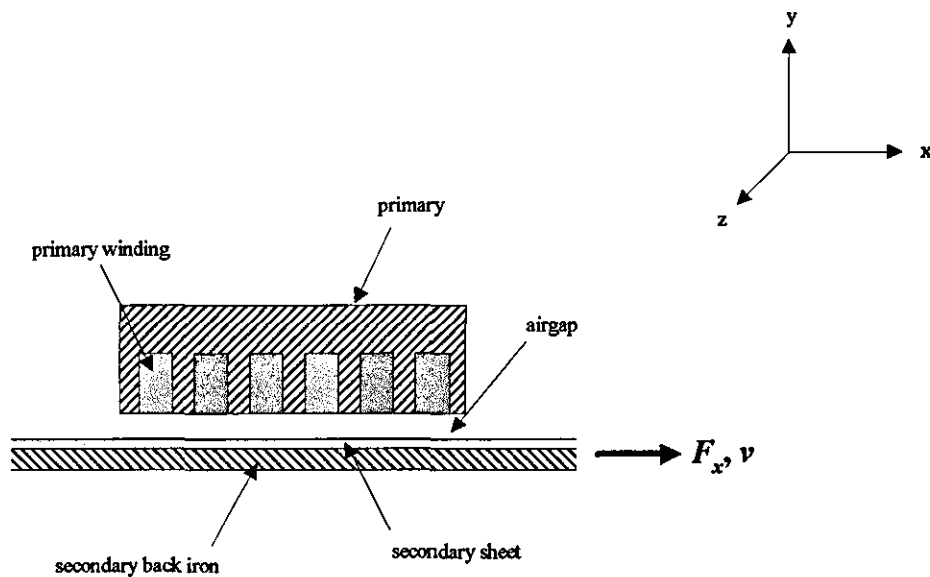


Figure 3-1 Side view of a short-stator flat-type single-sided linear induction motor

Motion in a LIM is produced in a similar way to that in a rotary machine. The three-phase primary winding currents produce a travelling magnetic field that induces currents in the secondary member, and by producing a reaction force on the rail causes it to move.

3.1.2 Goodness factor

The 'goodness factor' is used as a convenient guideline for assessing the quality of a LIM. Although, there are different ways of defining this quantity, the definition used in this thesis is [8]

$$G_e = \frac{2\tau^2 \sigma_e \mu_0 f_s}{\pi g_e}$$

A large air-gap need not necessarily produce a poor design if the pole-pitch is correspondingly large. Clearly, increasing this value has a beneficial effect on the performance if end-effects are ignored, but in practice it increases the end-effects and tends to detract from the performance. To allow for this, Boldia and Nasar [9] suggested an alternative measure of performance based on achieving zero total propulsive force at synchronous speed.

3.2 Differences between the linear and conventional induction motor

The key differences between the LIM and its rotating counterpart are

- The linear motor has a finite length of travel i.e. it has a 'beginning' and an 'end'. This gives rise to longitudinal end-effects that can have influence on factors such as the power factor and efficiency, especially in medium to high-speed motors.
- The secondary (rotor) or moving member is often either a solid steel plate or a composite rail formed by a layer of aluminium attached to a steel backing plate. As such, there are no conducting bars or coils in the secondary.
- A transverse edge-effect has an influence on the equivalent resistance of the secondary, but this is usually accounted for by using a transverse correction factor [10].
- In single-sided motors, a force exists perpendicular to the direction of travel, that may be either repulsive or attractive. This normal force can often be used to advantage, and should be considered in the design of LIM drives.
- The considerably larger air-gap results in a large leakage reactance.
- Rotor resistance variation is small since heat generated by the machine slip is easily dispersed through the larger surface area of the secondary.

The above factors must all be taken into account if the linear motor is to be modelled correctly.

3.3 Circuit analysis of a low-speed linear induction motor

Although a LIM can be studied either using field theory to give analytical expressions [11-15] or by an equivalent circuit [2, 16-20], the latter was chosen since it provides a model that is suitable for the analysis of the combined inverter-motor system. The lumped parameters of the machine are easily obtained from design parameters or, alternatively, from static tests.

The behavioural differences between the LIM and its rotary counterpart are usually attributed to the end-effect phenomenon due to the continuous replacement of the secondary material. The consequences of this are not easily expressed in terms of equivalent circuit components.

The present study is concerned with the low-speed application of LIMs, where end-effects are considered to have negligible influence on the overall machine performance, and are neglected in the initial analysis. A single-sided stator configuration is assumed, in which the secondary consists of an aluminium cap over a laminated steel core. However, a double-sided arrangement can easily be analysed in the same manner. Lamination of the back-iron reduces the effect of field diffusion (i.e. skin-effects) in the secondary [15], especially for low-speed operation.

3.3.1 Equivalent circuit

Since, all edge transients due to motion can be neglected in the evaluation of the performance of a low-speed LIM, the machine performance can be predicted with a fair degree of accuracy from the equivalent circuit for a conventional motor, with appropriate modifications to the parameter values [2, 18-20]. The per-phase equivalent circuit of the SLIM shown in Fig.3-2 can be derived, together with the equivalent circuit parameters.

Often, the secondary leakage reactance is ignored in the equivalent circuit, since the rotor current is concentrated into a thin conducting sheet [21, 22]. However, in this thesis, it is included so as to provide a complete circuit analysis, thus a more accurate model of the LIM.

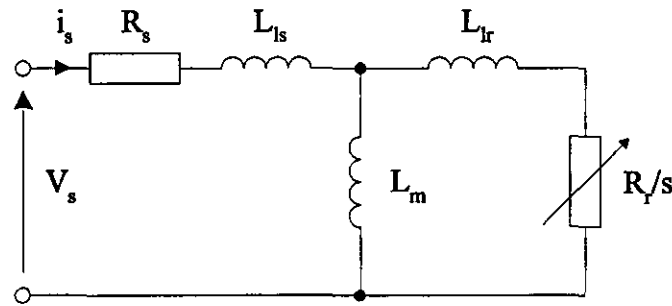


Figure 3-2 Per-phase equivalent circuit of the LIM without longitudinal end-effect

In deriving the equivalent circuit the following assumptions are made

- The motor is low speed.
- Longitudinal end-effects are neglected (since the speed is low).
- The design is of the flat-type.

The mutual and secondary impedance are easily derived from field theory [18, 19], and are speed and slip frequency dependant. Transverse distortion effects of the magnetic field caused by the flow of currents in the x-direction within the secondary rail and slotting-effects in the stator are taken into account by appropriate correction factors [10, 23]. Thus the actual LIM is replaced by an ideal LIM, whose equivalent parameters are evaluated with the aid of these correction factors. Iron losses are neglected, since the large air-gap leads to moderate flux densities in the core and hence, low core losses.

In fact, provided that the machine to be analysed has a fair number of poles (i.e. $2p \geq 4$) and a stack-length sufficiently large with respect to the pole-pitch, evaluation of the equivalent circuit parameters for the linear machine follows very closely that of a rotary machine.

3.3.2 Derivation of equivalent circuit parameters

In deriving the equivalent circuit parameters, the linear induction motor is initially analysed as a one-dimensional electromagnetic field problem as outlined in [13, 14], to

provide a basic understanding of the problems involved. Although, it is expected that a two-dimensional analysis of the LIM [14, 19] should give better results, it has been shown by Yamamura et al. [14] that in many situations such as in low-speed applications, a one-dimensional theory provides results of acceptable accuracy.

The one-dimensional air-gap equations are derived from the three-dimensional Maxwell's equations for a machine moving at a velocity v relative to a fixed reference frame. Thus, in terms of the magnetic vector potential A , [13]

$$\nabla_x \frac{1}{\mu} \nabla \bar{A} = -\sigma \frac{\partial \bar{A}}{\partial t} - (\bar{v} \cdot \nabla) \bar{A} \sigma + \bar{J}, \quad (3-1)$$

where, μ is the magnetic permeability, σ the material conductivity and J_s the source currents.

The following assumptions are made in the analysis of a LIM by the 'Continuous sheet' method [20], which allows Eq.(3-1) to be greatly simplified.

- The stator winding is replaced by an infinitely thin current sheet, with slotting-effects taken into account by Carter's coefficient [23].
- The current density distribution of the current sheet is equivalent to that of the actual slot-embedded conductor configuration. A sinusoidal distribution is assumed for the windings, which results in a sinusoidally varying air-gap field. The primary phase currents are represented by the current sheet,

$$j_s = \text{Re} \left[J_s \exp \left(j \left\{ \omega t - \frac{\pi x}{\tau} \right\} \right) \right] \quad (3-2)$$

where, J_s is the design current density of the primary sheet, and

j_s is the instantaneous current density acting on the primary surface.

- The effect of x-directed currents in the secondary are neglected, and only z-directed currents exist in the secondary conductor below the primary.

- Only a y-component of the magnetic flux and field density exist in the air-gap and the secondary conductor, since it is assumed that only z-directed currents exist in both the primary and secondary.
- With an aluminium-capped secondary the induced currents will flow in roughly elliptical patterns and have an x-component. The x-directed currents have an important influence on the secondary impedance especially when the stator core is too narrow with respect to the pole-pitch. This transverse edge-effect may be taken into account by the Russell and Norsworthy [10] correction factor, with all fields then assumed to be invariant in the z-direction.
- Magnetic saturation and hysteresis effects in both the primary and secondary core are neglected.

The above assumptions are valid for a stator length sufficiently large with respect to the stack and the air-gap length, and Eq.(3-1) can be written as

$$\frac{\partial^2 b_y}{\partial x^2} - \frac{\mu_0}{\rho_s g} \frac{\partial b_y}{\partial x} = \frac{\mu_0}{g} \frac{\partial j_s}{\partial x} \quad (3-3)$$

where b_y is the instantaneous magnetic flux density in the air-gap, g is the air-gap length, μ_0 is the permeability of free space, which is termed the air-gap field equation.

Neglecting the longitudinal end-effects, the steady-state solution of Eq.(3-3) is

$$b_y = \text{Re} \left[B_s \exp \left(j \left\{ \omega t - \frac{\pi x}{\tau} \right\} \right) \right] \quad (3-4)$$

where B_s , the peak steady-state air-gap flux density is

$$B_s = \frac{\tau \mu_0 J_s}{g_s \pi (sG_s - j)}$$

where

$$J_s = \frac{3\sqrt{2}i_s N k_\omega}{p\tau}$$

Once the linear motor has been identified as an electromagnetic field boundary value problem, the circuit theory components in the resistance matrix $[R]$, the inductance matrix $[L]$ and the motional inductance matrix $[G]$ can easily be obtained [24]. Alternatively, a set of equations can be derived to evaluate the equivalent circuit parameters, given the design parameters of the machine. The equivalent circuit parameters for a low-speed SLIM can be evaluated from [20].

$$X_m = \frac{12\mu_0\omega a_e k_w N^2 \tau}{\pi^2 p g_e} \quad (3-5)$$

$$R_r' = \frac{X_m}{G_e} = \frac{12a_e k_w N^2}{\pi p \sigma_e} \quad (3-6)$$

$$X_r' \approx 0 \quad (3-7)$$

$$R_s = \frac{1}{\sigma_e} \frac{(4a_e + 2l_{ce})}{Ni} J_s N^2 \quad (3-8)$$

$$X_{ls} = \frac{2\mu_0\omega}{p} \left[\left(\lambda_s \left(1 + \frac{3}{2p} \right) + \lambda_d \right) \frac{2a_e}{q} + \lambda_e I_{ce} \right] N^2 \quad (3-9)$$

where,

$$\lambda_s \approx \frac{1}{12} \frac{h_s}{w_s} (1 + 3\beta_1)$$

$$\lambda_d = \frac{5(g_e / w_s)}{5 + 4(g_a / w_s)}$$

$$\lambda_e = 0.3(3\beta_1 - 1)$$

3.3.3 Force computation

The force produced on the reaction plate of the LIM can be resolved into a propulsive force (thrust) along the direction of motion, and a force normal to the surface of the plate [25]. In addition to these two forces, the stator in a SLIM can be subject to a lateral force under asymmetric positioning [15]. The normal force can be either

repulsive or attractive, and is dependant on the type of reaction plate used. Thus, whereas a steel secondary will always produce an attractive force, with an aluminium composite secondary it is possible for the force to become repulsive. All three forces are dependant on slip-frequency.

The following analysis relies on a two-dimensional solution of the field distribution [14, 19], where the magnetic flux density in the air-gap has both a normal and tangential component. The thrust and normal forces per unit area of primary surface are [22]

$$F_x = \frac{1}{2} B_{sn} J_s \cos \phi \quad (3-10)$$

$$F_n = \frac{1}{4} \left(\mu_0 J_s^2 - \frac{B_{sn}^2}{\mu_0} \right) \quad (3-11)$$

where B_{sn} is the normal component of air-gap flux density, and a positive value of F_n denotes a repulsive force.

From Eq.(3-11), the normal force is seen as the difference between a term proportional to J_s and one proportional to B_{sn} . With a constant current drive J_s is constant, but B_{sn} is a function of slip. As the slip reduces B_{sn} increases, thus making the second term of Eq.(3-11) increasingly significant and leading to an attractive force at low slip.

For a low-speed LIM, the expression for the steady-state thrust and the normal force are greatly simplified [25],

$$F_x = \frac{m(i_r)^2 R_r'}{sv_s} \quad (3-12)$$

$$F_n = -0.5 \left(R_m s - \frac{1}{R_m s} \right) F_x \quad (3-13)$$

where the magnetic Reynolds number $R_m = \sigma_e \mu_0 v_s$.

It is important that these forces are taken into account in the design of a control system for variable speed drives, since the normal force can often be used to advantage. However, in this thesis, the normal and lateral forces are not evaluated for a SLIM.

3.4 Longitudinal end-effect

According to Yamamura et al. [14], the longitudinal end-effect can be interpreted as the superposition of two travelling air-gap magnetic flux density waves. The magnetic field is weakened at the entry edge by the incoming secondary sheet whereas at the exit edge it is intensified by the reflection of the travelling wave.

3.4.1. Principle of the phenomena

The general solution of Eq.(3-3) given below includes both the entry and exit end-effect waves [14].

$$b_y = \text{Re} \left(\begin{array}{l} B_s \exp j\left(\omega t - \frac{\pi x}{\tau}\right) \\ +B_1 \exp\left(\frac{-x}{\alpha_1}\right) \exp j\left(\omega t - \frac{\pi x}{\tau_e}\right) \\ +B_2 \exp\left(\frac{x}{\alpha_2}\right) \exp j\left(\omega t - \frac{\pi x}{\tau_e}\right) \end{array} \right) \quad (3-14)$$

The first term of Eq.(3-14) is the normal unattenuated wave travelling in the forward direction at synchronous speed $2\tau f_s$. The second term is the flux density wave due to the entry edge, decaying along the x-axis and travelling in the same forward direction. Finally, the third term is the flux density wave due to the exit edge, increasing exponentially along the x-axis, and travelling in the opposite direction. The travelling speed of both the end-effect waves is the same, where the half-wavelength of the end-effect waves τ_e is

$$\tau_e = 2\pi \left(\frac{\rho_s g_e}{4\omega\mu_0} \right) \quad (3-15)$$

and the distance of penetration of the entry and exit end-effect wave are

$$\alpha_1 = \frac{2\rho_s g_e}{\rho_s g_e X - \mu_0 v} \quad (3-16)$$

$$\alpha_2 = \frac{2\rho_s g_e}{\rho_s g_e X + \mu_0 v} \quad (3-17)$$

where,

$$X = \frac{\mu_0 v}{\rho_s g_e}$$

The last two terms in Eq.(3-14) are responsible for the main reduction in the LIM performance when compared with its rotary counterpart. In general α_1 is larger than α_2 , and the entry edge wave has therefore a much greater influence on performance than the exit edge wave. It can also be deduced that these end-effects play a significant role in the design of a high-speed LIM [15], and at low slip where

$$\tau_e \cong \tau(1-s) \approx \tau \quad (3-18)$$

the two waves cancel over much of the primary length. However, the end-effects are a more dominant factor in the performance of a LIM with a sheet reaction rail than a solid-steel rail, at higher speeds.

It can also be shown [13, 14] that the arbitrary constants B_1, B_2 can be found from simple boundary conditions:

- there is no fringing at the stator ends, and therefore the net flux under the stator is zero

$$\int_0^L b_y dx = 0$$

- with no fringing flux, at $x = 0$,

$$b_y = \frac{\rho_s}{v} j_s$$

In the next section an equivalent circuit is presented which takes into account the longitudinal end-effects.

3.4.2 Modified equivalent circuit

So far the development of the equivalent circuit resembles that of its rotary counterpart, but does not take into account the so called 'end-effects'. However, recent papers by Duncan [2], and Gieras et al. [17] suggest that the rotary-motor model can easily be modified to account for this behaviour through the use of the usual equivalent circuit components.

Eddy currents in the motor secondary have a demagnetizing effect on the primary magnetizing current, which accounts for the gradual build up of flux density in the air-gap of the LIM. For the short stator machine under consideration, a high velocity will lead to a significant loss of flux at the leading edge. In fact, the lower the speed the smaller the loss of flux, and hence the less influence the end-effect has on the behaviour of the machine.

The paper by Gieras et al. [17] introduced an end-effect factor by evaluating the induced voltage in the primary winding due to the first two terms in Eq.(3-14). To account for the end-effect in the equivalent circuit, an impedance Z_e (i.e. the end-effect impedance) is connected in parallel with the magnetizing branch inductance L_m .

$$Z_e = \left(\frac{1 - k_e}{k_e} \right) Z_{1\alpha}$$

where,

$$Z_{1\alpha} = \frac{Z_g Z'_{sec}}{Z_g + Z'_{sec}}$$

and k_e is the end-effect factor, Z_g the mutual impedance and Z'_{sec} the secondary impedance referred to the primary. Since, the exit-end effect wave is considered to produce much less degradation in LIM performance than the entry-end-effect wave, it is not taken into account.

The paper by Duncan [2] introduced the so called ' Q ' quantity as a measure of the ability of the motor to resist the loss in output performance due to end-effects. In fact, the actual value of Q is dependant upon several criteria,

- The velocity,
- The secondary resistance R_r ,
- The magnetizing branch inductance L_m .

and it is evaluated from

$$Q = \left(\frac{T_v}{T_2} \right) = \frac{LR_r}{(L_m + L_r)v} \quad (3-19)$$

where, L is the motor effective length.

The demagnetizing effect of the secondary eddy currents is taken into account by simply placing an inductance in parallel with the magnetizing inductance L_m , so as to divert current away from L_m , and in effect to create a loss of excitation. The value of this parallel circuit in terms of an equivalent series circuit is

$$L'_m = L_m \left(1 - \frac{1 - e^{-\varrho}}{Q} \right) \quad (3-20)$$

As a result of the eddy currents circulating in the motor secondary, ohmic losses are produced. It has been shown that these are sufficiently accounted for by a resistance R_m placed in series with the magnetizing branch, where

$$R_m = R_r \left(\frac{1 - e^{-\varrho}}{Q} \right) \quad (3-21)$$

Figure 3-3 shows the modified equivalent circuit of the LIM taking end-effects into account. However, this model is only valid when the inductive element dominates the impedance of the magnetizing branch.

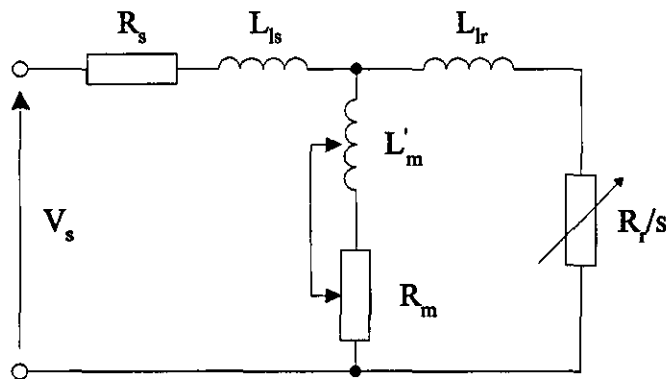


Figure 3-3 Modified equivalent circuit taking end-effects into account

Clearly, both the above methods take the longitudinal end-effect into account by modifying the air-gap electromotive force (EMF) of a T-type equivalent circuit. However, the method proposed by Duncan is chosen since it provides a more accurate analysis of the longitudinal end-effect by taking both entry and exit-end-effect waves into account.

For a complete analysis of the short stator machine, no easy equivalent circuit is possible, and the simplest way to calculate the performance of such a machine is to evaluate the back emf generated and to obtain the total input voltage as a function of slip with a constant current drive.

3.5 Dynamic equation

Having previously carried out a transient analysis of the rotary induction motor, the aim now is to predict the current and force transients for a LIM in a similar fashion. The electrical angles must clearly be expressed as a function of the linear distance travelled by the machine, rather than as an angular distance. This is easily achieved using the transformation,

$$\theta = kx$$

where,

$$k = \frac{2\pi}{\lambda} = \frac{\pi}{\tau}$$

Similarly, the inertia of the LIM is the mass of its moving member. The mechanical equation of motion is now

$$\frac{dv}{dt} = \frac{1}{mass}(F_x - F_l - F_f) \quad (3-22)$$

and it can be shown [18, 22] that the thrust F_x produced by the machine and the frictional force F_f are

$$F_x = \frac{\pi}{L} p [i_m]^T [G_m] [i_m] \quad (3-23)$$

$$F_f = mass \cdot k_\mu \quad (3-24)$$

where k_μ is the friction coefficient in N/kg.

According to Luda [22], the value of friction coefficient is dependant on both the wheel and axle diameter, and the type of wheel bearings used. For the experimental machine in question, a value of 0.068N/kg is assumed.

3.6 Simulated results

The transient and steady-state performance of a SLIM with sheet secondary is analysed using the equivalent circuit technique presented in this Chapter. The equivalent circuit and design parameters for the experimental machine are given in Appendix C. The former parameters were obtained using standard rotary motor tests [2], with measurements made at the machine terminals. The phase parameters are then derived from the per-phase equivalent circuit, using the relationships given in Appendix A.

Figs 3-4 to 3-7 show the predicted starting performance for the LIM with a line voltage of 140V and a supply frequency of 10Hz. The speed and phase currents are displayed as a function of time, and it is evident from Fig.3-4 that the synchronous speed of the machine is around the expected figure of 5.74ms^{-1} . End-effects were not taken into consideration during this analysis, and no unbalance among the primary three-phase currents can therefore be observed.

The thrust-speed characteristic is shown in Fig.3-5, where the marked points indicate the computed results obtained for the thrust at different speeds. For speeds above 6ms^{-1} , the thrust and phase current waveforms will resemble those of the rotary induction motor. In fact, the overall shape of the thrust-speed characteristic is dependant on the motor parameters, with reaction rail resistance and inductance largely governing the overall shape.

In comparison to the conventional induction motor, the LIM starting current is low. From the stator phase current waveform shown in Fig.3-6, it is also evident that the current drawn by the machine remains almost constant from standstill up to synchronous speed. This applies to linear motors with synchronous speeds of between 3 and 6ms^{-1} . Under no-load conditions and with only a small frictional force, the rotor phase current eventually decays to a value close to zero.

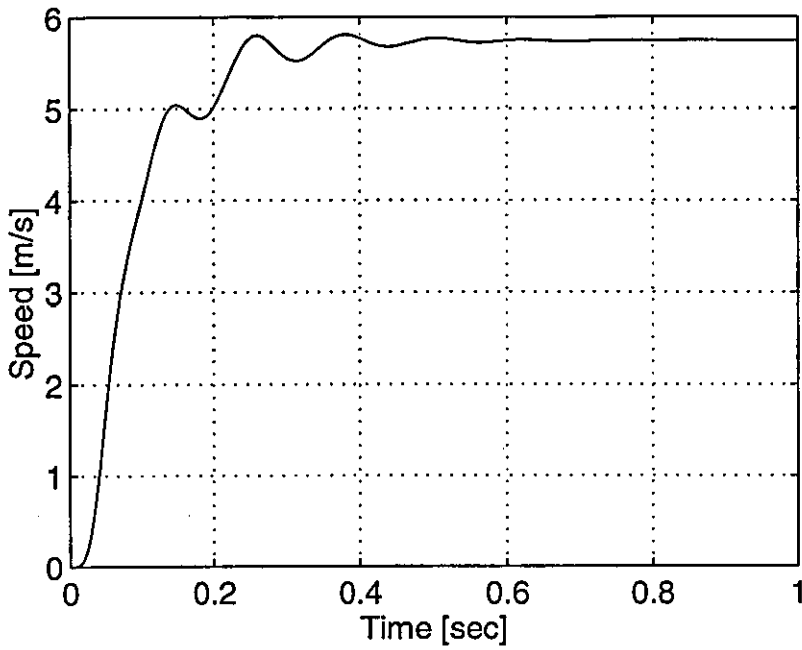


Figure 3-4 Computed results - Speed characteristic for start-up of a Linear Induction Motor - Sine wave input

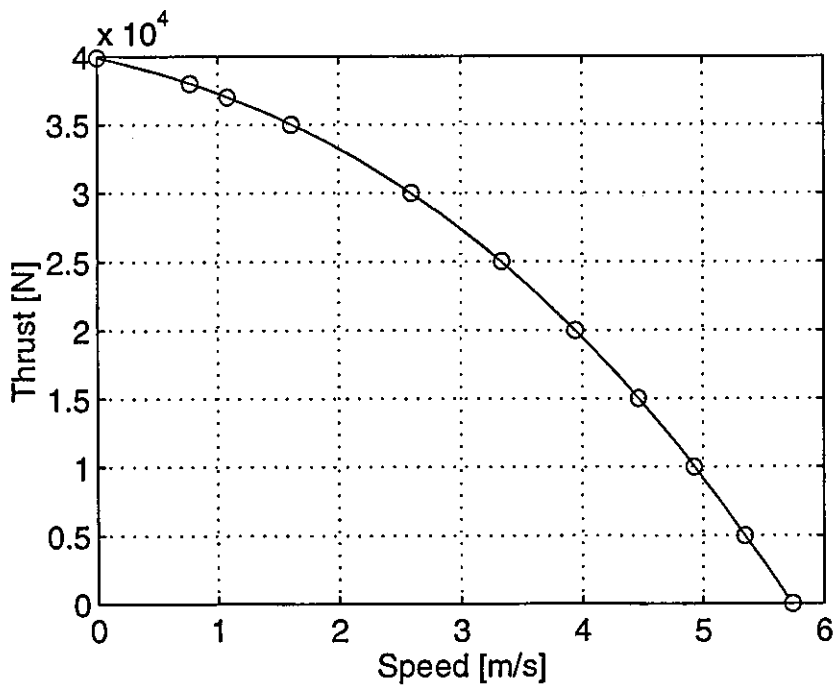


Figure 3-5 Computed results - Thrust-speed characteristic for start-up of a Linear Induction Motor - Sine wave input

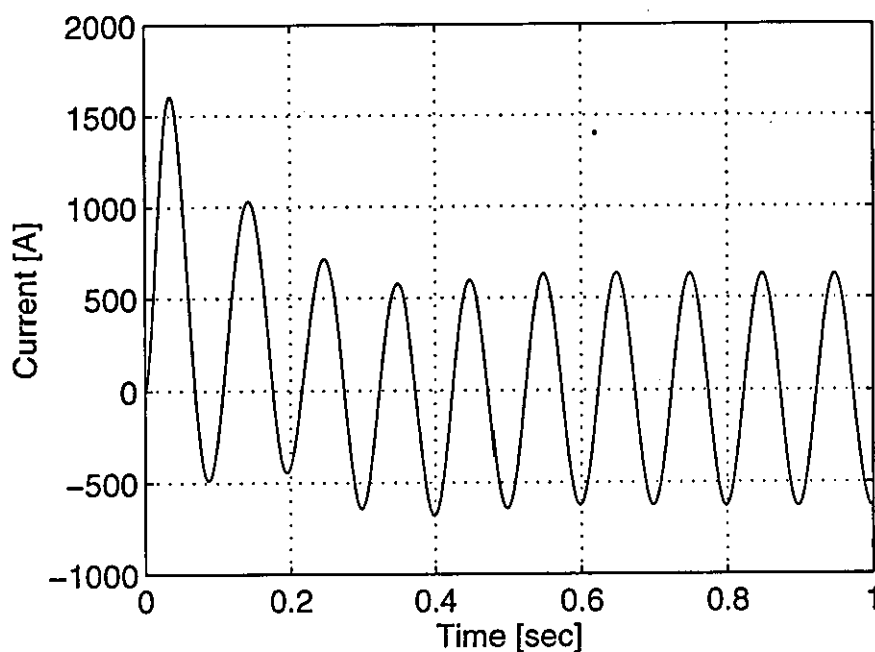


Figure 3-6 Computed results - Stator phase current characteristic for start-up of a Linear Induction Motor - Sine wave input

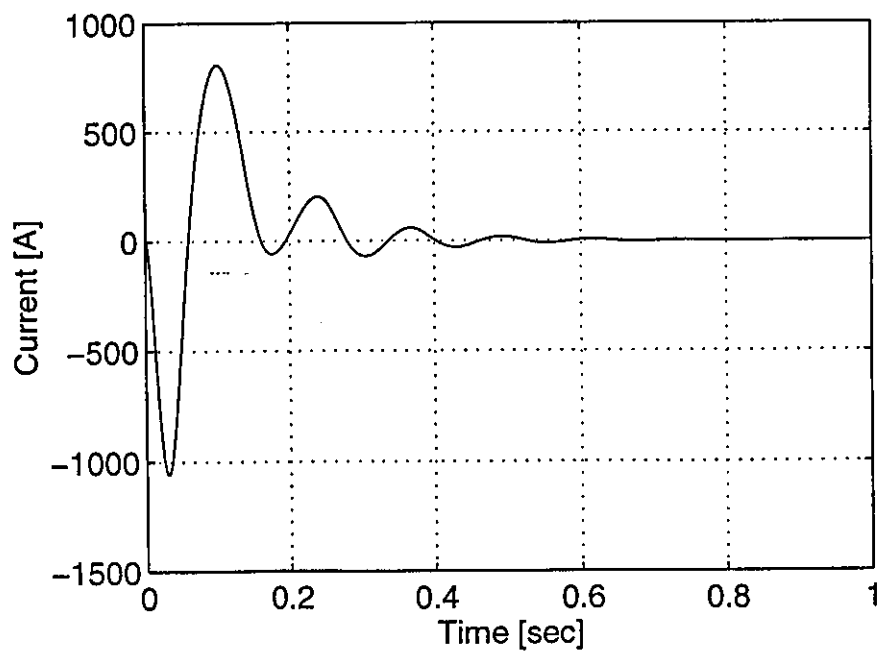


Figure 3-7 Computed results - Rotor phase current characteristic for start-up of a Linear Induction Motor - Sine wave input

**CHAPTER
FOUR**

THE INVERTER

Inverters are generally of the *constant-voltage* or *constant-current* type. The former type is usually fed from a rectifier with a large parallel-connected capacitor, to ensure that the source voltage remains almost constant. The latter type has a larger series inductor in the dc link, which effectively keeps the source current constant [26]. Bulky commutating capacitors and inductors, and poorer speed regulation [27] explain why constant-current inverters are nowadays confined mostly to medium and high-power drives. The voltage-source inverter (VSI) is usually used for high-performance motor drives and this thesis concentrates on this type of inverter.

4.1 The voltage-source inverter

Inverter drives provide a major means of controlling the speed of an induction motor, with emphasis now placed on the voltage-source inverter (VSI). The basic circuit of such an inverter resembles that of a three-phase rectifier bridge, as shown in Fig.4-1. The inverter is controlled so that each semiconductor switch conducts for a fixed period of the output cycle, either 120° or 180° . This results in a quasi-squarewave line voltage which may cause a motor connected on the ac side to become unstable at speeds below around 5Hz due to harmonic torques produced within the motor.

When inverters were first developed they used conventional thyristors, since these were the only devices available. These inverters required complex and extensive commutation networks involving both capacitors and inductors, to reduce the anode current to zero and to apply a reverse voltage for sufficient time to enable the thyristor to regain its blocking state.

With the introduction of the gate turn-off thyristor, device turn-off can be controlled by the gate, and although this eliminates the need for commutation networks it is at the expense of more complex gate circuits.

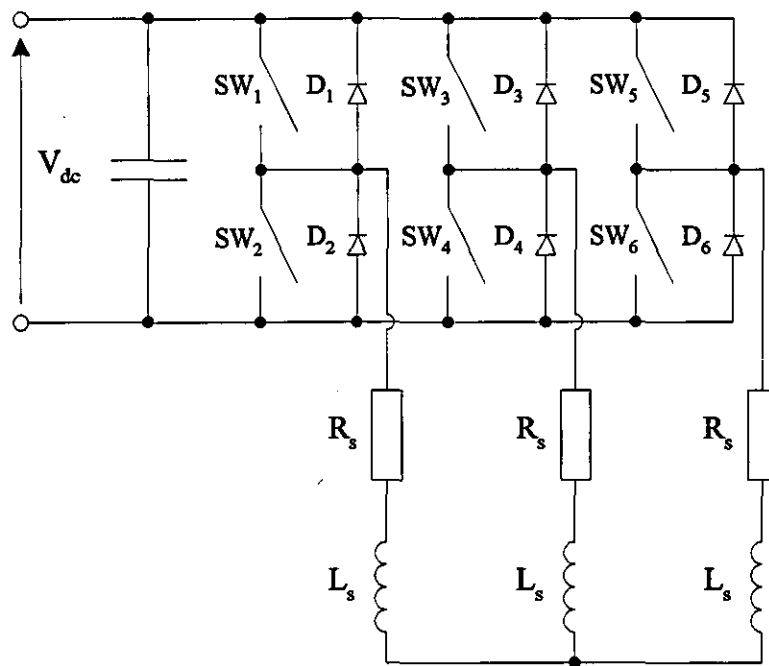


Figure 4-1 *Voltage-source inverter*

The transistor family of devices is now the most commonly used switching device in low and medium power inverter circuits. These may be bipolar transistors, which offer faster switching times than thyristors, power MOSFETs which are extremely fast devices or IGBTs which have a switching time between that of the bipolar transistor and the MOSFET. Since the commutation times of all these devices are very small in comparison with the inverter output frequency, their switching action may be regarded as instantaneous.

4.2 Pulse-width-modulated switching schemes

With the development of fast switching devices, the pulse-width-modulated (PWM) inverter became an improved alternative to the traditional quasi-squarewave inverter. This thesis concentrates on sinusoidal and current-regulated PWM switching schemes, since these are best suited for the proposed control schemes for the inverter-induction motor drive.

4.2.1 Sinusoidal pulse-width modulation

The inverter to be modelled is supplied by a constant dc voltage-source, as shown in Fig.4-1, with the amplitude and frequency of the output waveform determined by the way in which the inverter switches are modulated. Although various switching schemes exist, sinusoidal PWM is often implemented when it is necessary to shape the output voltages to be as near to sinusoidal as possible.

In sinusoidal PWM, three reference sinewaves modulate a high-frequency triangular wave to generate the signals that drive the inverter switches. The frequency of the triangular waveform determines the switching frequency of the inverter, while the frequency of the sinusoidal control voltage is chosen to correspond to the required supply frequency for the motor. Controlling the modulation ratio allows the magnitude of the output voltage to be controlled.

When power MOSFETs are used, switching frequencies up to 50kHz can easily be realised. Increasing the switching frequency reduces low-order harmonics, but this is at the expense of increased switching losses. High-order current harmonics are naturally attenuated with an inductive load such as an induction motor, which results in the motor current being almost sinusoidal without the need for a filter.

Figure 4-2 shows a sinewave of frequency f_m , compared with a triangular waveform of frequency f_s . The modulation ratio is the ratio of the amplitude of the sinewave to that of the modulating waveform, and switches SW_1 to SW_6 of Fig.4-1 are controlled by comparing the amplitude of the reference sinewaves with that of the modulating waveform. The algorithm used for the inverter leg of SW_1/SW_2 is

- If ($v_{controla} > v_{triangular}$) then turn-off SW_2 and turn-on SW_1 ,
- If ($v_{controla} < v_{triangular}$) then turn-off SW_1 and turn-on SW_2 .

The same criteria also apply to both of the other inverter legs. To prevent short-circuiting of the supply, which would damage the switches, no two switches in the same leg can conduct simultaneously. Time must be allowed for each device to turn-off before turning-on the complementary device in the same leg, and this is ensured by incorporating a delay in switching between the two devices.

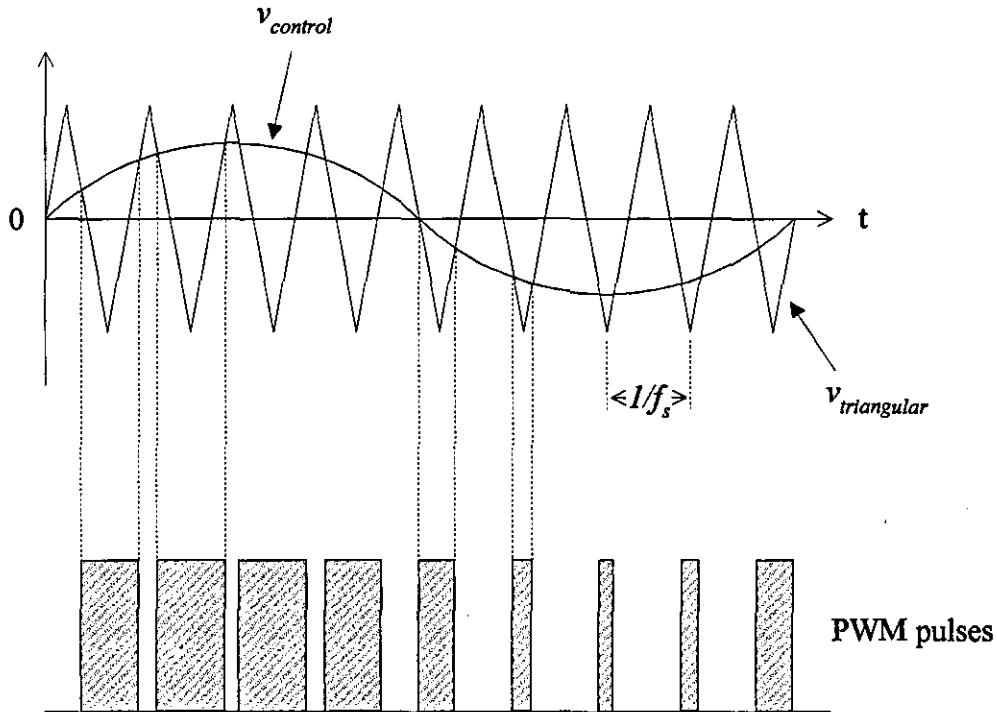


Figure 4-2 Sinusoidal PWM switching pattern

With this type of control, one device in each leg is conducting at all times, connecting the corresponding motor line to either the positive or negative voltage rail. To generate a balanced three-phase output voltage, the same triangular waveform is compared with three sinusoidal control voltages mutually displaced by 120° .

4.2.2 Current-regulated pulse-width modulation

A current-controlled voltage-source inverter provides a rapid control of the inverter output line currents by including a current feedback loop for each phase. With a current loop controller, the torque and speed of the induction machine can be controlled by changing the amplitude and the frequency of the stator current.

The tolerance band method of current control is used to obtain the gating signals needed to drive the inverter switches, and therefore to achieve current control. This method is commonly referred to as hysteresis control and is chosen in preference to other forms of current control because of its inherent simplicity. It compares the actual stator phase currents with a demanded current, and if the magnitude of the error

exceeds a preset level, the appropriate switching signals are generated to either increase or reduce the current.

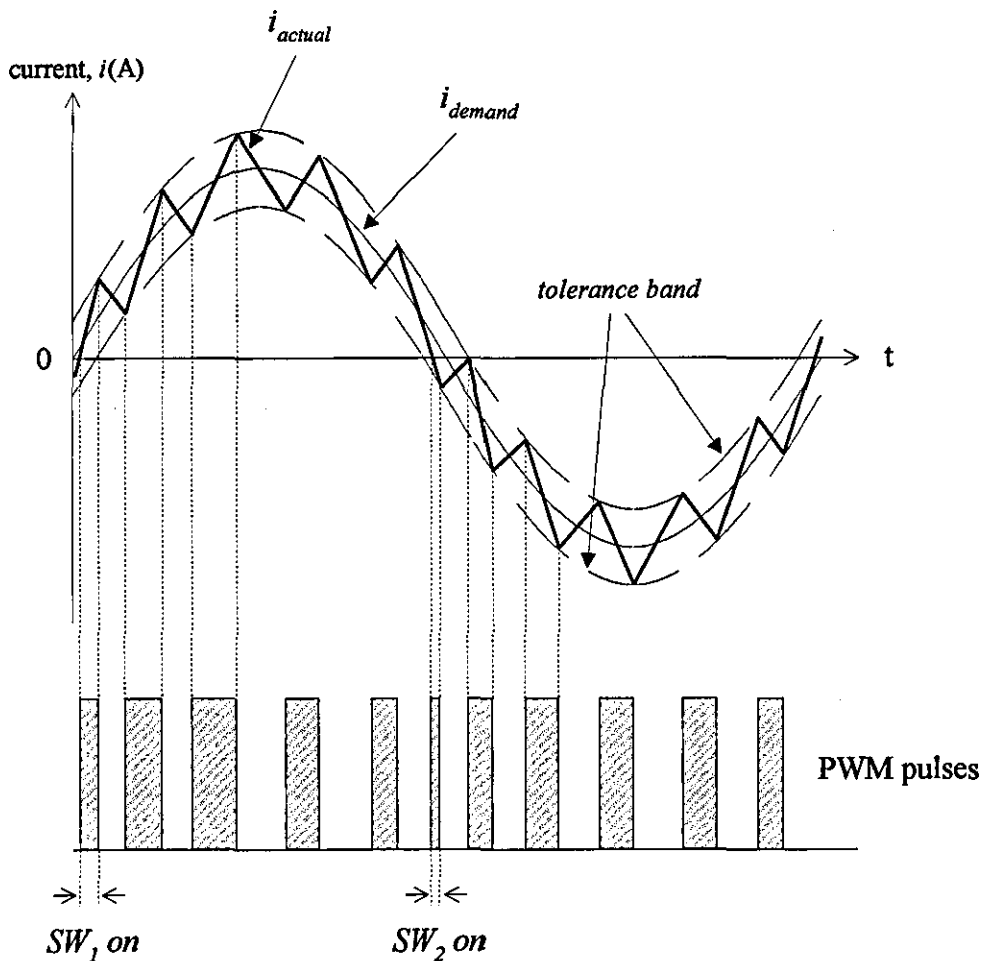


Figure 4-3 Switching waveform for tolerance band control

For example, if SW_1 is on, and the current increases beyond the upper tolerance band, the same switch is turned-off to decrease the current. If the actual current tries to fall below the lower tolerance band, then SW_1 is turned-on to increase the current, as shown in Fig. 4-3. For a hysteresis bandwidth of h , the algorithm used for the inverter leg of SW_1/SW_2 is

- If $(i_s^* > 0)$ AND $(i_s > (i_s^* + h/2))$ then turn-off SW_1 ,
- If $(i_s^* > 0)$ AND $(i_s < (i_s^* - h/2))$ then turn-on SW_1 ,
- If $(i_s^* < 0)$ AND $(i_s > (i_s^* + h/2))$ then turn-on SW_2 ,
- If $(i_s^* < 0)$ AND $(i_s < (i_s^* - h/2))$ then turn-off SW_2 ,

Clearly, the switch to be turned-on or off is dependant on both the sign of the error and the demanded current i_s^* . A disadvantage with this method of control is that the switching frequency is not constant, and it depends on motor parameters, the speed and the dc link voltage.

Alternatively, the control current is either sampled at a fixed frequency or the control signal generated by the tolerance band comparator is compared with a triangular waveform of known frequency to ensure a constant switching frequency, but this is at the expense of a poorer transient response and current error. In the latter method, the appropriate switching signals are generated in a manner similar to the sinusoidal PWM technique, where the amplitude of the modulating waveform (in this case the error signal) is compared to a triangular carrier waveform of frequency f_{sw} as shown in Fig. 4-4.

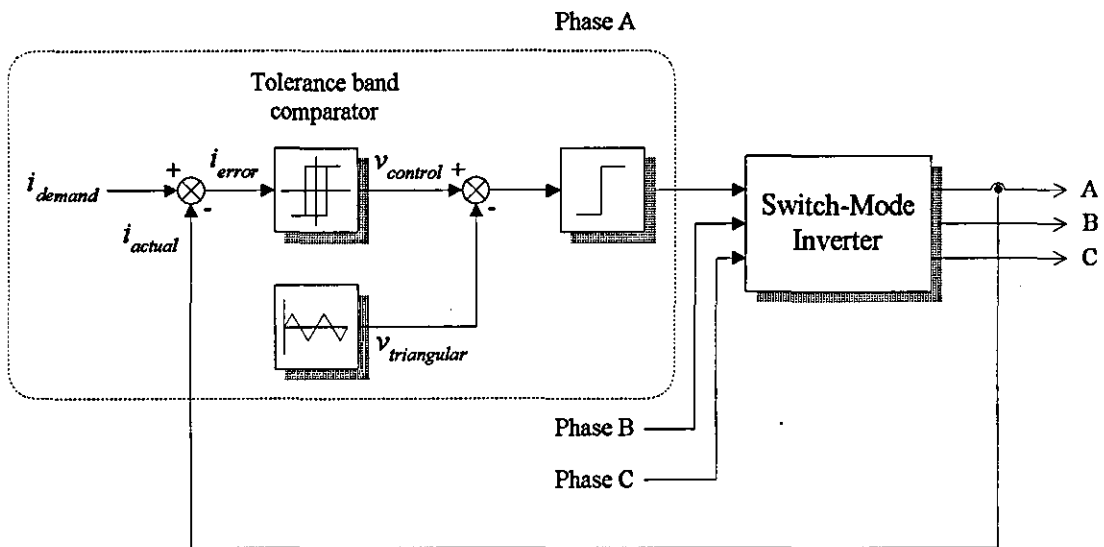


Figure 4-4 Fixed frequency tolerance band current control

4.3 An analysis of the inverter

There are several methods for analysing switching circuits which have a continuously changing circuit topology, with the common aim of each method being to provide the correct set of differential equations that describes a particular topology.

A common approach has been to assume that the motor is supplied from a precisely defined voltage waveform. While this approach is feasible for steady-state conditions, it is unsuitable for analysing transient behaviour, since the motor operating conditions and the supply impedance both influence the inverter output waveform. To overcome these problems, a tensor technique based on the work of Kron [28] is employed in this thesis, because it deals efficiently with the varying circuit topology of the inverter and also

- The approach is valid for any bridge topology.
- The analysis can be easily extended to include the motor circuit i.e. additional terms are accommodated in enlarged system tensors.
- The analysis can be applied to various motor operating conditions by a simple modification to the transformation tensors, with the remaining analysis remaining unchanged.
- The addition of external components such as filtering capacitors can be easily catered for.

It allows for the switching action of the diode and semiconductor switches by producing automatically the correct transformation tensor required to set-up the system differential equations that describe a particular topology. Consequently, the system equations can be solved simultaneously, and the tensor technique is therefore chosen for the analysis of the complete inverter-motor system as described in Chapter 5.

In addition, since the inverter circuit contains both capacitive and inductive elements, it is most convenient to use a step-by-step numerical integration of the system differential equations in the form

$$\frac{dx}{dt} = f(x,t)$$

for both the steady-state and transient behaviour.

4.3.1 Tensor technique

To simplify the analysis, the following assumptions are made

1. The inverter supply is initially represented by an adjustable direct voltage V_{dc} with the supply impedance incorporated in the impedance of the filter inductance in the dc link, and represented by $R_f + j\omega L_f$
2. Each switch/diode in the bridge is treated as a branch since they never conduct simultaneously.
3. The switches and diodes are regarded as instantaneous switching devices, since at normal operating frequencies their commutation times are very short in comparison with the inverter output frequency.
4. The inverter is assumed to supply a star-connected inductive load. The complete inverter-motor system can be easily modelled at a later stage by the simple addition of the rotor circuit.

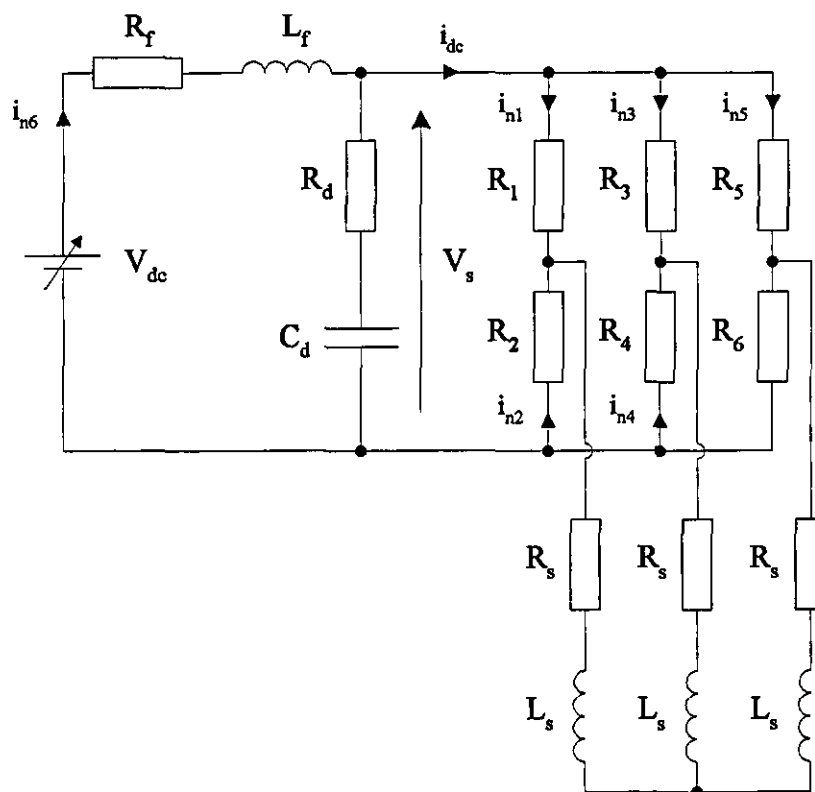


Figure 4-5 Basic network of the inverter system

The primitive network is defined by the following equation,

$$[V_B] = [R_p][i_p] + [L_p] \frac{d}{dt} [i_p] + [SQ_p] - [V_p] \quad (4-1)$$

where, the tensors for the primitive resistance $[R_p]$, the primitive inductance $[L_p]$ and the primitive capacitor voltage $[SQ_p]$ are given by

$$[R_p] = \text{diag}[R_1 \ R_2 \ R_3 \ R_4 \ R_5 \ R_6 \ R_s \ R_s \ R_s \ R_d \ R_f]$$

$$[L_p] = \text{diag}[0 \ 0 \ 0 \ 0 \ 0 \ 0 \ L_s \ L_s \ L_s \ 0 \ L_f]$$

$$[SQ_p] = [0 \ 0 \ 0 \ 0 \ 0 \ 0 \ 0 \ 0 \ 0 \ 0 \ Q/C_d \ 0]^T$$

The tensors for the primitive current $[i_p]$, the primitive voltage-source $[V_p]$ and the branch voltage $[V_B]$ are given by

$$[i_p] = [i_1 \ i_2 \ i_3 \ i_4 \ i_5 \ \dots \ i_{11}]^T$$

$$[V_p] = [0 \ 0 \ 0 \ 0 \ 0 \ 0 \ 0 \ 0 \ 0 \ 0 \ 0 \ V_{dc}]^T$$

$$[V_B] = [V_1 \ V_2 \ V_3 \ V_4 \ V_5 \ \dots \ V_{11}]^T$$

A capacitor voltage tensor is used to describe the capacitor, to reduce the number of equations to be solved in the final system. The charge stored in the capacitor is given by

$$Q = \int i_{10} dt$$

4.3.1.2 Basic network

Having determined the primitive voltage equations, the equations for the independent system may be established using tensor relationships i.e. with the six independent currents defined as shown in Fig.4-5, the relationship between the primitive and independent current tensor is given by the transformation matrix,

The relationship between the old and new set of independent currents $[i_{nn}]$ is

$$\begin{bmatrix} i_{n1} \\ i_{n2} \\ i_{n3} \\ i_{n4} \\ i_{n5} \\ i_{n6} \end{bmatrix} = \begin{bmatrix} S_1 & & & & & \\ S_2 & & & & & \\ & S_3 & & & & \\ & S_4 & & & & \\ -S_5 & -S_5 & & & & \\ & & & & & 1 \end{bmatrix} \begin{bmatrix} i_{nn1} \\ i_{nn2} \\ i_{nn3} \end{bmatrix}$$

and denoted in standard matrix form as

$$[i_n] = [C_n][i_{nn}] \quad (4-3)$$

where S_x refers to the conduction state of the inverter switch/diode x - a value of '1' indicates that device is conducting, and '0' non-conducting.

The tensor $[C_n]$ refers to a given conduction pattern in the inverter, and has to be re-generated each time the conduction state of any of the devices changes. As an example, consider the transformation when switches 1, 3 and 6 are in the on-state. The reduced network is shown in Fig.4-7, where the transformation is now given by

$$[i_n] = \begin{bmatrix} 1 & & & & \\ 0 & & & & \\ & 0 & & & \\ & 1 & & & \\ -1 & -1 & & & \\ & & & & 1 \end{bmatrix} \begin{bmatrix} i_{nn1} \\ i_{nn2} \\ i_{nn3} \end{bmatrix}$$

The new equation describing the reduced network is

$$[V_{nn}] = [R_{nn}][i_{nn}] + [L_{nn}] \frac{d}{dt} [i_{nn}] + [SQ_{nn}] \quad (4-4)$$

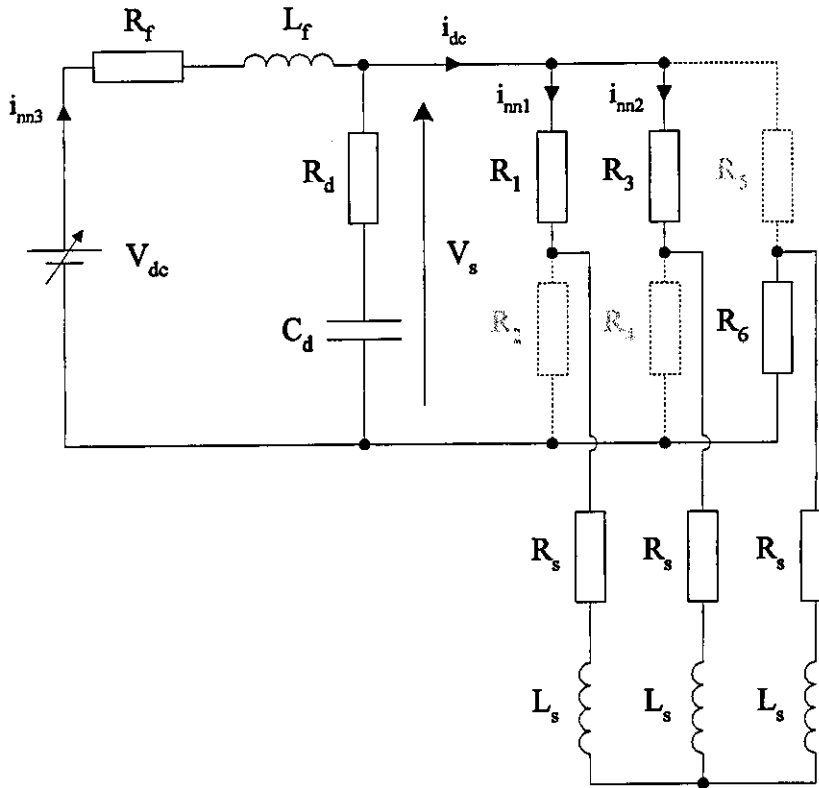


Figure 4-7 Reduced network for the above example

Based on power invariance considerations, the following transformations are used to evaluate the new circuit tensors $[R_{mn}]$, $[L_{mn}]$, $[SQ_{mn}]$ and $[V_{mn}]$.

$$[R_{mn}] = [C_n]^T [R_n] [C_n]$$

$$[L_{mn}] = [C_n]^T [L_n] [C_n]$$

$$[SQ_{mn}] = [C_n]^T [SQ_n]$$

$$[V_{mn}] = [C_n]^T [V_n]$$

4.3.2 Numerical solution of the inverter equations

Equation (4-4) may be arranged in an alternative form which is suitable for numerical integration as

$$\frac{d}{dt} [i_{nn}] = [L_{nn}]^{-1} \{ [V_{nn}] - [R_{nn}] [i_{nn}] - [SQ_{nn}] \} \quad (4-5)$$

Using this equation, new values for the reduced set of independent currents may be determined, and using the relationships defined in Equations (4-2) and (4-3), the new values for the basic and primitive current tensors can also be evaluated. In the same manner, the basic and primitive current derivative tensors are calculated and the new branch voltage tensor $[V_B]$ then obtained from

$$[V_B] = [R_p] [i_p] + [L_p] \frac{d}{dt} [i_p] + [SQ_p] - [V_p] \quad (4-6)$$

The inverter phase voltages are given by branches 7, 8, and 9, respectively. Likewise the dc link voltage V_s is the voltage across branch number 10. The inverter supply current i_{dc} is evaluated from the primitive current tensor by adding the currents, i_1 , i_3 , and i_5 .

4.4 Simulated and experimental results

A program was written in *FORTRAN77* using the method presented in this chapter to analyse an inverter. The inverter parameters and a brief flow chart are given in Appendices C and E, respectively. The program employs a fourth-order Runge-Kutta numerical integration routine with an integration step length of $10\mu s$ to ensure integration stability and provide results with a good accuracy.

4.4.1 Quasi-squarewave inverter

To validate the program, experimental results were obtained from [1] for an inductively-loaded inverter with quasi-square wave switching and compared with computed results. The system parameters are

- supply voltage $V_{dc} = 50V$,
- $R_s = 10\Omega$ and $L_s = 0.022H$,
- output frequency = 50Hz.

Steady-state experimental waveforms for the output phase voltage, phase current and inverter supply current are given in Figs 4-8 to 4-10. Since the load is inductive, the current in each phase lags its voltage as shown in Fig.4-9, and contains exponential transient components. The frequency of the supply current ripple is six times the output frequency. Good agreement clearly exists between the experimental and theoretical results, suggesting that the inverter is being accurately modelled.

4.4.2 Sinusoidal pulse-width-modulated inverter

Using the same system parameters, but with PWM switching, computed results for the output phase voltage and current, and the supply current are given in Figs 4-14 to 4-16. The modulation ratio is 1, and the switching frequency is 1kHz. With this form of control, one or other of the devices in each leg of the inverter is conducting at all times, connecting the load to either the positive or negative side of the supply.

The phase voltage (measured with respect to the star point of the load) shown in Fig.4-14 is a PWM wave, whereas the phase current is close to sinusoidal. The peak amplitude of the waveform is equal to two-thirds the inverter dc link voltage V_s , and since the load is inductive, the inverter output line current lags its voltage.

Phase Voltage (V)

Scale : 25V/div
time 10ms/div

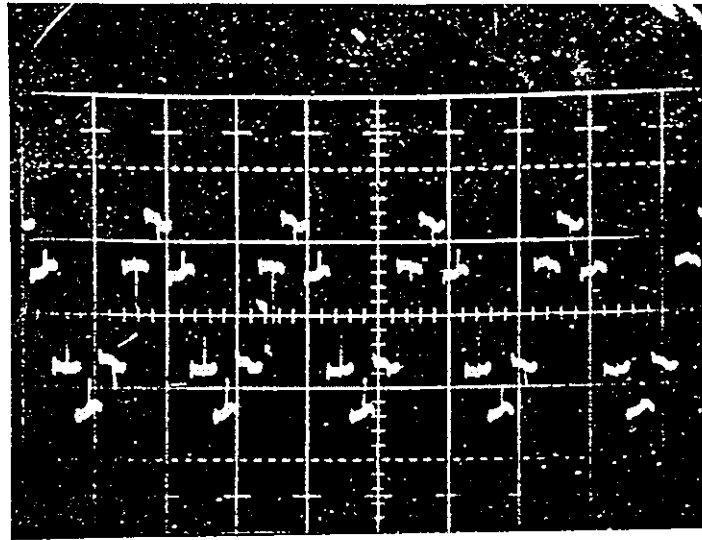


Figure 4-8 Experimental results - Phase voltage characteristic for an inductively loaded 180° Inverter

Phase Current (A)

Scale : 1A/div
time 10ms/div

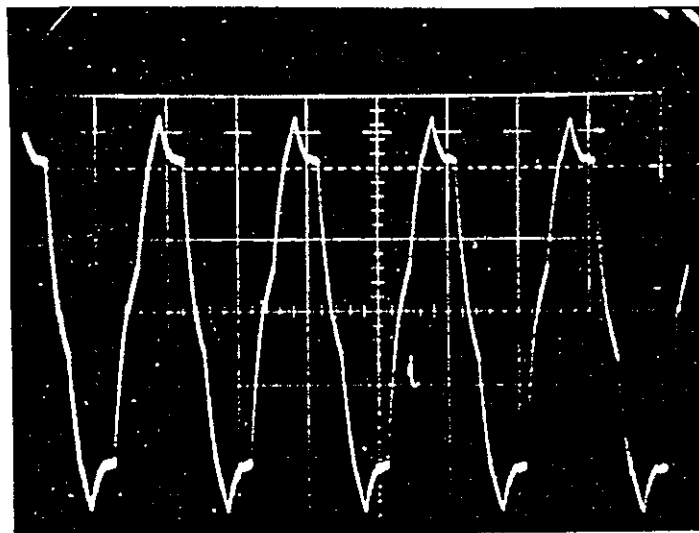


Figure 4-9 Experimental results - Phase current characteristic for an inductively loaded 180° Inverter

Current (A)
 Scale : 1A/div
 time 10ms/div

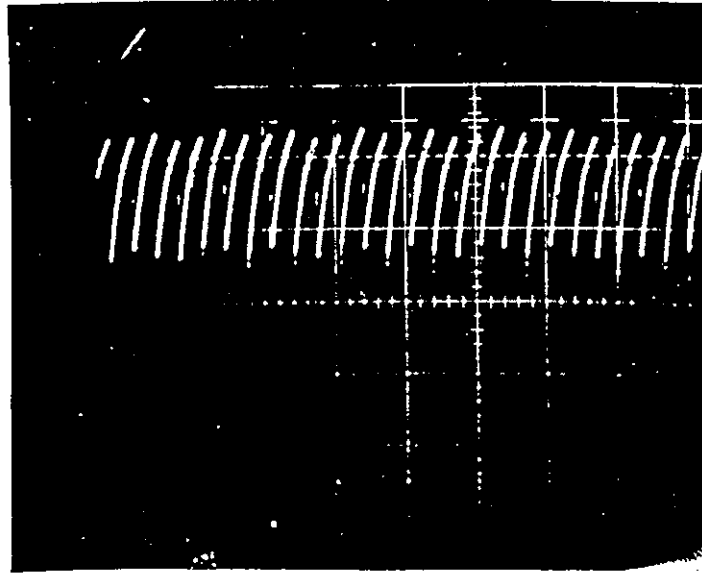


Figure 4-10 Experimental results - Inverter current characteristic for an inductively loaded 180° Inverter

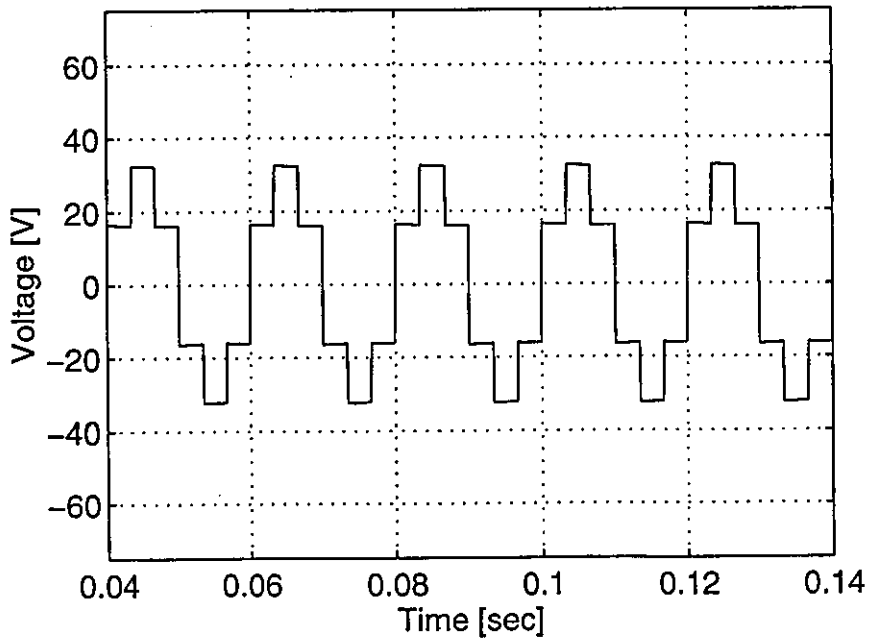


Figure 4-11 Computed results - Phase voltage characteristic for an inductively loaded 180° Inverter

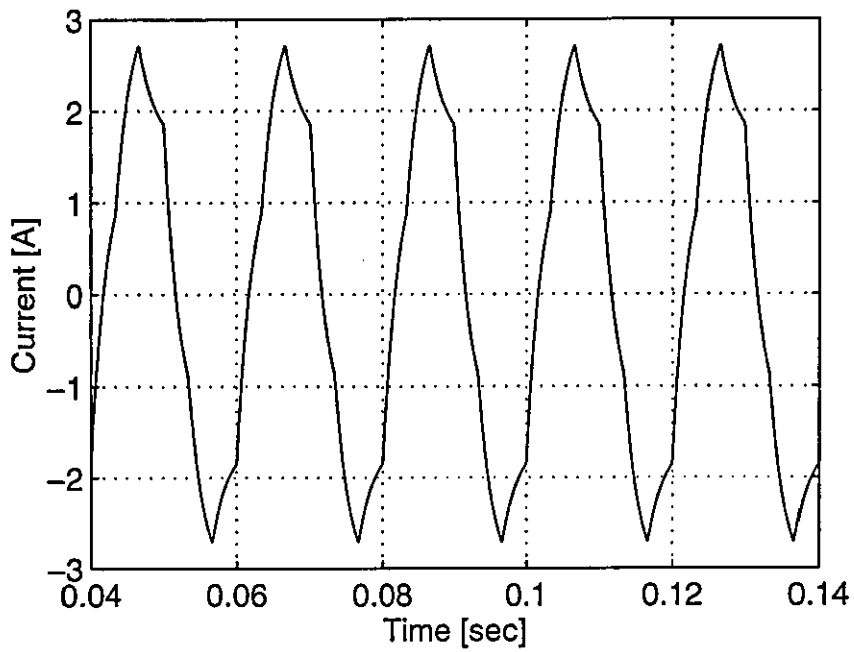


Figure 4-12 Computed results - Phase current characteristic for an inductively loaded 180° Inverter

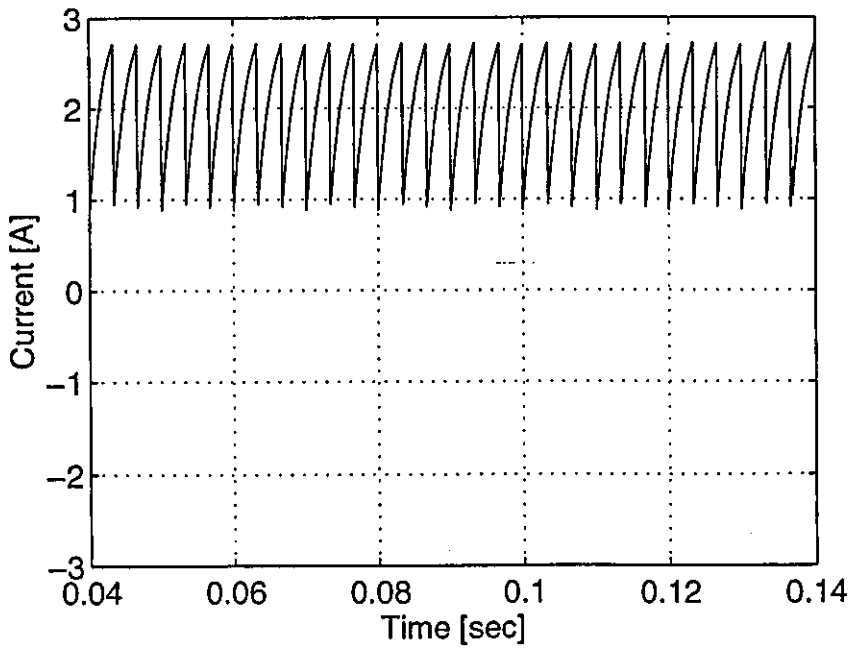


Figure 4-13 Computed results - Inverter current characteristic for an inductively loaded 180° Inverter

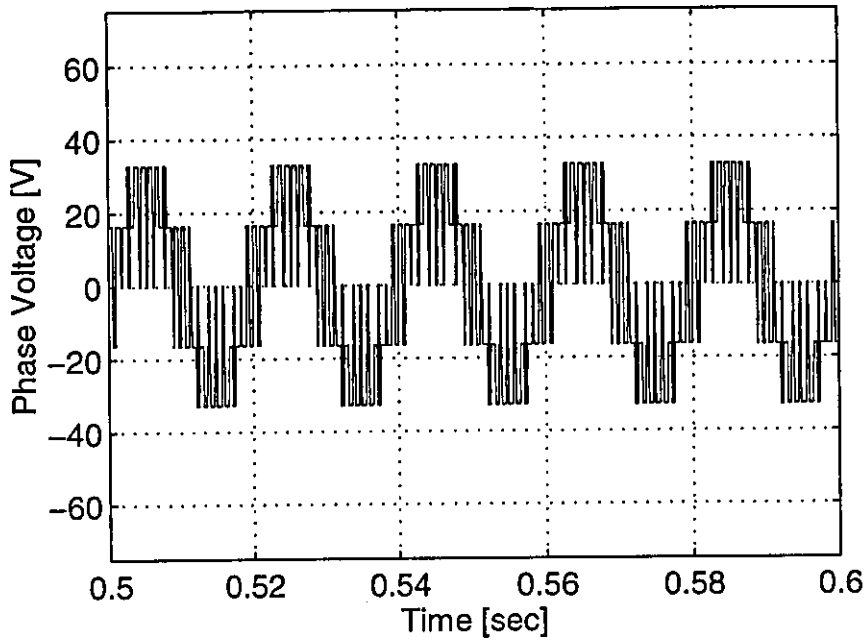


Figure 4-14 Computed results - Phase voltage characteristic for an inductively loaded PWM Inverter

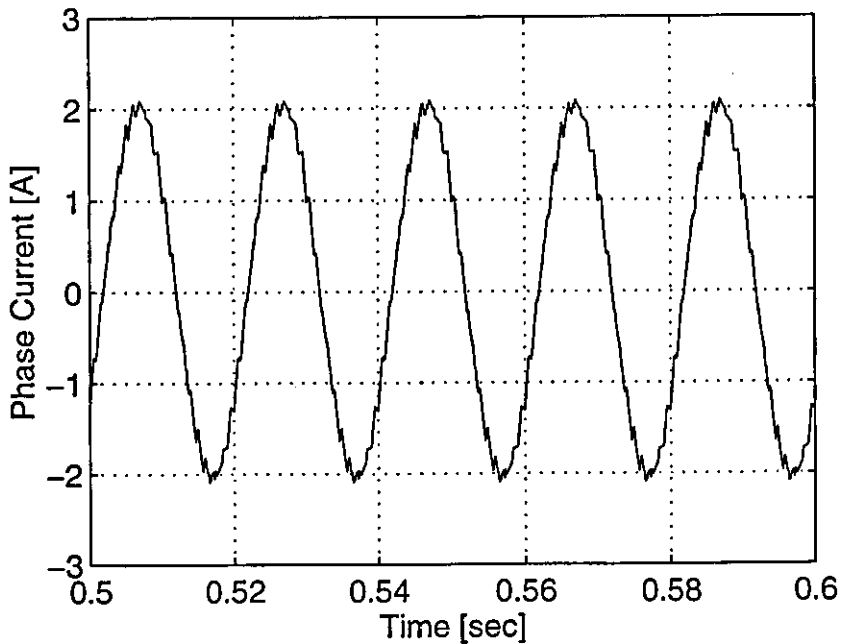


Figure 4-15 Computed results - Phase current characteristic for an inductively loaded PWM Inverter

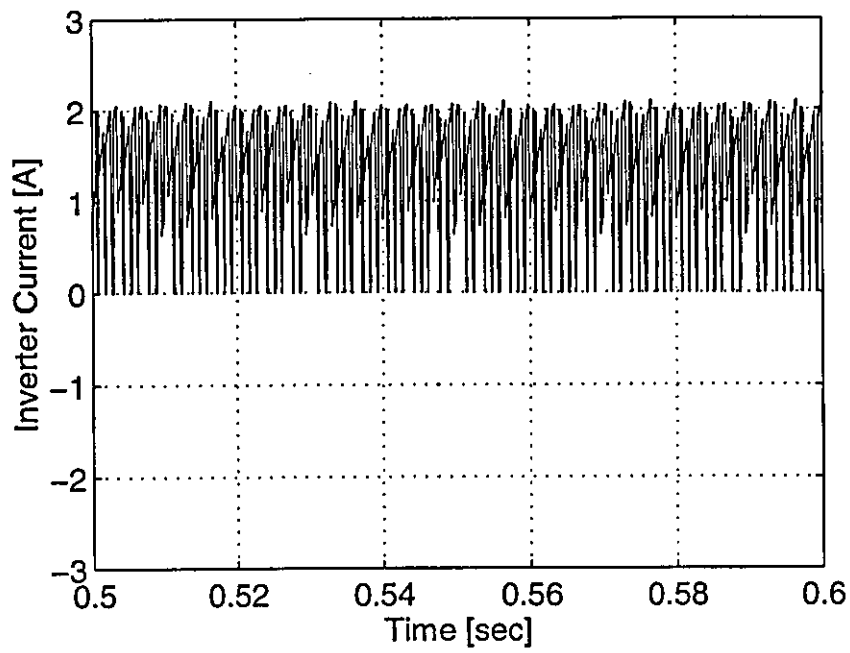


Figure 4-16 Computed results - Inverter current characteristic for an inductively loaded PWM Inverter

THE INVERTER-FED INDUCTION MOTOR

With a voltage-source inverter (VSI) drive, the voltage applied to the motor terminals is controlled, and the current is determined by the motor operating conditions. The characteristics of a PWM inverter were discussed in the previous chapter and clearly, an inverter with this type of switching scheme offers several advantages over other switching schemes.

- The phase currents are nearly sinusoidal because of the inductance which has a smoothing effect,
- A diode rectifier can be used to supply the inverter since it operates with a constant dc link voltage.
- Finally, the choice of switching frequency is a compromise between the purity of the sinusoidal output waveform, and the switching losses - generally, the higher the switching frequency, the more sinusoidal the output waveform.

The proposed method of vector control requires instantaneous control of the phase currents, which can be achieved by a current-regulated voltage-source inverter (CR-VSI). Since, a model for the VSI has been developed, it is now necessary to implement the current-regulated modulation strategy.

5.1 Mathematical model of the inverter-motor system

To model the inverter-fed induction motor, the direct-phase model of the induction motor (developed in Chapters 2 and 3) is combined with the inverter model developed in the previous Chapter.

With the independent equations of the basic network being derived from the various primitive system tensors, all that is required is the addition of the rotor circuit and dynamic equation of the motor to develop the complete system, as shown in Fig.5-1.

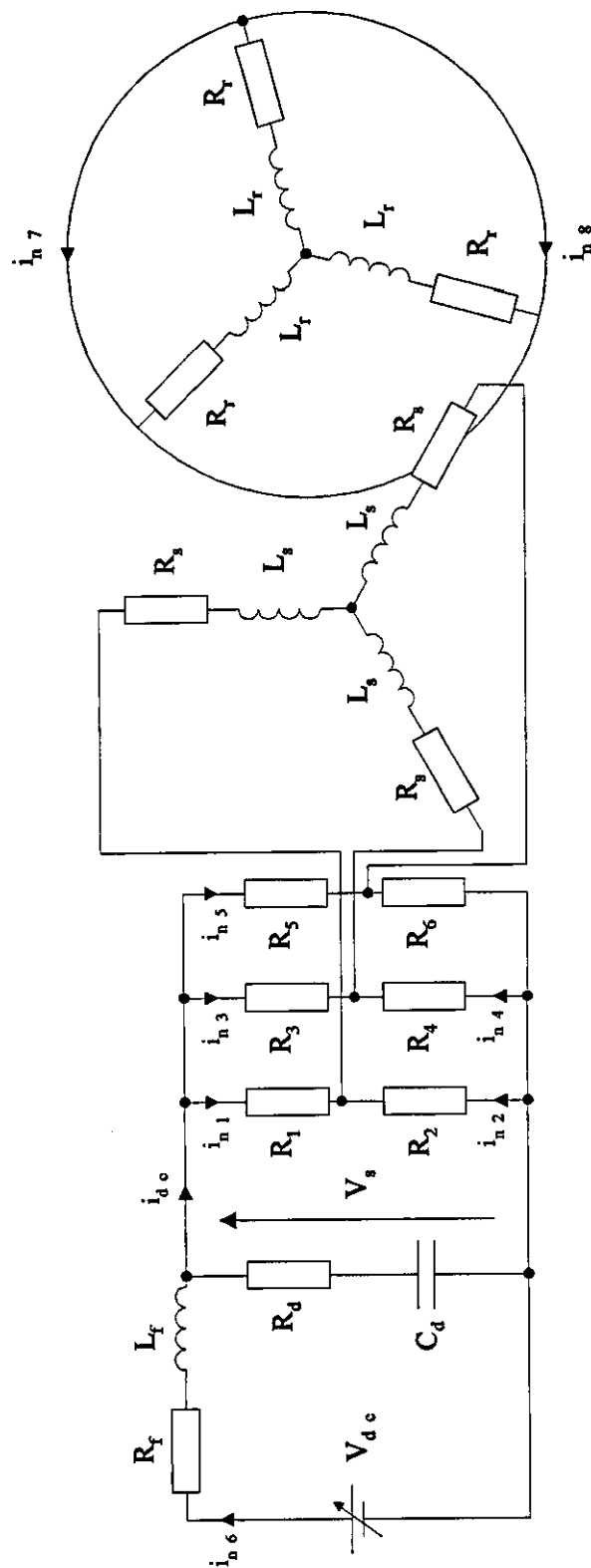


Figure 5-1 Basic network for the inverter-fed motor drive

- Primitive resistance tensor, R_p

Three additional resistance terms for the rotor circuit are included in the diagonal of the primitive resistance tensor, $[R_p]$.

$$[R_p] = \text{diag}[R_1 \ R_2 \ R_3 \ R_4 \ R_5 \ R_6 \ R_s \ R_s \ R_s \ R_d \ R_f \ R_r \ R_r \ R_r]$$

- Primitive tensors SQ_p , i_p , V_p , and V_B

Each of these tensors are increased in size by an additional three rows to accommodate the new elements i.e.

$$[SQ_p] = [0 \ 0 \ 0 \ 0 \ 0 \ 0 \ 0 \ 0 \ 0 \ Q/C_d \ 0 \ 0 \ 0 \ 0 \ 0]^T$$

$$[i_p] = [i_1 \ i_2 \ i_3 \ i_4 \ i_5 \ \dots \ i_{14}]^T$$

$$[V_p] = [0 \ 0 \ 0 \ 0 \ 0 \ 0 \ 0 \ 0 \ 0 \ 0 \ 0 \ V_{dc} \ 0 \ 0 \ 0]^T$$

$$[V_B] = [V_1 \ V_2 \ V_3 \ V_4 \ V_5 \ \dots \ V_{14}]^T$$

- Primitive inductance tensor, L_p

The primitive inductance tensor is no longer diagonal because of the mutual coupling present between the phases. It now takes the form

$$[L_p] = \begin{bmatrix} 0 & 0 & 0 & 0 & 0 & 0 & 0 & 0 & 0 & 0 & 0 & 0 & 0 & 0 \\ 0 & 0 & 0 & 0 & 0 & 0 & 0 & 0 & 0 & 0 & 0 & 0 & 0 & 0 \\ 0 & 0 & 0 & 0 & 0 & 0 & 0 & 0 & 0 & 0 & 0 & 0 & 0 & 0 \\ 0 & 0 & 0 & 0 & 0 & 0 & 0 & 0 & 0 & 0 & 0 & 0 & 0 & 0 \\ 0 & 0 & 0 & 0 & 0 & 0 & 0 & 0 & 0 & 0 & 0 & 0 & 0 & 0 \\ 0 & 0 & 0 & 0 & 0 & 0 & 0 & 0 & 0 & 0 & 0 & 0 & 0 & 0 \\ 0 & 0 & 0 & 0 & 0 & 0 & L_s & M_{12} & M_{13} & 0 & 0 & M_{14} & M_{15} & M_{16} \\ 0 & 0 & 0 & 0 & 0 & 0 & M_{21} & L_s & M_{23} & 0 & 0 & M_{24} & M_{25} & M_{26} \\ 0 & 0 & 0 & 0 & 0 & 0 & M_{31} & M_{32} & L_s & 0 & 0 & M_{34} & M_{35} & M_{36} \\ 0 & 0 & 0 & 0 & 0 & 0 & 0 & 0 & 0 & 0 & 0 & 0 & 0 & 0 \\ 0 & 0 & 0 & 0 & 0 & 0 & 0 & 0 & 0 & 0 & L_f & 0 & 0 & 0 \\ 0 & 0 & 0 & 0 & 0 & 0 & M_{41} & M_{42} & M_{43} & 0 & 0 & L_r & M_{45} & M_{46} \\ 0 & 0 & 0 & 0 & 0 & 0 & M_{51} & M_{52} & M_{53} & 0 & 0 & M_{54} & L_r & M_{56} \\ 0 & 0 & 0 & 0 & 0 & 0 & M_{61} & M_{62} & M_{63} & 0 & 0 & M_{64} & M_{65} & L_r \end{bmatrix}$$

5.2 Numerical solution of the system equations

The system is described by the equation,

$$\frac{d}{dt} [i_{nn}] = [L_{nn}]^{-1} \left\{ [V_{nn}] - [R_{nn}] [i_{nn}] - [G_{nn}] \frac{d\theta}{dt} [i_{nn}] - [SQ_{nn}] \right\} \quad (5-1)$$

together with the mechanical system equations. The primitive tensor $[G_p]$ is transformed in the same way as the inductance and resistance tensors, to give the tensor $[G_{nn}]$ describing the reduced network.

A step-by-step integration routine is used to evaluate the new values for the reduced set of independent currents, and using the relationships of Eqs (4-2) and (4-3), the primitive current tensor can be obtained and hence, the dc link voltage and current, and the phase voltages.

5.3 Non-regenerative supply

For simplicity, a constant voltage-source in series with a supply impedance is used in place of the rectifier in supplying the inverter. This assumption is only valid if power flows from the dc link to the inverter, but under certain operating conditions, an inverter-fed induction motor will re-generate and the dc current will reverse, returning energy to the dc link capacitor. A diode is placed in series with the constant voltage-source to simulate the rectifier and block energy from being fed back to the supply, as shown in Fig.5-2.

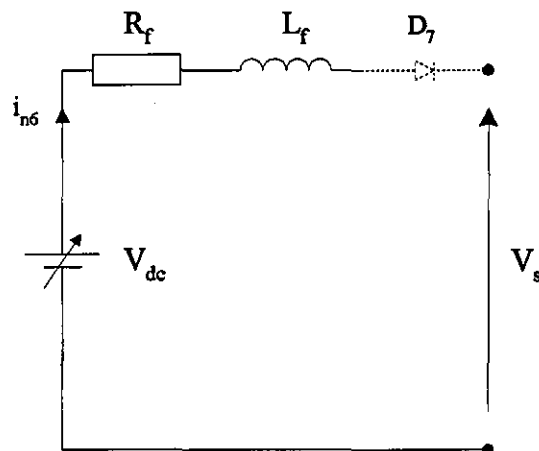


Figure 5-2 Inverter supply including rectifier diode

This strategy is implemented in the software, by treating the diode as a switch in a manner similar to the other inverter switches. The diode current is monitored at every integration step, and as soon as it drops to zero, the column in the transformation tensor $[C_n]$ corresponding to the source current i_f is removed, thereby disabling the supply. From then on, the potential difference across the diode is evaluated by subtracting the voltage across the capacitor from the supply voltage, and as this goes positive the diode becomes forward biased and the supply is switched back on. Hence, the presence or absence of the column in $[C_n]$ corresponding to the source current is dependant on the state of the diode whether conducting or non-conducting.

5.4 Simulated and experimental results

As an illustration of the validity of the inverter-induction motor model, experimental [1] and simulated results are initially obtained for a quasi-square wave inverter-fed induction motor drive with an output frequency of 25Hz. The motor and inverter parameters are given in Appendix C, and a flowchart for the program is given in Appendix E. For system stability, the integration step-length was set at $10\mu s$.

The initial conditions for the independent variables are

- all the currents are set to zero,
- the rotor speed ω_r is set to zero,
- the initial capacitor charge is set to $C_d V_{dc}$.

5.4.1 Quasi-squarewave inverter

With the inverter supplied from a 240V dc source, experimental and computed results for start-up of the induction motor under 180° inverter operation are shown in Figs 5-3 and 5-4, and Figs 5-5 to 5-8 respectively. The motor does not present a simple load to the inverter, as it reacts differently to each harmonic component in the voltage waveform. This explains the nature of the phase current waveform shown in Fig.5-3. A good agreement exists between the practical and computed results.

5.4.2 Sinusoidal pulse-width-modulated inverter

Using the same system parameters for the sinusoidal PWM inverter, with a modulation ratio of 1 and a switching frequency of 1kHz, the motor was allowed to run-up to rated speed. Computed results for the speed, torque, stator-phase current and inverter current are shown in Figs 5-9 to 5-12.

Although a higher switching frequency of the PWM results in a smoother transient torque response, the inverter switching losses are increased. At steady-state, sufficient torque is generated to overcome the frictional losses, but the harmonics generated by the inverter give rise to a pulsating torque shown in Fig.5-10. The pulsating torque at low frequency particularly can have an effect on the motor speed.

The line current shown in Fig.5-11 resembles closely the waveform obtained with a mains supplied induction motor. The initial amplitude of the stator phase current is about 8A, but this decays to about 1.5A at running speed. The rotor phase currents, on the other hand, vary in both amplitude and frequency. Due to the low slip for the no-load condition, both the amplitude and frequency of the rotor currents eventually decay to a value close to zero.

5.4.3 Linear induction motor drive under constant current excitation

To validate the program, further dynamic simulations were performed for a current-regulated PWM LIM drive whose parameters are given in Appendix C. With the inverter supplied from a 600V dc source, and a constant excitation current of 465A and input frequencies from 10Hz to 40Hz, the motor was allowed to run-up to rated speed. Practical and predicted results for the variation of the motor thrust with speed are shown in Figs 5-13 and 5-14. Transient and steady-state waveforms for velocity, thrust and phase currents for both 10Hz and 40Hz operation are given in Figs 5-15 to 5-18 and Figs 5-19 to 5-22 respectively.

In practice, the magnetic gap is not constant but varying. In effect, a tapered gap is produced which varies with load and speed, and this might account for the higher values of thrust produced under test than those obtained from the model. This increase in thrust is caused by an increase in coupling with the secondary, due to the reduced air-gap.

To illustrate the effect of changes in both the gap and rail resistance, two calculated curves for the thrust are shown in Fig.5-13. These have been calculated by Duncan [2], using the maximum range of both the average air-gap and secondary resistance.

To illustrate the longitudinal end-effect, two calculated curves for the thrust are shown in Fig.5-14. One was calculated by taking the end-effect factor into account and the other by ignoring it. In both cases, the mean gap and rail resistance is assumed. Clearly, the thrust calculations including the end-effect are closer to the test results than those obtained without the end-effect, especially at higher input frequencies. Since for low speeds the end-effect is considered negligible.

It is evident from Figs 5-15 and 5-19 that the synchronous speed of the machine is around the expected figures of 5.74ms⁻¹ and 23ms⁻¹ respectively. The high-frequency torque ripples shown in Fig 5-16 and 5-20 are caused by the motor current harmonics.

The stator phase current waveforms shown in Figs 5-17 and 5-21 resemble those of the input reference currents, with a peak amplitude of approximately 657A. This was expected, since the phase currents are forced to track the reference current to within a specified band limit. However, the phase current waveforms are not perfectly sinusoidal because of the harmonic contents in the output voltage.

The back iron of the secondary was laminated using 3mm thick steel, to avoid saturation over the range of interest and therefore, to ensure that the equivalent circuit constants obtained through static tests were not too dependant on frequency. Hence, the simple equivalent circuit provides an accurate prediction of the performance of the linear motor, and is suitable for evaluating the field-orientation control principle.

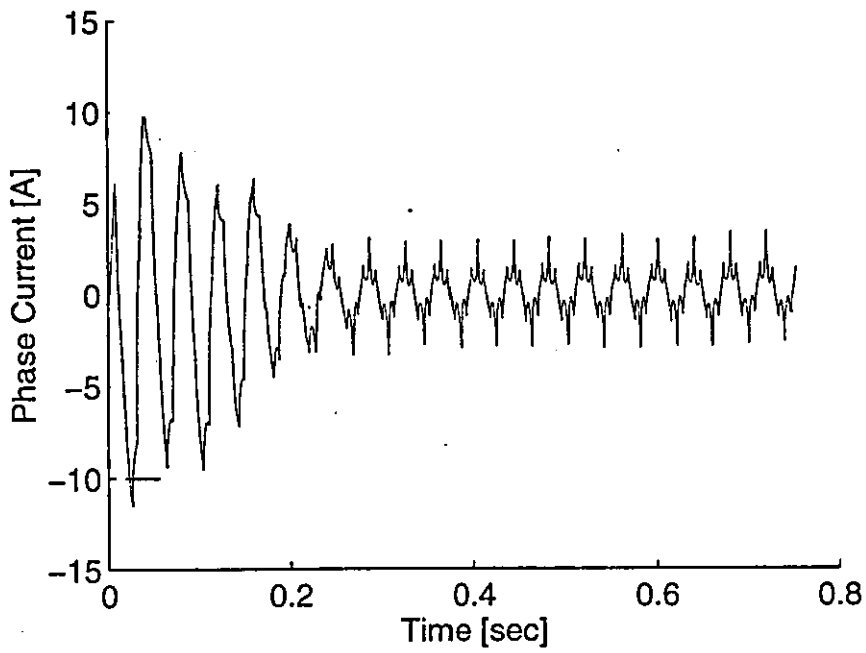


Figure 5-3 Experimental results - Phase current characteristic for start-up of a 180° Inverter-fed Induction Motor

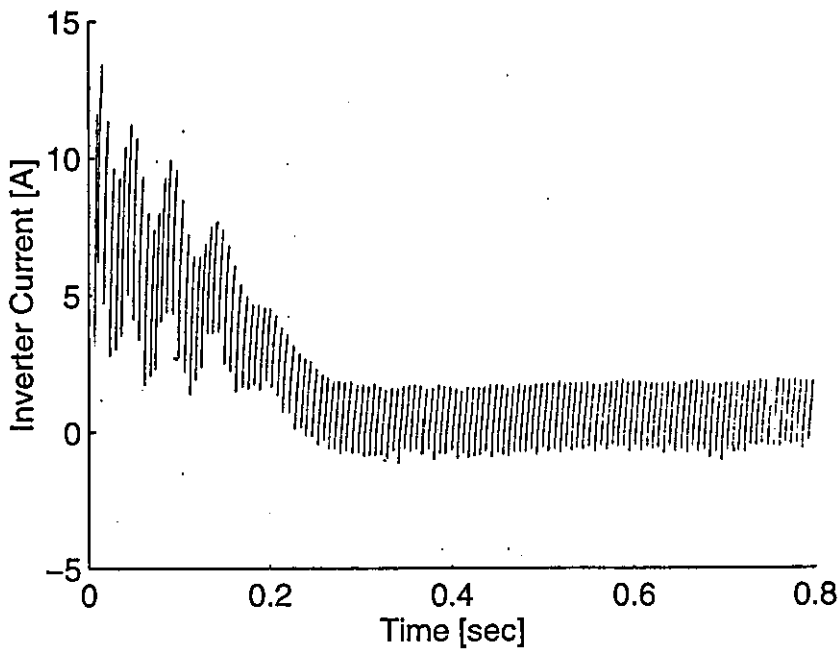


Figure 5-4 Experimental results - Inverter current characteristic for start-up of a 180° Inverter-fed Induction Motor

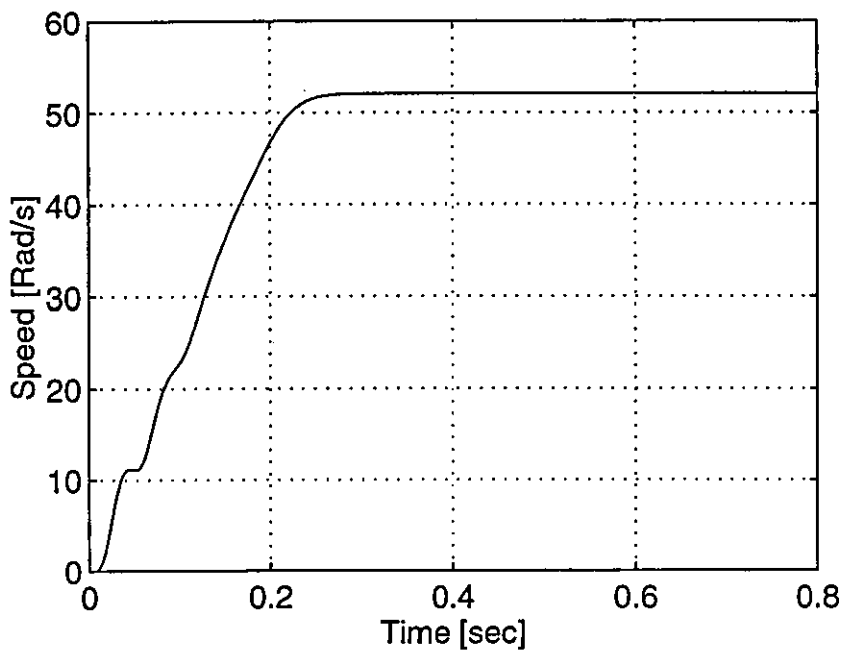


Figure 5-5 Computed results - Speed characteristic for start-up of a 180° Inverter-fed Induction Motor

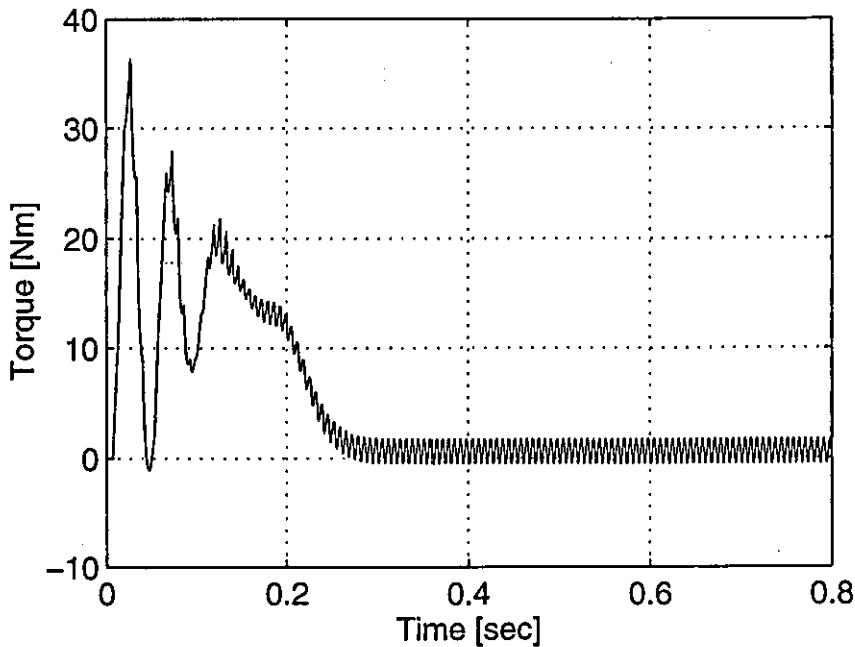


Figure 5-6 Computed results - Torque characteristic for start-up of a 180° Inverter-fed Induction Motor

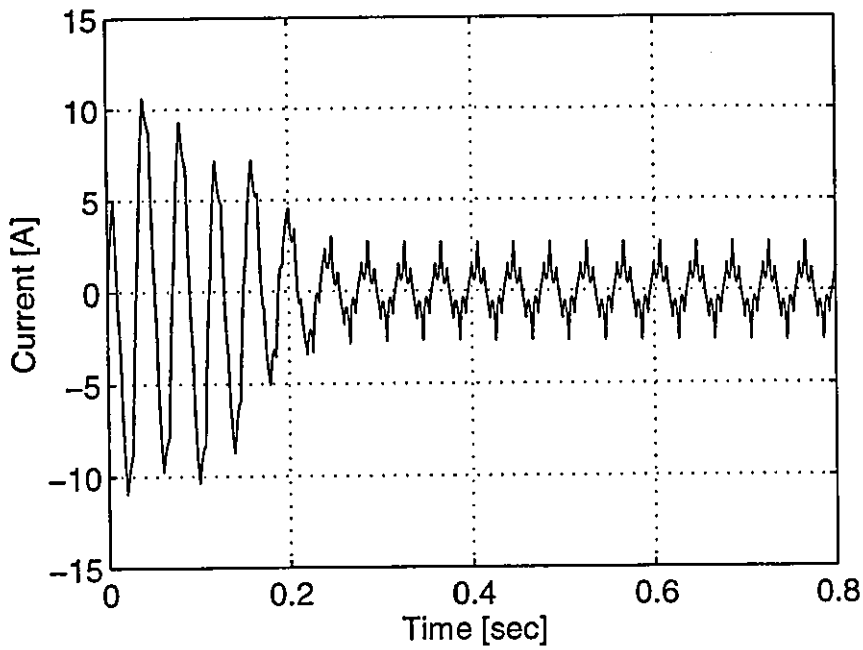


Figure 5-7 Computed results - Stator phase current characteristic for start-up of a 180° Inverter-fed Induction Motor

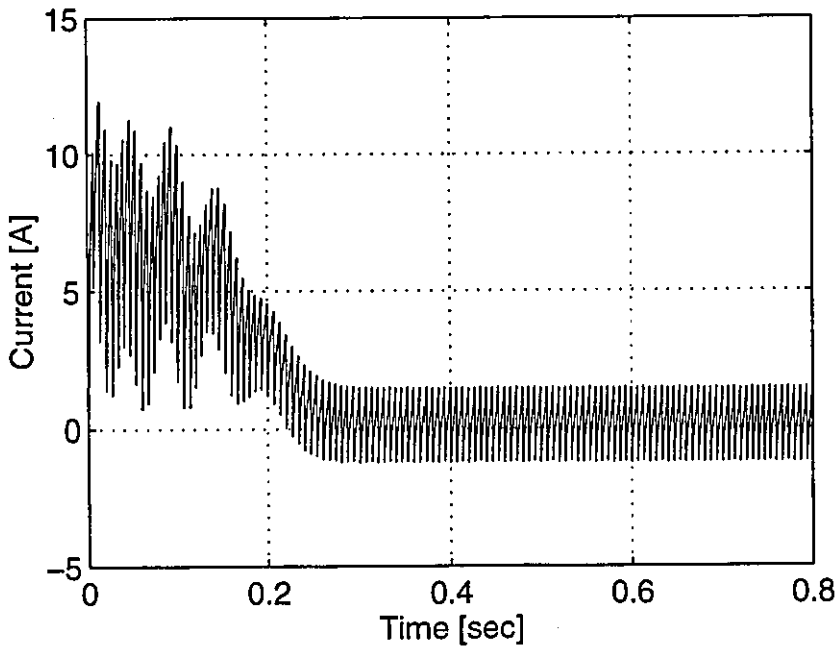


Figure 5-8 Computed results - Inverter current characteristic for start-up of a 180° Inverter-fed Induction Motor

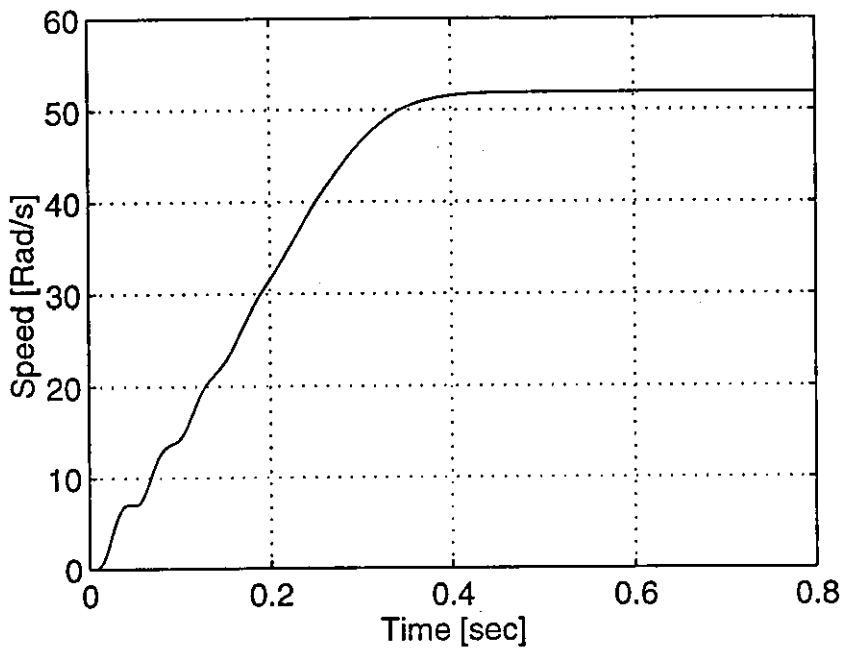


Figure 5-9 Computed results - Speed characteristic for start-up of a Sinusoidal-PWM Inverter-fed Induction Motor

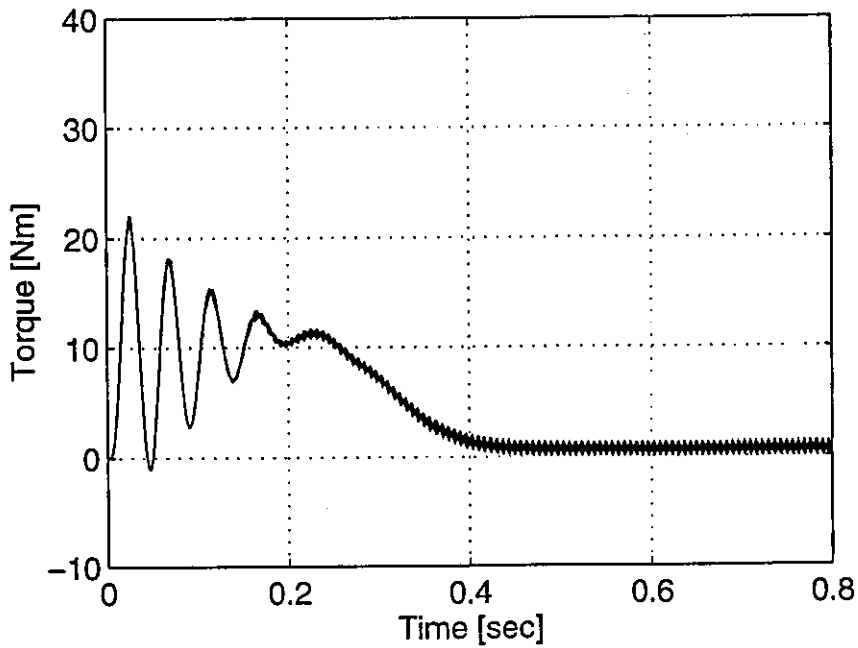


Figure 5-10 Computed results - Torque characteristic for start-up of a Sinusoidal-PWM Inverter-fed Induction Motor

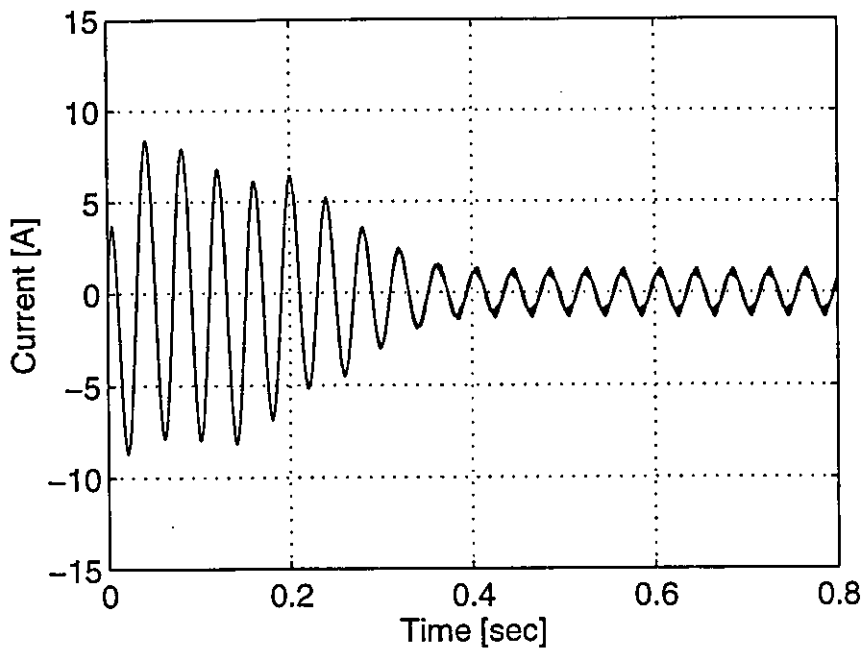


Figure 5-11 Computed results - Phase current characteristic for start-up of a Sinusoidal-PWM Inverter-fed Induction Motor

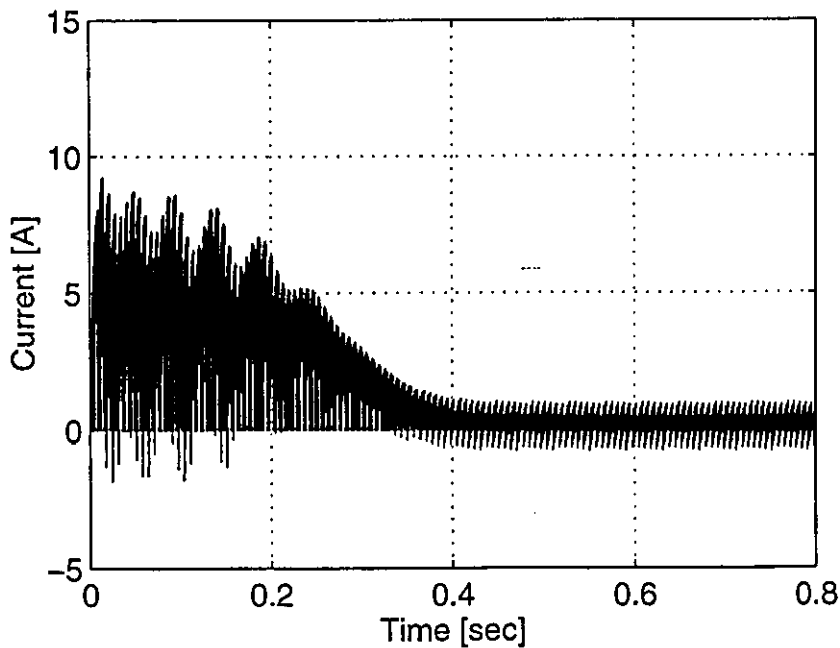


Figure 5-12 Computed results - Phase voltage current characteristic for start-up of a Sinusoidal-PWM Inverter-fed Induction Motor

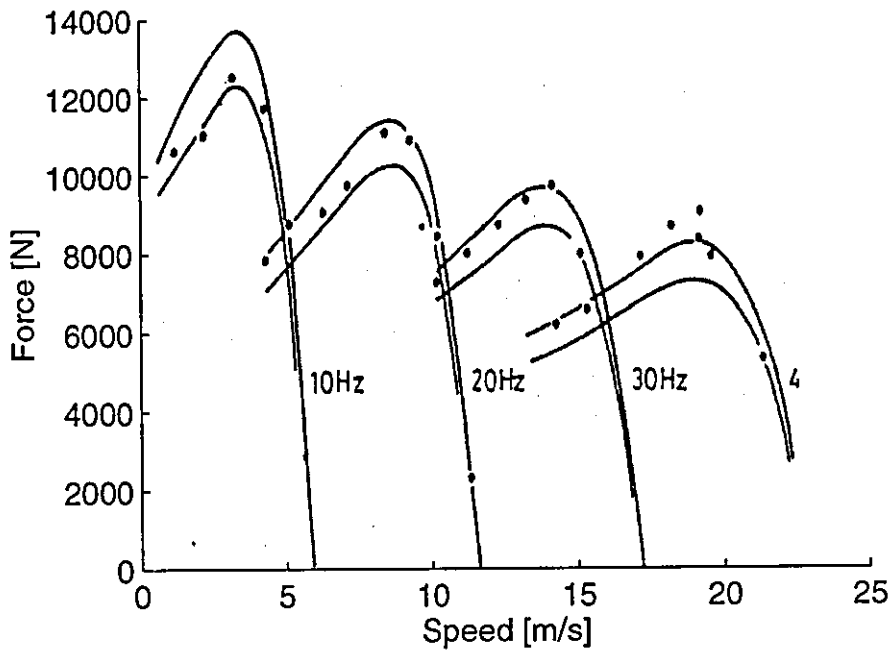


Figure 5-13 Thrust plotted against speed for a constant current of 465 rms at various supply frequencies

— calculated • experimental

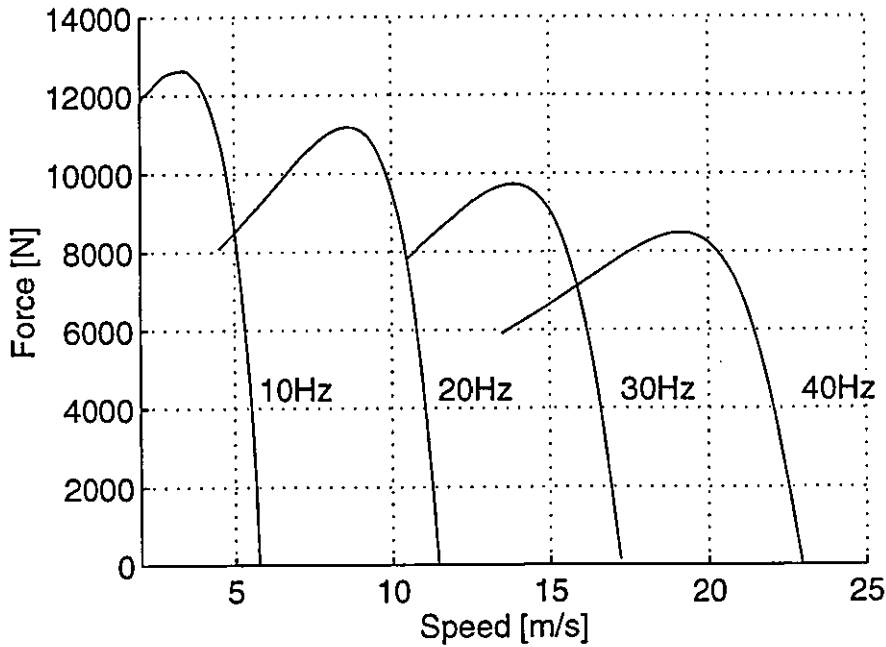


Figure 5-14 Computed results - Thrust plotted against speed for a constant current of 465 rms at various supply frequencies

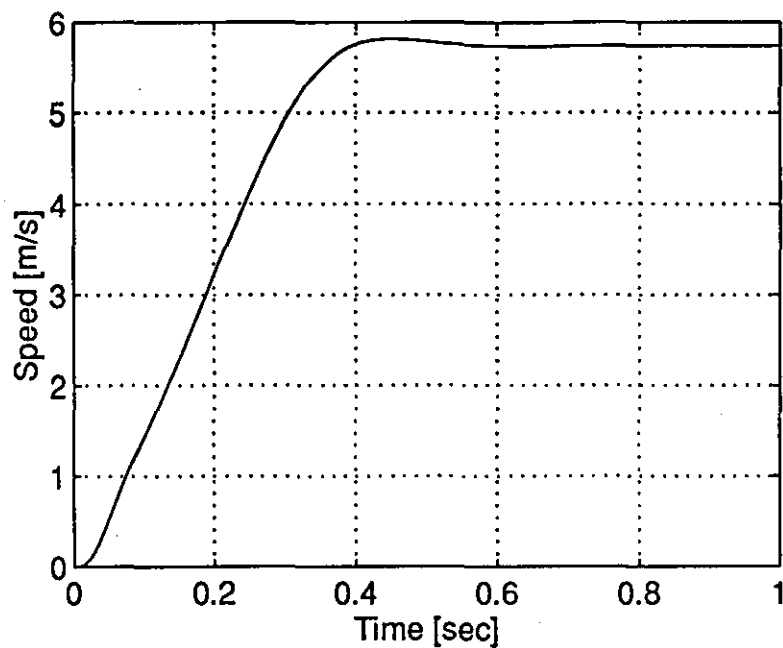


Figure 5-15 Computed results - Speed characteristic for start-up of a current-regulated PWM Inverter-fed LIM at 10Hz

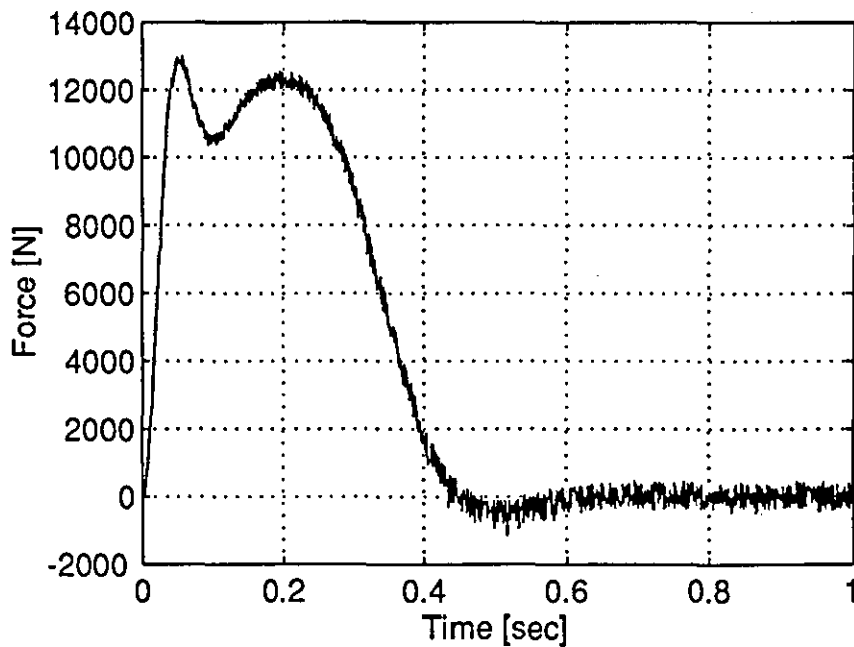


Figure 5-16 Computed results - Thrust characteristic for start-up of a current-regulated PWM Inverter-fed LIM at 10Hz

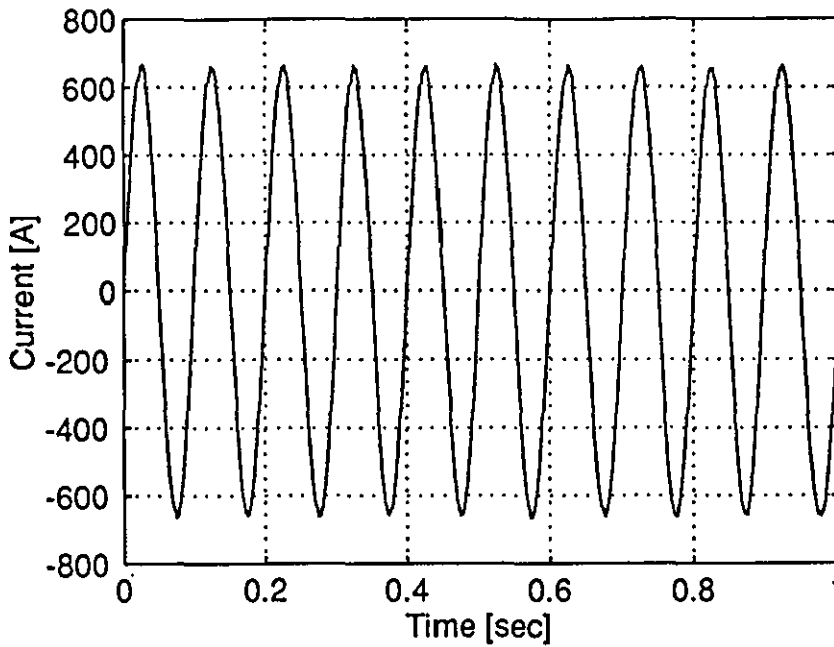


Figure 5-17 Computed results - Stator phase current characteristic for start-up of a current-regulated PWM Inverter-fed LIM at 10Hz

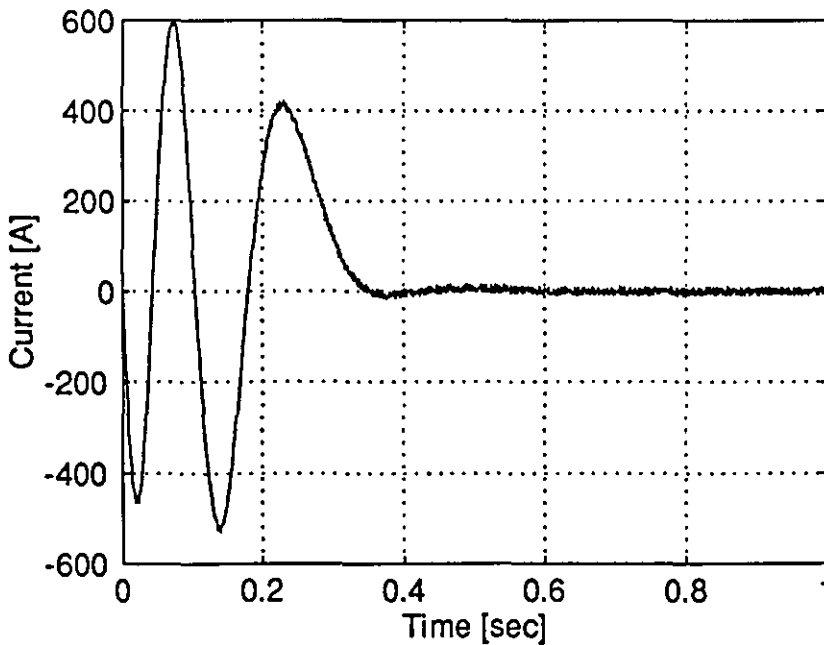


Figure 5-18 Computed results - Rotor phase current characteristic for start-up of a current-regulated PWM Inverter-fed LIM at 10Hz

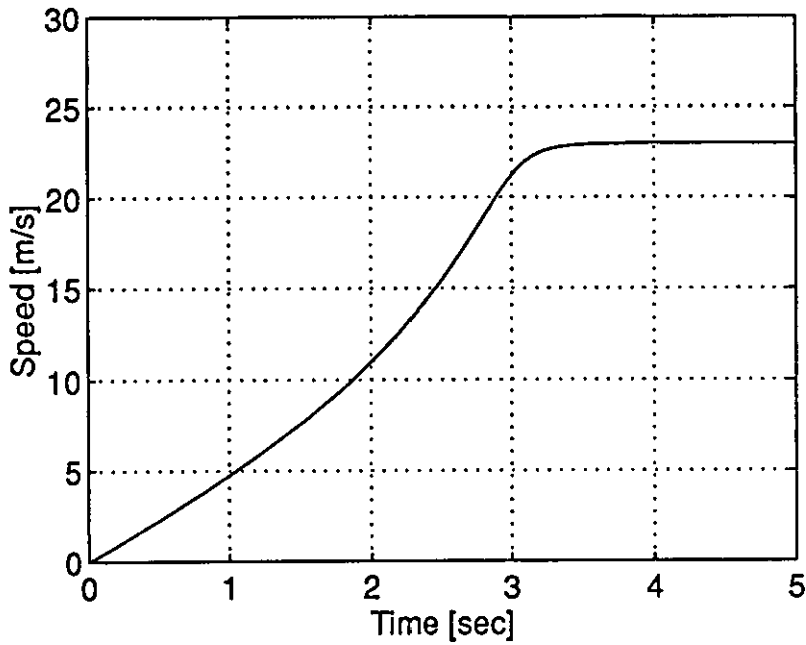


Figure 5-19 Computed results - Speed characteristic for start-up of a current-regulated PWM Inverter-fed LIM at 40Hz

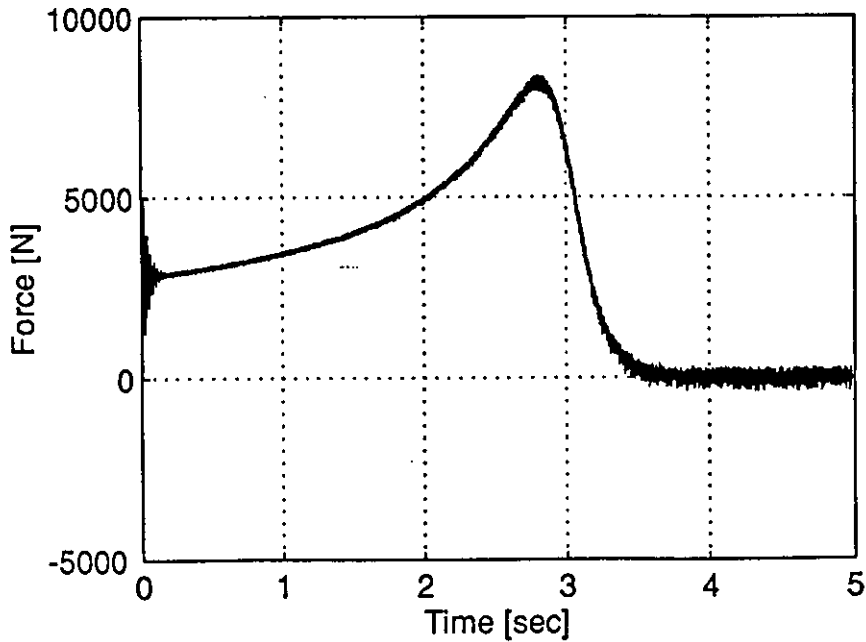


Figure 5-20 Computed results - Thrust characteristic for start-up of a current-regulated PWM Inverter-fed LIM at 40Hz

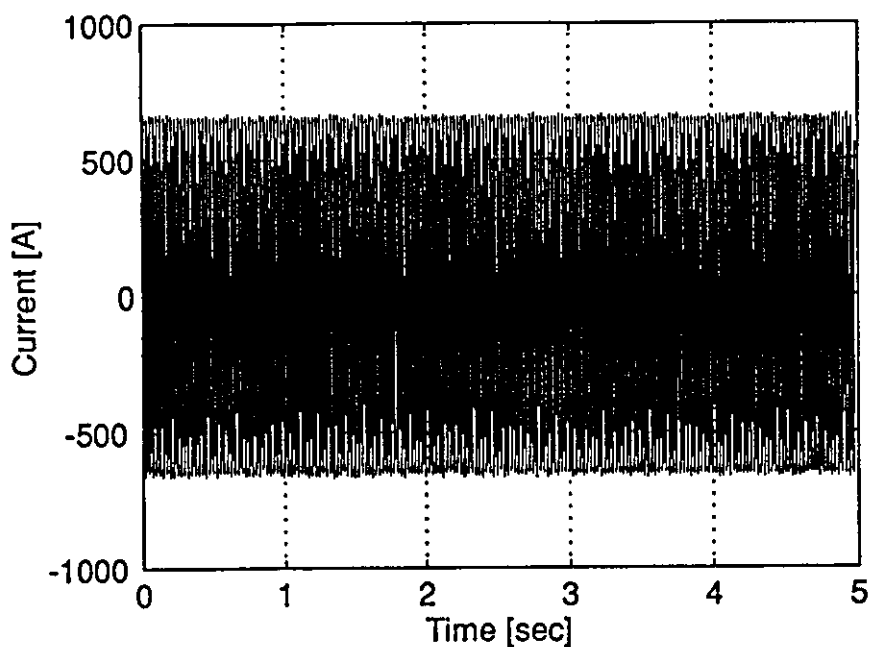


Figure 5-21 Computed results - Stator phase current characteristic for start-up of a current-regulated PWM Inverter-fed LIM at 40Hz

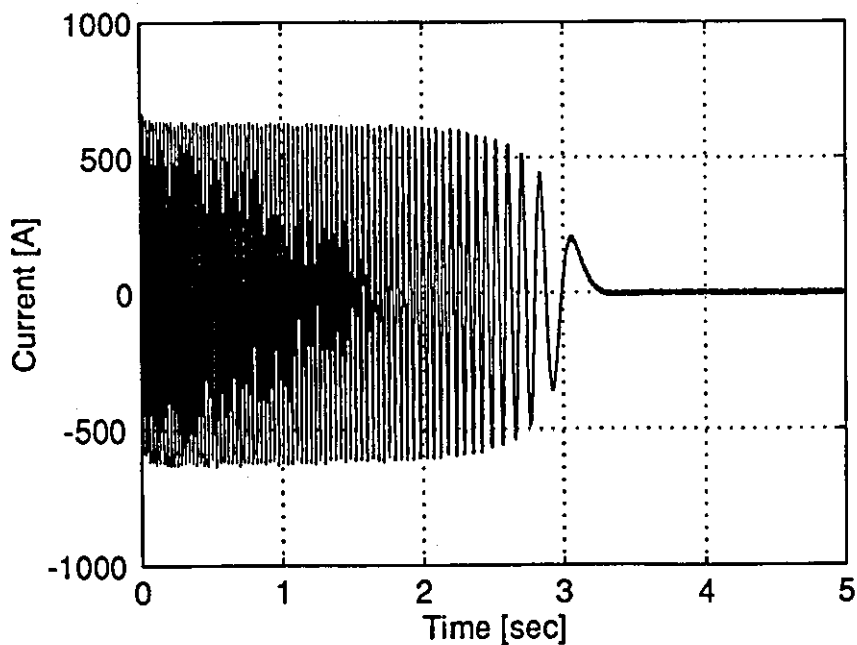


Figure 5-22 Computed results - Rotor phase current characteristic for start-up of a current-regulated PWM Inverter-fed LIM at 40Hz

INDUCTION MACHINE CONTROL

Although, various methods have been developed for controlling the torque and speed of a three-phase induction motor, the vector control [29, 30] and direct torque control methods [32-35] are of main importance. Vector control focuses on the separation of the torque and flux components in field coordinates, whereas, the direct torque method relies on manipulating the instantaneous value of the stator flux vector to achieve the required torque demand, while the currents are indirectly controlled. The latter control principle only works well for induction machines with a large rotor time constant, since the assumption is that the rotor flux is stable and changes slowly compared with the stator flux. A linear induction machine has a small time constant because of the low inductance value of its secondary member, and as such the vector control principle seems more appropriate.

6.1 Vector control

The induction motor torque is a non-linear function of the primary current and this makes direct control of the motor torque impossible. Vector control aims to provide decoupled control of torque and flux similar to that achieved in a dc machine, where control of the armature current allows direct control of the torque. Vector control gives the ac drive a similar performance, combining the control characteristics of the dc motor with the advantages of an induction motor so that the motor

- is generally smaller, and cheaper,
- is more robust, and therefore, requires less maintenance.

6.2 Principle of Operation

A vector controller uses an external controller to re-produce the field relationships that occur in a separately excited dc machine. Its chief merit is a good dynamic response to rapidly changing loads. The major problem associated with implementing a suitable control strategy is the determination of the position of the flux vector, and the methods

of achieving this are classified as either direct [36-39] or indirect field orientation [40-42], together with a newer method called Natural Field Orientation (NFO) [43-47].

In traditional vector control, an estimation is required of the magnitude and spatial position of the rotor flux vector within the induction motor, since this is taken as the frame of reference for the stator voltages and currents. Without a proper knowledge of the rotor flux, field orientation cannot be completely achieved.

To help decide which vector control scheme is most appropriate for low-speed applications, the advantages and disadvantages of the three methods will be looked at in greater detail.

6.2.1 Indirect field orientation

- *Indirect field-oriented control* - or flux-feedforward vector control. With this method, the stator current reference vector is evaluated, based on the rotor coordinate, utilising the motor parameters. As such, there is no flux-feedback loop in the block diagram of Fig.6-1.

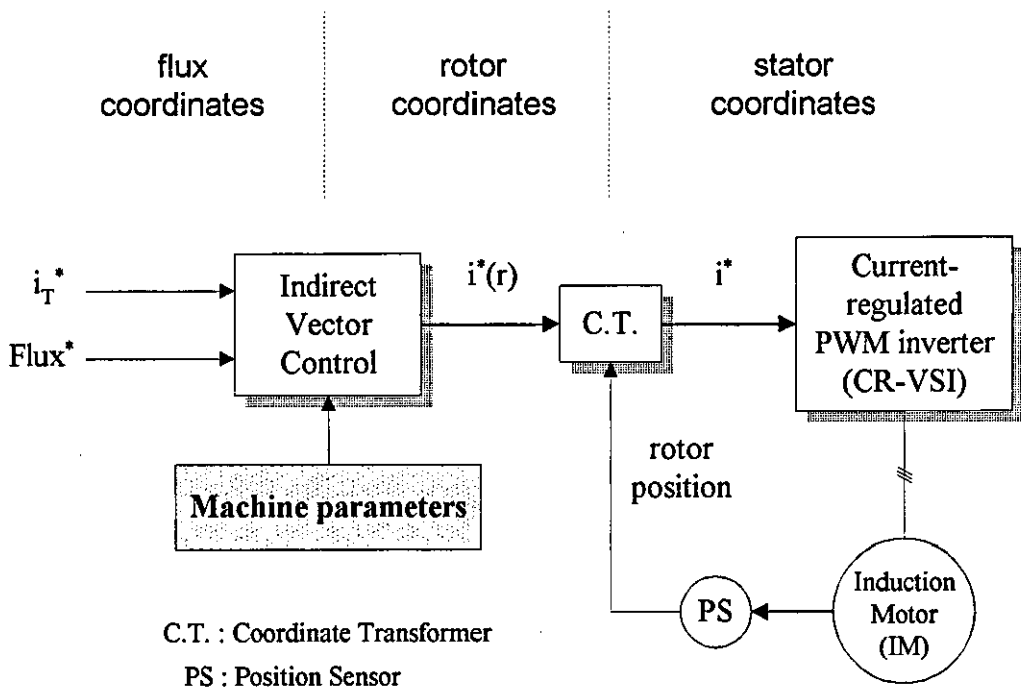


Figure 6-1 Feedforward vector control scheme

The advantages and disadvantages of this scheme are

1. No detector or calculator is needed in determining the rotor flux vector, which helps to keep the complexity of the control system to a minimum.
2. The machine parameters are required in the control algorithm, and consequently the drive is limited to a specific machine. However, with advances in control techniques, drives are being introduced that automatically tune themselves and both improve the overall performance and simplify commissioning [48, 49].
3. An estimate of the motor slip constant is required.
4. A sensor is required on the rotor shaft to determine the rotor speed, and this can be both expensive and troublesome to install. Several field-oriented methods without rotational transducers have been proposed in the literature [40-42] with an evaluation of various slip estimation techniques made in [50].
5. To maintain field orientation, motor parameter variations such as changes in the rotor resistance with operating temperature have to be taken into account, using either
 - Adaptive type controllers that employ self-tuning [41, 42], or
 - an appropriately designed outer control loop.

Otherwise, the control system will have a transient response to a torque command which involves changes in both the torque and flux levels of the machine.

6. Small low-efficiency machines are much less affected by 'detuning' than large high-efficiency machines.

6.2.2 Direct field orientation

- *Direct field-oriented control* - or flux-feedback vector control. In this method the amplitude and position of the flux linkage is either detected by direct measurement with field sensors in the air-gap of the machine [39] or calculated using a flux calculator [36-38]. A block diagram for the flux-feedback vector control scheme is shown in Fig.6-2.

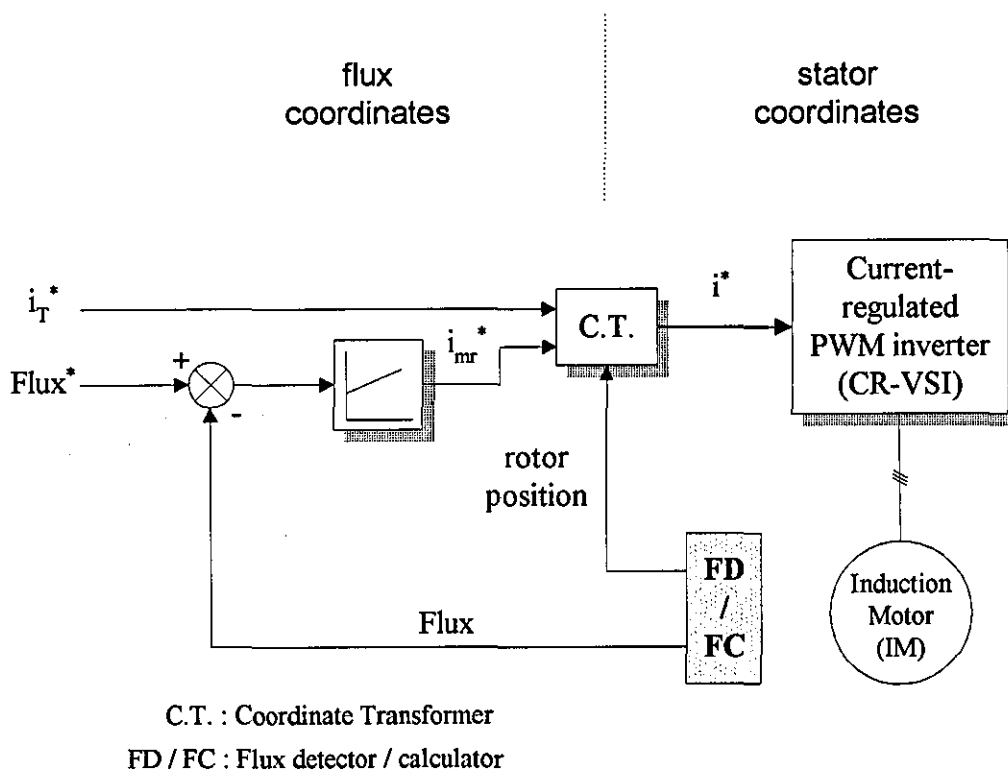


Figure 6-2 Feedback vector control scheme

The advantages and disadvantages of this scheme are

1. The control system is less sensitive to parameter variations, such as changes in the rotor resistance with operating temperature than the feedforward system. However, at low speed, the system becomes very sensitive to changes in the stator resistance.
2. The rotor flux vector is estimated from the stator currents and rotor speed on the basis of the rotor circuit equations for an induction motor. This enables the

rotor flux vector to be calculated even at standstill, since no integration is required.

3. A flux detector or calculator is needed to determine the position and magnitude of the flux vector.

On the basis of the advantages and disadvantages of the direct and indirect vector control schemes, the tendency is to use the feedforward system because of the lack of need for either a flux detector or a calculator.

6.2.3 Natural Field Orientation

An alternative vector approach is to implement a control system based on the concept of Natural Field Orientation [43-47], which relies on the induction motor establishing a correct field orientation due to its inherent properties. This eliminates any need either to measure or estimate the magnetic field.

This approach offers significant advantages over the previous two methods, since it presents no problems in operation at low speed or at standstill. Likewise, no sensor is required on the rotor shaft for speed or position control, and the control system is suited for both open and closed-loop operation.

Since the control system is able to work correctly at zero speed i.e. zero frequency, it follows that the motor can react immediately to a change in the torque command without the need to build-up the magnetic field before the torque is created. In comparison with indirect field orientation, the system is insensitive to rotor parameter variations, since all the necessary calculations are performed in the stator circuit.

6.3 Vector transformation

A characteristic feature of field-oriented control is the use of different coordinate systems. The motor is described in a stationary reference frame, whereas the control is performed in field coordinates. In creating a stator coordinate system which rotates and follows the magnetic field, it allows the machine to be effectively controlled by dc quantities. Similar to that achieved in a dc motor, where we have a stationary magnetic

field vector and stationary current vectors. The phasor diagram of the induction motor in field coordinates is shown in Fig.6-3.

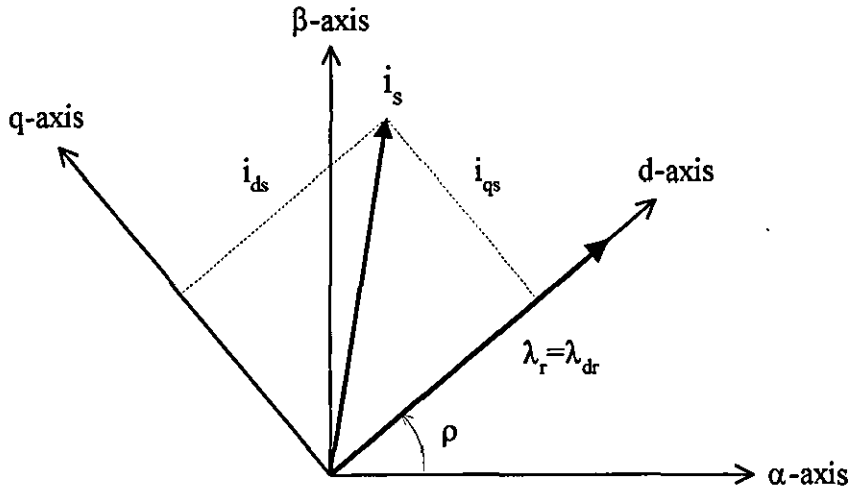


Figure 6-3 Induction motor phasor diagram in field-coordinates

The transformation from stator to field coordinates, or vice versa, is achieved by vector rotation or the so called vector transformation. To obtain the required current components in field coordinates, the stator current vector i_s is firstly divided into orthogonal components i_α and i_β , and then transformed into the required field coordinates by vector rotation. The required transformations in matrix form are

$$[T(\rho)] = \begin{bmatrix} \cos \rho & \sin \rho \\ -\sin \rho & \cos \rho \end{bmatrix} \begin{bmatrix} \frac{2}{3} & -\frac{1}{3} & -\frac{1}{3} \\ 0 & \frac{\sqrt{3}}{3} & -\frac{\sqrt{3}}{3} \end{bmatrix} \quad (6-1)$$

$$[T(\rho)^{-1}] = \begin{bmatrix} 1 & 0 \\ -\frac{1}{2} & \frac{\sqrt{3}}{2} \\ -\frac{1}{2} & -\frac{\sqrt{3}}{2} \end{bmatrix} \begin{bmatrix} \cos \rho & -\sin \rho \\ \sin \rho & \cos \rho \end{bmatrix} \quad (6-2)$$

where,

$$\begin{bmatrix} i_{ds} \\ i_{qs} \end{bmatrix} = [T(\rho)] \begin{bmatrix} i_{\alpha s} \\ i_{\beta s} \end{bmatrix} \quad \text{and} \quad \begin{bmatrix} i_{\alpha s} \\ i_{\beta s} \end{bmatrix} = [T(\rho)^{-1}] \begin{bmatrix} i_{ds} \\ i_{qs} \end{bmatrix}$$

and ρ is the angle of the rotor flux vector with the stator reference axis.

6.4 Implementation of the vector control schemes

There are several methods for implementing the control scheme in moving coordinates, since more than one realisation exists. Instead of feeding the motor with impressed stator currents, the stator currents may be controlled in their field coordinate components i_{qs} and i_{ds} , while the motor is fed with impressed voltages. In the latter case, the current controllers process steady-state dc quantities, and with the PWM now included in the digital part of the controllers, the way is open to more advanced modulation schemes.

In this thesis, the current impression scheme is chosen so that hysteresis current control of the inverter switches is made possible. The field-oriented controller sets up the three-phase reference currents that control the VSI. It generates these currents in a way that orients the magnetic field of the stator with respect to that of the rotor, by basically regulating the stator current magnitude and phase with respect to the rotor position.

While the traditional field orientation scheme is based on the alignment of the rotor flux vector, it has been established that there exists a generic scheme which is capable of de-coupling torque and flux in either the rotor, air-gap or stator flux reference frame [51, 52]. The implementation of the traditional control scheme by either direct or indirect methods is discussed in the following sub-sections.

6.4.1 Indirect field orientation

With field-oriented control, it is normally assumed [53, 54] that

$$\lambda_{dr}^* = L_m i_{mr}^* = \text{constant} \quad (6-3)$$

$$i_{qr}^* = 0 \quad (6-4)$$

$$\omega_{slip} = \frac{L_m R_r i_{qs}^*}{L_{rr} \lambda_{dr}^*} = \frac{L_m i_{qs}^*}{\tau_r \lambda_{dr}^*} \quad (6-5)$$

where i_{mr} is the magnetizing current, and τ_r the rotor time constant.

As mentioned earlier, the objective of field-oriented control is to establish and maintain an explicit angular relationship (the so called orientation) between the stator current vector and the rotor flux. Equation (6-5) expresses the relationship between the slip and the current components required to attain correct field orientation. In a feedforward system, this relationship is employed directly to obtain the correct subdivision by regulating the slip of the machine to the value given by Eq.(6-5). In effect, field-oriented control attempts to align the rotor flux vector with the d-axis component of the stator current vector as shown in Fig.6-4, to allow independent control of the machine flux and torque. Subdivision of the stator current is basic to field orientation controllers.

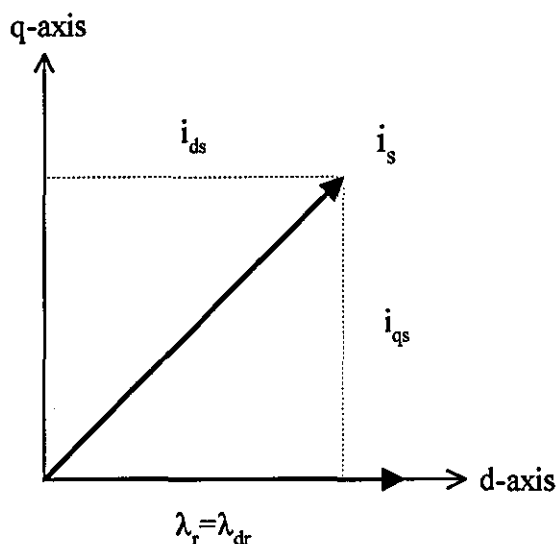


Figure 6-4 Quadrature and direct axis components of the stator current vector

It follows from Eq.(6-5) that for λ_{qr} to be equal to zero,

$$\lambda_{dr}(\omega - \omega_r) = \left(\frac{L_m R_r}{L_r}\right) i_{qs} \quad (6-6)$$

where ω is the synchronous speed.

To achieve a dynamic performance similar to that of a dc machine, a control strategy similar to that of a dc machine is required. This is achieved by controlling the stator currents and thereby omitting the stator voltage drops.

The relationship between the d-axis component of the stator current and the rotor flux is

$$|\lambda_r| = \lambda_{dr} = \frac{L_m i_{ds}}{R_r + \frac{d}{dt} L_{rr}} \quad (6-7)$$

and the electromagnetic torque can be expressed as

$$\begin{aligned} T_{em} &= \frac{3p}{2} \left(\frac{L_m}{L_{rr}} \right) (\lambda_{dr} i_{qs}) \\ &= k (i_{mr} i_{qs}) \end{aligned} \quad (6-8)$$

assuming, that $\lambda_{qr} = 0$ i.e. perfect field orientation.

Equation (6-8) shows that if the rotor flux λ_{dr} is kept constant, by maintaining constant the d-axis component of the stator current, the torque can be directly controlled by the q-axis component of the stator current. The control structure to achieve this is shown in Fig.6-5.

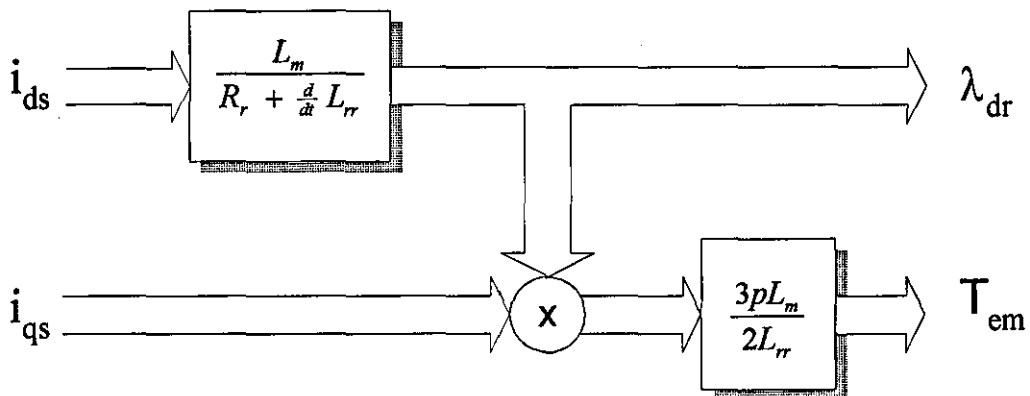


Figure 6-5 Dynamic control structure

The analogy with a dc motor is now obvious, with i_{mr} representing the field and i_{qs} the armature current. If it is feasible to control both currents independently, the aim of controlling the machine like a dc motor is achieved.

Assume, initially that the electromagnetic torque T_{em} and the magnetizing current i_{mr} are known quantities. By re-arranging Eq.(6-8), the torque component of current can be evaluated.

$$i_{qs}^* = \left(\frac{T_{em}^*}{k i_{mr}^*} \right)$$

Substituting i_{qs}^* into Eq.(6-5) gives

$$\omega_{slip}^* = \left(\frac{T_{em}^*}{k i_{mr}^{*2} \tau_r} \right) \quad (6-9)$$

Eq.(6-9) is then integrated, giving the slip angle θ_{slip} , which is added to the rotor angle. Finally, the sum of the two angles is used to control the vector rotator which transforms the input signals for current control into three-phase reference currents as shown in Fig.6-6.

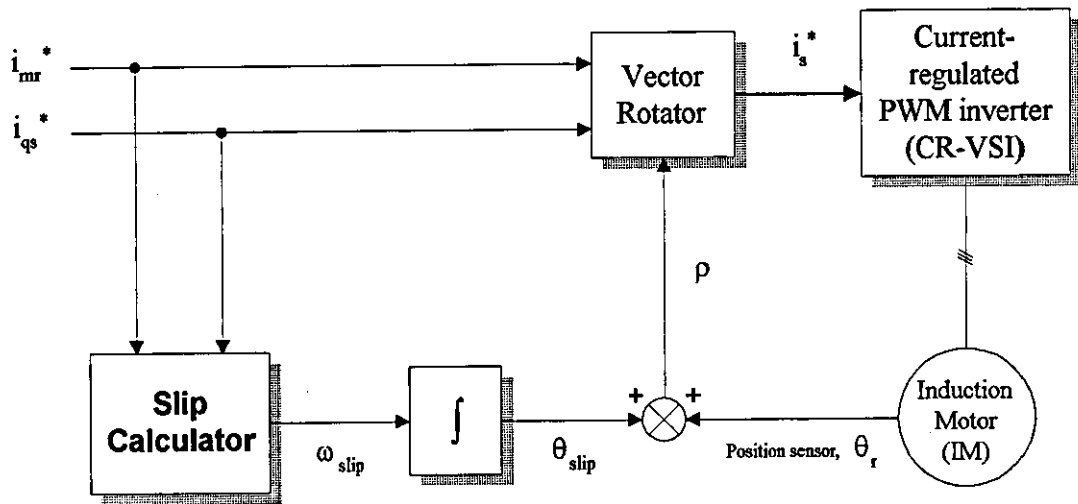


Figure 6-6 Feedforward field-oriented control system

6.4.1.1 Evaluation of the rotor flux vector

Using the matrix transformation of Eq.(6-1), the orthogonal components of the stator current vector in field coordinates is evaluated. Using the initial assumptions of field-oriented control, the position and magnitude of the rotor flux vector can then easily be found. Since the relationship between i_{ds} and the rotor flux λ_{dr} is a first-order low pass function,

$$i_{ds} = i_{mr} + \tau_r \frac{di_{mr}}{dt} \quad (6-10)$$

Re-arranging Eq.(6-10), gives

$$\frac{di_{mr}}{dt} = \frac{(i_{ds} - i_{mr})}{\tau_r} \quad (6-11)$$

substituting Eq.(6-3) into Eq.(6-5) gives the slip speed

$$\omega_{slip} = \frac{i_{qs}}{\tau_r i_{mr}} \quad (6-12)$$

The slip speed may be added to the rotor speed and integrated over a given time interval to determine the new position of the rotor flux vector.

$$\omega = \frac{d\rho}{dt} = \omega_r + \left(\frac{i_{qs}}{\tau_r i_{mr}} \right) \quad (6-13)$$

When the stator current vector is transformed into field coordinates using Eq.(6-1) orthogonal components i_{ds} and i_{qs} are generated. The steady-state value for the magnetizing current vector i_{mr} is evaluated by integrating Eq.(6-11), and substituting this value into Eq.(6-3) gives the required magnitude of the flux vector. A block diagram of the model to evaluate the necessary control signals in field coordinates is given in Fig.6-7.

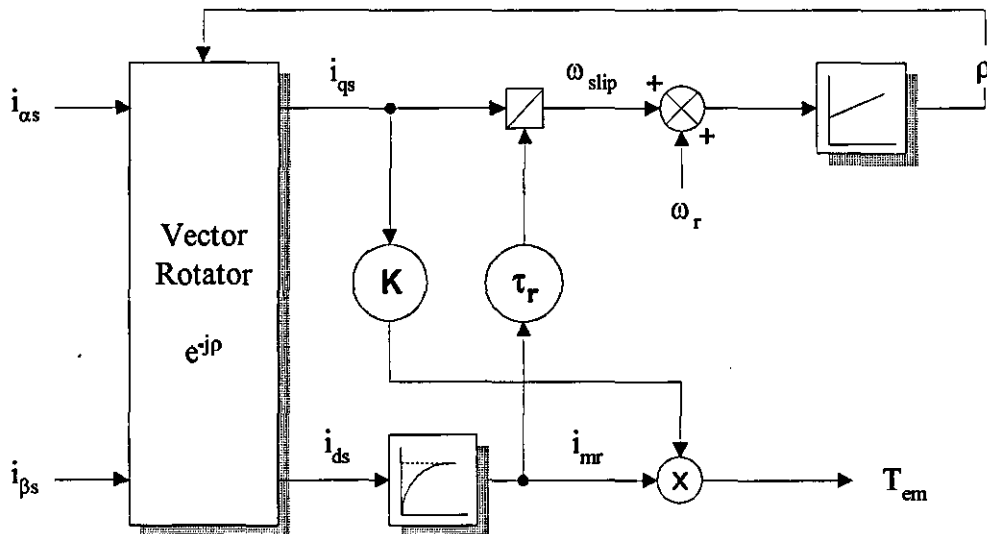


Figure 6-7 Model for obtaining variables required for control in field coordinates

6.4.2 Direct field orientation

Direct field orientation is the oldest of the three vector methods presented in this thesis. In direct field orientation, the angular position of the magnetic field is either obtained by direct measurement, or evaluated using a flux calculator. Detection by direct measurement is considered impractical, as it requires either Hall sensors [39] or search coils to be placed in the air-gap of the machine. In this approach, the instantaneous magnitude and position of either the stator, air-gap or rotor flux vector is determined by voltage and current measurements [36-38]. In fact, an induction motor controlled with a constant magnetic flux can generate up to six times the rated torque [47].

Although stator flux orientation is easier since only the stator resistance is required in the calculation process, operating the machine with a constant stator flux or air-gap flux, yields a pull-out torque which might be disadvantageous at over-load. Rotor flux orientation is therefore performed, and a block diagram of the proposed direct control scheme is shown in Fig.6-8.

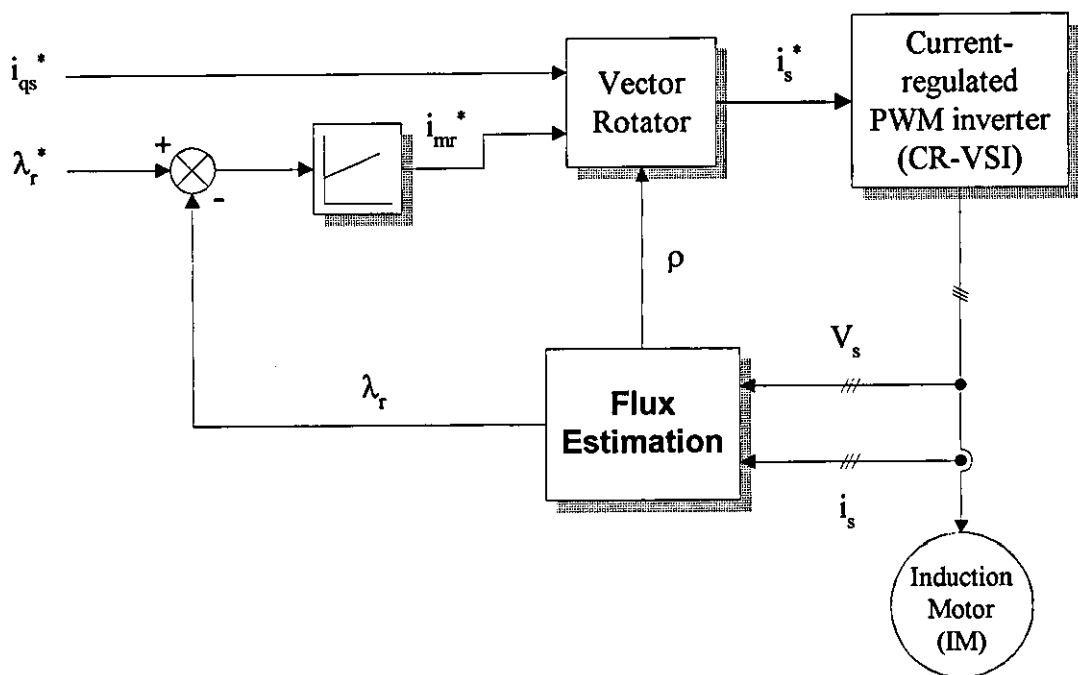


Figure 6-8 Induction machine torque control with rotor flux orientation

The control variables are determined in field coordinates. The flux regulator establishes the magnetizing current i_{mr} and the necessary information about the location of the rotor flux is obtained by voltage and current measurements on the stator side. This enables the current control variables to be transformed from field to stator coordinates. For direct current control the reference currents are applied to three independent hysteresis controllers that generate the required gating signals to drive the inverter switches.

By applying the constant phase transformation i.e. from 3-phase to 2-phase, the current and voltage vectors can be expressed in orthogonal components in a stationary reference frame as

$$V_s = v_{\alpha s} + jv_{\beta s} \quad (6-14)$$

$$i_s = i_{\alpha s} + ji_{\beta s} \quad (6-15)$$

The stator flux λ_s can be expressed in terms of the stator voltage, current and machine parameters as

$$\lambda_{\alpha s} = \int (v_{\alpha s} - R_s i_{\alpha s}) dt \quad (6-16)$$

$$\lambda_{\beta s} = \int (v_{\beta s} - R_s i_{\beta s}) dt \quad (6-17)$$

and the air-gap flux λ_m can be obtained from the stator flux as

$$\lambda_{\alpha m} = \lambda_{\alpha s} - L_{ls} i_{\alpha s} \quad (6-18)$$

$$\lambda_{\beta m} = \lambda_{\beta s} - L_{ls} i_{\beta s} \quad (6-19)$$

Having determined the air-gap flux, the rotor flux can be evaluated from

$$\lambda_{\alpha r} = \frac{L_{rr}}{L_m} \lambda_{\alpha m} - L_{lr} i_{\alpha s} \quad (6-20)$$

$$\lambda_{\beta r} = \frac{L_{rr}}{L_m} \lambda_{\beta m} - L_{lr} i_{\beta s} \quad (6-21)$$

and the magnitude and angular position of the rotor flux vector to the stator reference frame are respectively

$$\lambda_r = \sqrt{(\lambda_{\alpha r})^2 + (\lambda_{\beta r})^2} \quad (6-22)$$

$$\rho = \tan^{-1}\left(\frac{\lambda_{\beta r}}{\lambda_{\alpha r}}\right) \quad (6-23)$$

Clearly, the stator resistance, and stator and rotor leakage inductances are essential in the calculation of the rotor flux. At low speed, the control system becomes sensitive to changes in leakage inductance and stator resistance with temperature. A method has been presented in literature [37] that tries to compensate for changes in the stator parameters.

6.4.3 Natural Field Orientation

With Natural Field Orientation there is no dependency on the rotor parameters and likewise no need to measure or estimate the rotor flux vector. This clearly eliminates most of the problems associated with both direct and indirect field-oriented control, especially the difficulties faced when operating at low speed and at standstill.

As mentioned earlier, to achieve a correct field orientation and therefore a good decoupling of torque and flux, involves keeping a 90° phase difference between the magnetizing current i_{mr} and the torque demand i_{qs} . In the feedback system the flux vector is estimated, while in the feedforward system the instantaneous position of the rotor flux is determined by summing the rotor position with a demanded slip position signal.

In this scheme, field-orientation is achieved by indirect measurement of the air-gap voltage, with quadrature conditions maintained between the magnetizing current and rotor current, with the magnitude of the magnetizing current kept constant. The magnetizing current is a function of the air-gap voltage E and can be expressed as

$$i_{mr} = \frac{E}{j2\pi f_s L_m} \quad (6-24)$$

Clearly, maintaining a fixed relationship between the air-gap voltage and the supply frequency f_s will keep the amplitude of i_{mr} constant, and this is the basis of NFO. By rearranging Eq.(6-24), the optimal stator frequency ω can be expressed as

$$\omega = \frac{E}{L_m i_{mr}} \quad (6-25)$$

6.4.3.1 Evaluation of the air-gap voltage

To maintain field orientation, an accurate determination of the air-gap voltage is essential to ensure a correct value for the stator frequency. To calculate the air-gap voltage, the terminal voltage V_s and the stator current i_s are measured. The terminal voltage of the equivalent circuit of the induction motor is given by

$$V_s = E + i_s \left(R_s + \frac{dl}{dt} \right) \quad (6-26)$$

from which E can be determined as

$$E = V_s - i_s \left(R_s + \frac{dl}{dt} \right) \quad (6-27)$$

The stator and rotor leakage inductances are combined to one single stator leakage inductance l . A block diagram of the proposed control system neglecting the inductive voltage drop in the stator is shown in Fig.6-9.

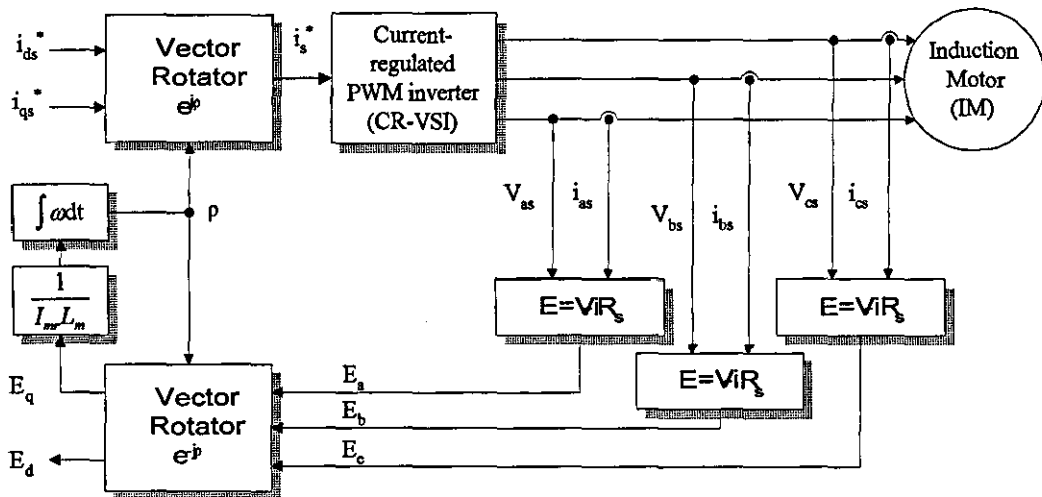


Figure 6-9 Natural Field Orientation with current control

The result of the measurement and calculation is a rotating voltage vector (E_a, E_b, E_c) in stator coordinates. Similar to other field-oriented control systems, the rotating air-gap voltage vectors are then converted into field coordinates by vector rotation. This transformation gives rise to an air-gap voltage E_q and an orthogonal error component E_d . Should all the measurements and calculations be correct, the value of E_d will be zero.

Using Eq. (6-25), the modulation frequency is calculated and integrated to give a new control angle for the vector rotators. However, the modulation frequency is only used as a secondary control variable for keeping the magnetizing current constant. The main control function of the system is to achieve current control of the rotor circuit.

6.5 Conclusions

The vector controller can meet the requirements of a high-performance induction machine drive by providing a fast torque response below base frequency and constant power with adequate response above base frequency. However, the cost and complexity associated with the controller restricts the field-oriented drive to applications where the performance requirements prevent the use of a volts-per-hertz drive.

A major contributory factor to the complexity and expense of the drive, especially with direct field-oriented control lies in the implementation of the control algorithm. This requires a knowledge of the machine parameters to tune the current and torque loops, and therefore restricts the drive to a specific machine.

Having looked at the advantages and disadvantages of each system, it was decided that NFO is most suited to control the linear induction machine. The simplicity of the control algorithm and its accuracy are considered to be of great importance. Current control is the most powerful version of NFO, because of the increased bandwidth achieved by eliminating the time delay caused by the leakage inductances, and it was chosen therefore in preference to voltage control. The leakage inductances dictate the rate of current build up in the rotor, and therefore the torque response of an induction machine. The linear induction motor has a secondary member with a low leakage factor which, with this type of control system, leads to a very fast torque response.

VECTOR CONTROL OF A LINEAR INDUCTION
MOTOR

In Chapter 6 the principles of the direct, indirect and natural field-oriented control methods were discussed, and it seems that Natural Field Orientation is most suited for the control a linear induction motor because of its inherent simplicity. This chapter compares the performance characteristics of the LIM under the direct and indirect field-oriented control schemes.

7.1 Control system design

The main part of the control system involves current control in the rotor circuit. With current control, the control vector is split into field-oriented components i_{mr} and i_{qs} . Since i_{mr} corresponds to the magnetizing current, it is maintained constant, and the control variable i_{qs} is used to control the motor thrust in the same way as armature current control of a dc machine.

The proposed control system accepts flux and thrust references as inputs. The command thrust and rotor flux linkage in field coordinates are evaluated from

$$F_x^* = \frac{3\pi p}{L} \left(\frac{L_m}{L_r} \right) \lambda_{dr}^* i_{qs}^* \quad (7-1)$$

and
$$\lambda_{dr}^* = L_m i_{mr}^* \quad (7-2)$$

By re-arranging Eqs.(7-1) and (7-2), the thrust and magnetizing components of current can be evaluated.

$$i_{qs}^* = \frac{L}{3\pi p} \left(\frac{L_r}{L_m} \right) \frac{F_x^*}{\lambda_{dr}^*} \quad (7-3)$$

$$i_{mr}^* = \frac{\lambda_{dr}^*}{L_m} \quad (7-4)$$

The vector rotator then transforms the control signals from field coordinates to stator coordinates, where the position of the magnetic field in the motor is determined by either the direct or indirect field-oriented methods.

7.1.1 Indirect field orientation

The proposed indirect vector control scheme shown in Fig.7-1 is composed of a current-controlled PWM inverter, a vector rotator, and controller that contains several functions.

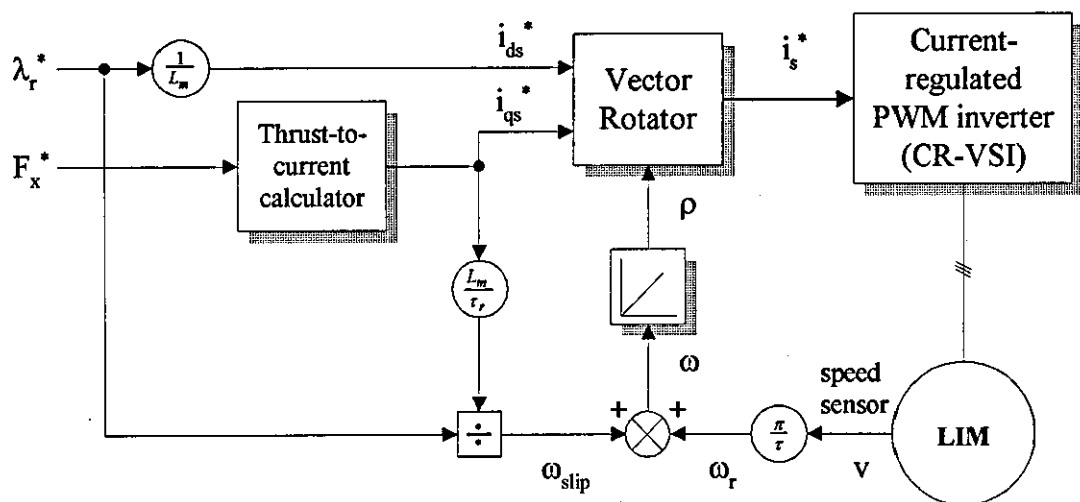


Figure 7-1 Indirect field-oriented control of a LIM

The control scheme is based on a feedforward approach that involves performing a slip calculation to coordinate the values of machine flux and thrust. Clearly, the rotor resistance and self-inductance are required in the slip frequency calculation, which makes the control system sensitive to parameter variations.

7.1.2 Direct field orientation

In direct field orientation, the required field orientation angle is directly calculated from the estimated rotor flux. The rotor flux is estimated using an open-loop non-linear observer that requires knowledge of the stator resistance, stator and rotor leakage

inductances, and the ratio of rotor inductance to magnetizing inductance. Thus, the rotor flux measurement is dependant on the stator resistance, which makes this control scheme sensitive to the field angle computation when the speed is low. In fact, stator resistance thermal variation can lead to thrust variation in the low-speed range. A block diagram of the proposed direct vector control scheme is shown in Fig.7-2.

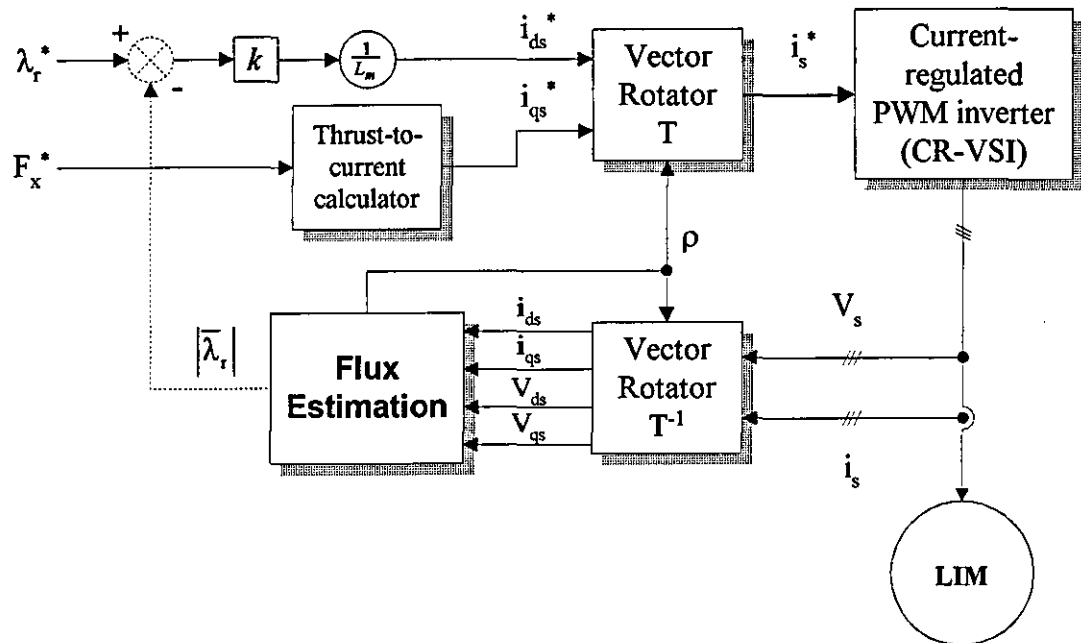


Figure 7-2 Direct field-oriented control of a LIM

Since the relationship between the demand and actual flux is a first-order low pass function, a closed-loop control of flux can be used to transiently supply a large d-axis component of the stator current in order to speed-up flux response.

7.2 Simulated results

Simulated results are provided for both control schemes, when the drive is operating under constant flux control. The motor is fed by a current-regulated voltage-source inverter (CR-VSI) with a tolerance-band control, and a supply voltage of 600V dc. The system parameters are given in Appendix C, and a brief flowchart provided in Appendix E. An integration step-length of $10\mu\text{s}$ is used to ensure integration stability and provide results with a good accuracy.

The motor with pure inertia load is initially at steady-state with zero thrust and the desired flux linkage of 2.95 Wb. A thrust demand of $\pm 2500\text{N}$ is applied to both field-oriented control systems, and the computed transient and steady-state waveforms for speed, thrust, rotor flux and phase current for both schemes are shown in Figs.7-3 to 7-8 and Figs.7-9 to 7-14 respectively.

The influence of the magnetizing inductance variation, due to the longitudinal end-effect, on the system dynamic response for both the direct and indirect field orientation schemes is shown in Figs.7-15 to 7-20 and Figs.7-21 to 7-26 respectively.

7.2.1 Indirect field orientation

The thrust and flux waveforms shown in Figs.7-4 and 7-6 respectively, confirm that field orientation is achieved, even on speed reversal through zero speed. The machine thrust follows the demanded thrust profile shown in Fig.7-5 closely, and during the large changes in thrust, the rotor flux is maintained constant.

The high-frequency ripples observed in the thrust waveform, are caused by the motor current harmonics. However, these high-frequency harmonics are not reflected in the machine flux owing to the first-order filtering effect between the demand and actual flux.

Fig.7-15 shows the oscillatory behaviour of the thrust response for a step-change in the thrust command when the magnetizing inductance variation is not taken into account by the controller. The mismatch in inductance value results in a reduced rotor flux shown Fig.7-18, and this implies that field orientation is not achieved.

7.2.2 Direct field orientation

The resulting thrust, flux, the stator and rotor current waveforms for operation at both low and moderate speeds are shown in Figs.7-9 to 7-14, and Figs.7-21 to 7-26 respectively. It is evident from the waveforms at low speed that field orientation is achieved, since there is no transient in the flux.

The direct field orientation system is, however, more sensitive to magnetizing inductance variation than the indirect method. The thrust pulsations shown in Fig.7-22, are due to the ripples in the estimated rotor flux. Hence, field orientation is not maintained.

7.3 Conclusions

An overview and comparison of the direct and indirect methods of field-oriented control of a LIM has been presented. The usefulness of field orientation and its decoupled control characteristics has also been illustrated. The vector drive is inevitably a closed-loop control system, regardless of whether it is used as an open-loop torque or thrust controller, or open or closed-loop speed or position controller.

Both the field-oriented control schemes are machine parameter dependant. Although the effects of machine parameter variations on the control performance has not been fully examined, a mismatch between the parameter values used in the controller and those of the actual machine, does introduce steady-state offsets in the thrust and flux control.

The direct field-oriented control method may be less sensitive to changes in the rotor resistance but it is more sensitive to variations in stator resistance and transient inductance during low-speed operation. To compensate for variations in the stator and rotor resistances with temperature, and maintain decoupled control, a parameter identification scheme may be required.

It is concluded that both the field orientation schemes provide an adequate means of controlling the thrust and flux of a LIM, if parameter variations due to magnetic saturation and changes in temperature are ignored. Clearly, the choice of controller to implement will depend on several criteria. These include the speed range of operation, complexity and cost. Although, the indirect field orientation technique requires an encoder or speed transducer to be fitted to the motor, in many high performance applications where position or velocity feedback is essential, this is available at no additional cost. This makes indirect field orientation more popular in high performance control, especially at low speed.

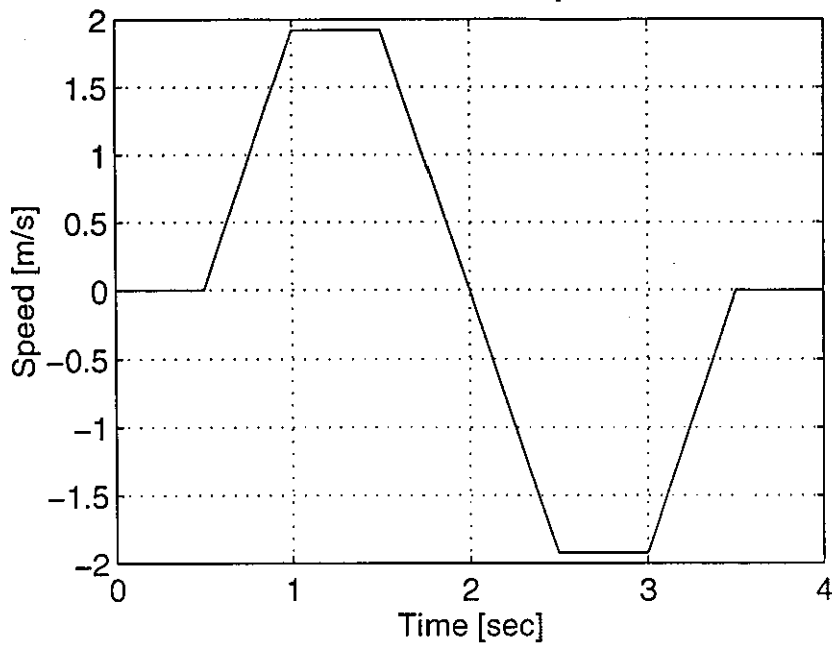


Figure 7-3 Computed results - Speed characteristic for indirect field-oriented control of a LIM

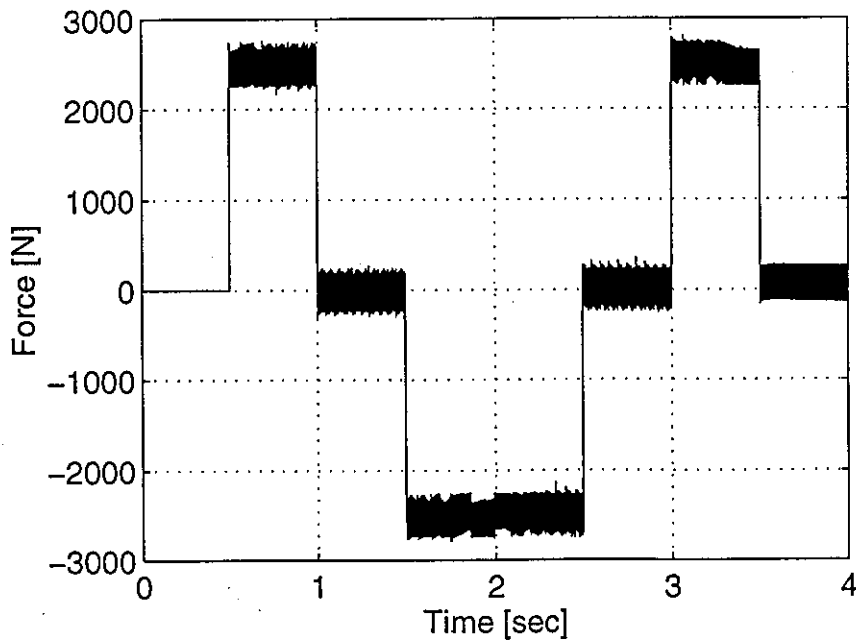


Figure 7-4 Computed results - Thrust characteristic for indirect field-oriented control of a LIM

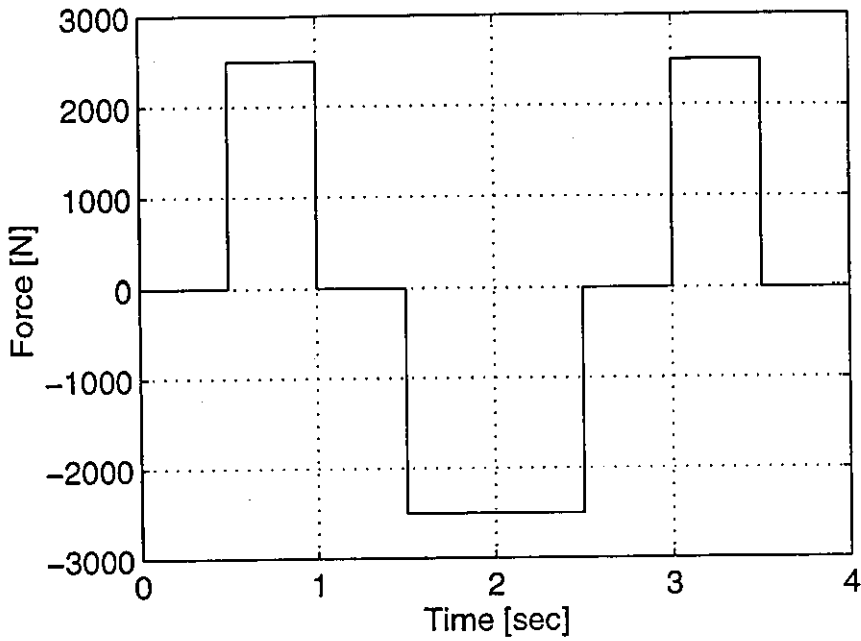


Figure 7-5 Computed results - Thrust demand characteristic for indirect field-oriented control of a LIM

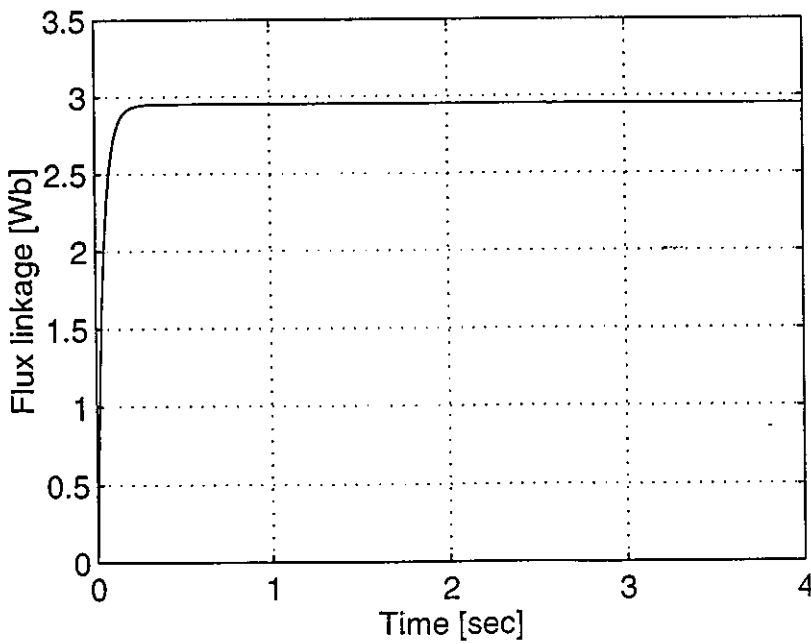


Figure 7-6 Computed results - Flux characteristic for indirect field-oriented control of a LIM

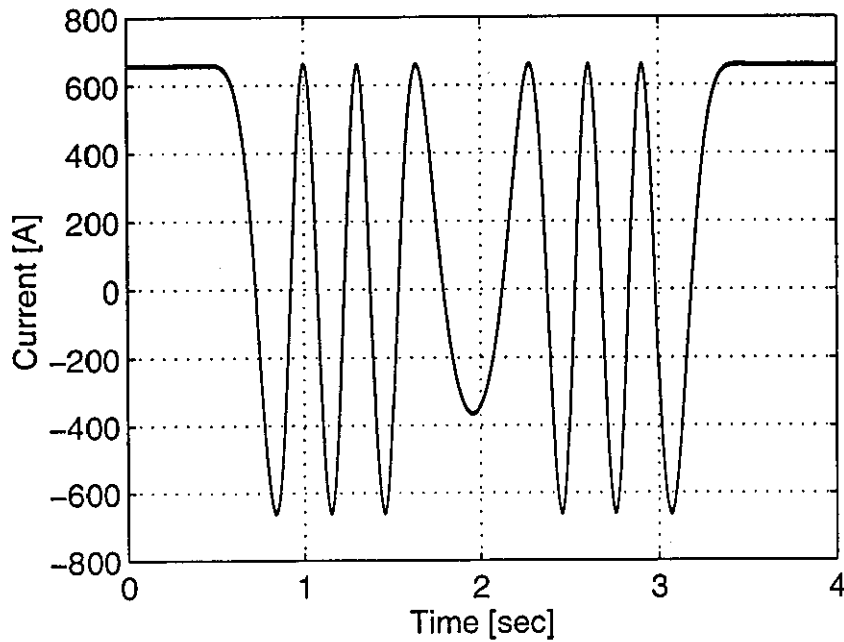


Figure 7-7 Computed results - Stator phase current characteristic for indirect field-oriented control of a LIM

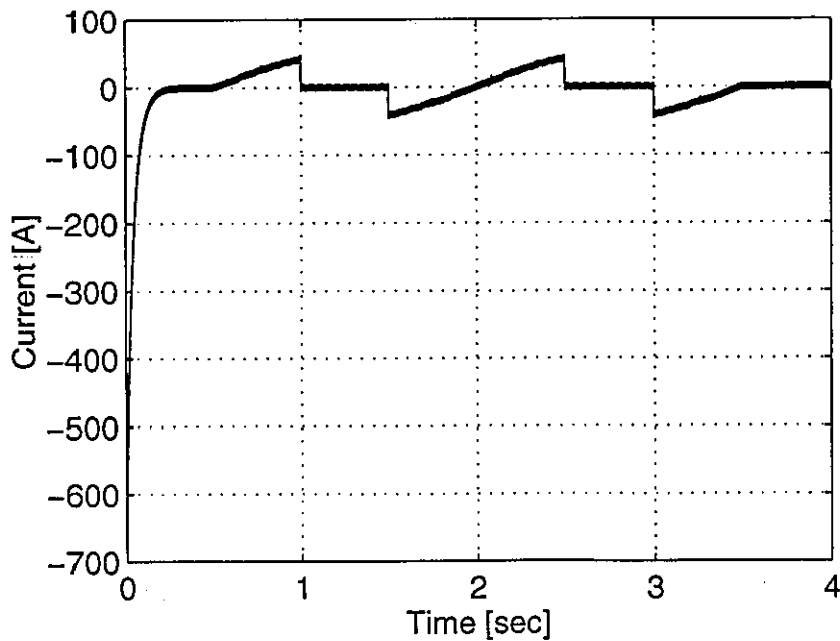


Figure 7-8 Computed results - Rotor phase current characteristic for indirect field-oriented control of a LIM

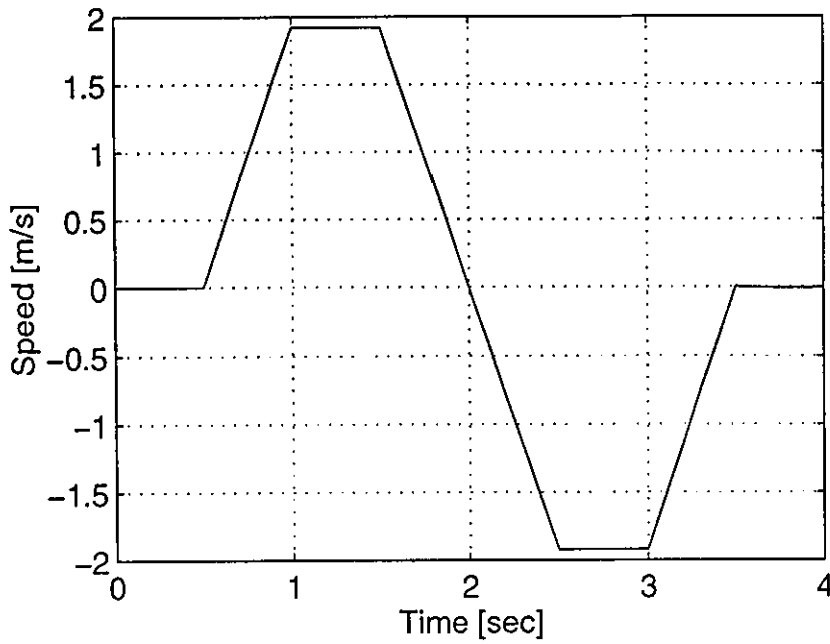


Figure 7-9 Computed results - Speed characteristic for direct field-oriented control of a LIM

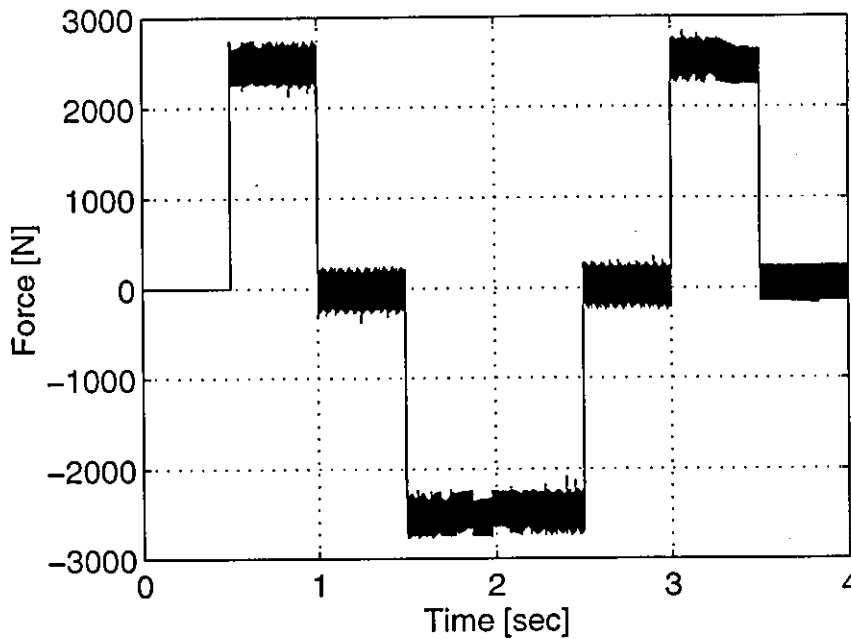


Figure 7-10 Computed results - Thrust characteristic for direct field-oriented control of a LIM

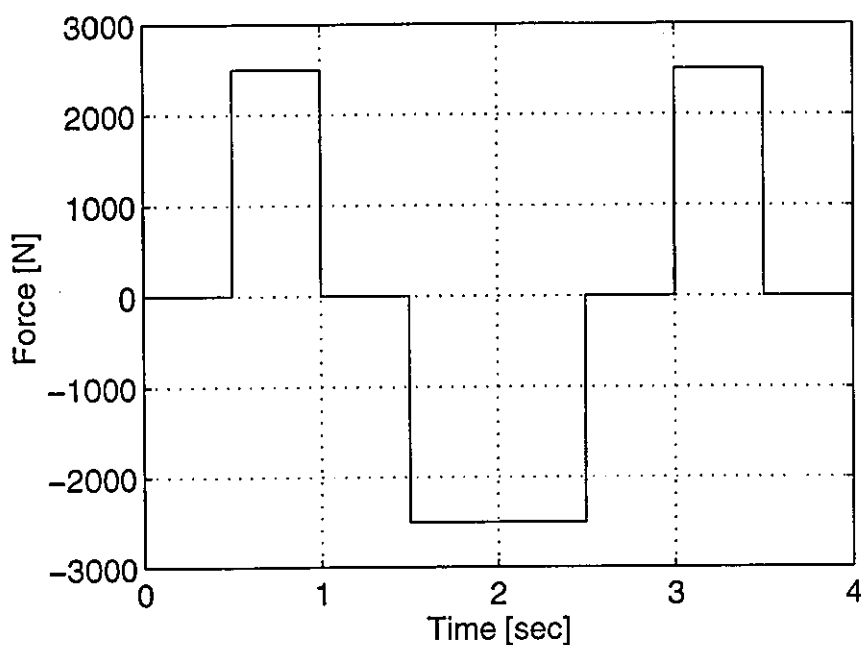


Figure 7-11 Computed results - Thrust demand characteristic for direct field-oriented control of a LIM

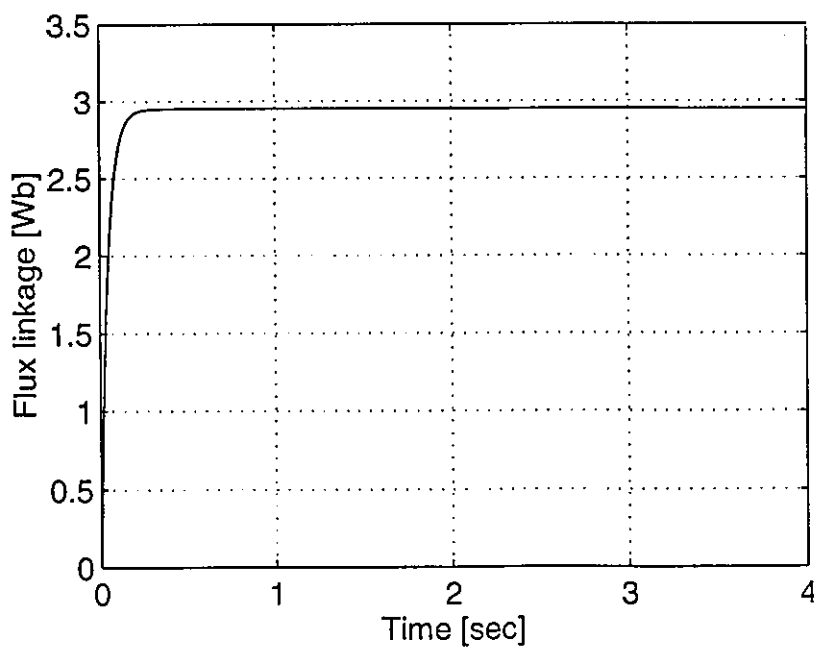


Figure 7-12 Computed results - Flux characteristic for direct field-oriented control of a LIM

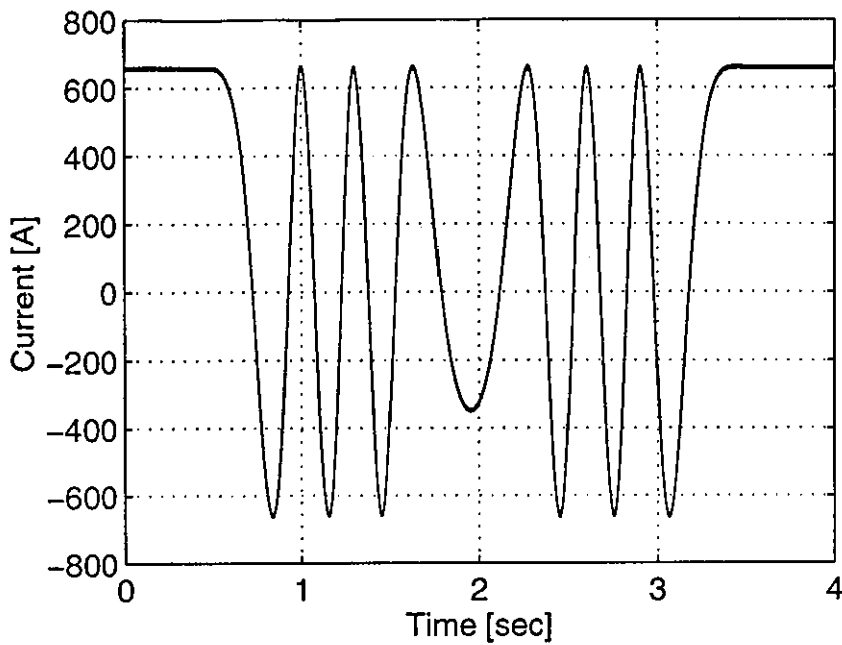


Figure 7-13 Computed results - Stator phase current characteristic for direct field-oriented control of a LIM

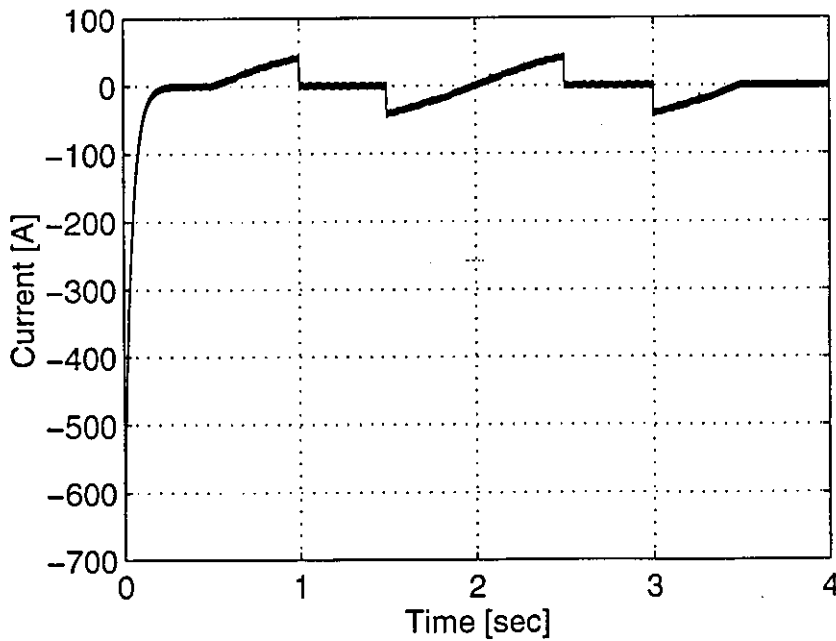


Figure 7-14 Computed results - Rotor phase current characteristic for direct field-oriented control of a LIM

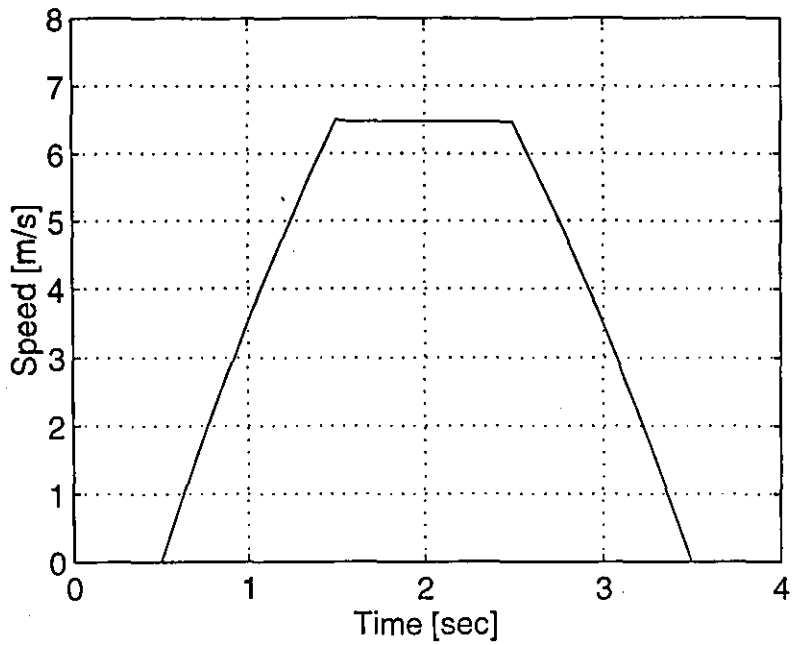


Figure 7-15 Computed results - Speed characteristic for indirect field-oriented control of a LIM at moderate speed

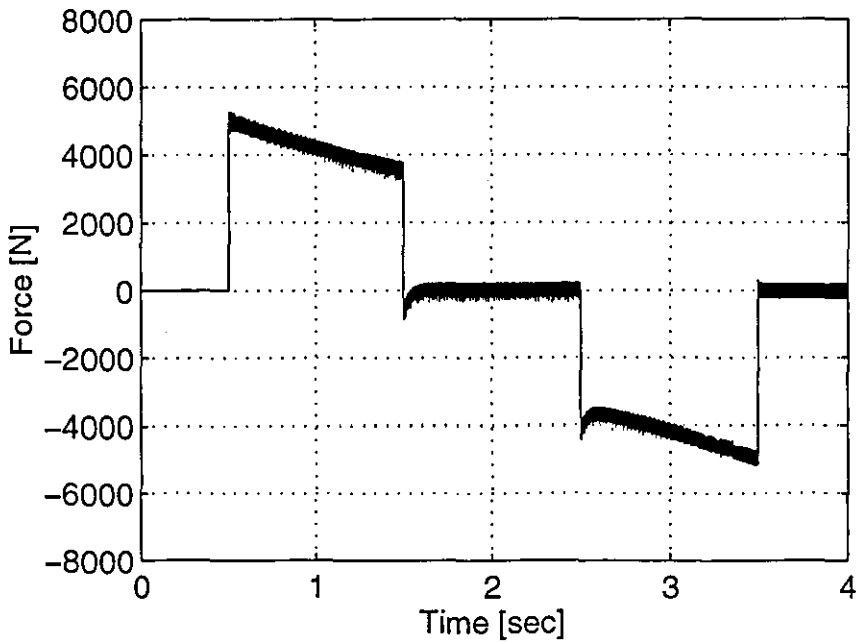


Figure 7-16 Computed results - Thrust characteristic for indirect field-oriented control of a LIM at moderate speed

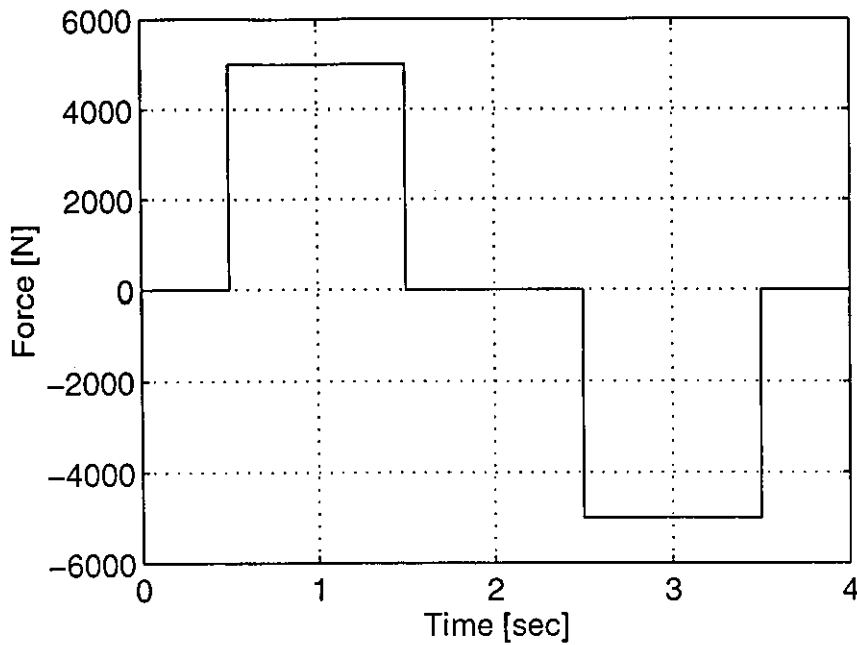


Figure 7-17 Computed results - Thrust demand characteristic for indirect field-oriented control of a LIM at moderate speed

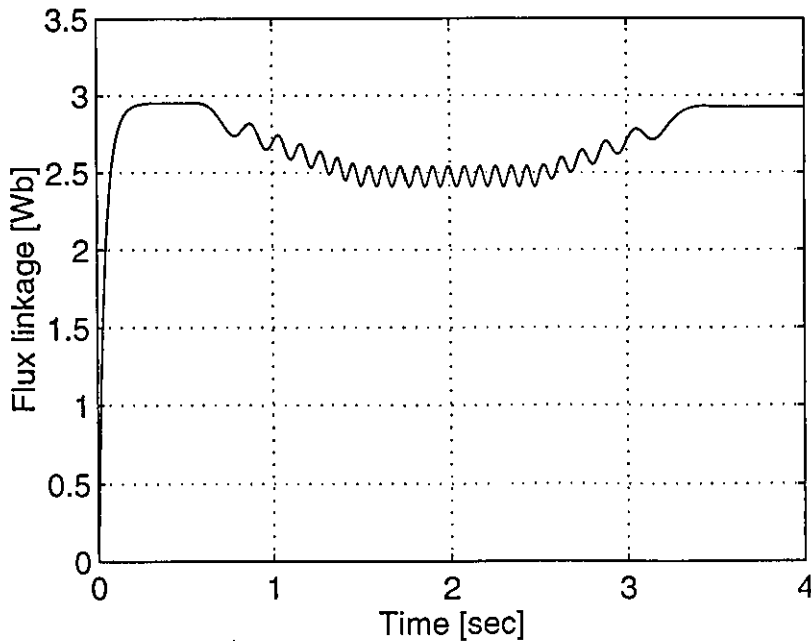


Figure 7-18 Computed results - Flux characteristic for indirect field-oriented control of a LIM at moderate speed

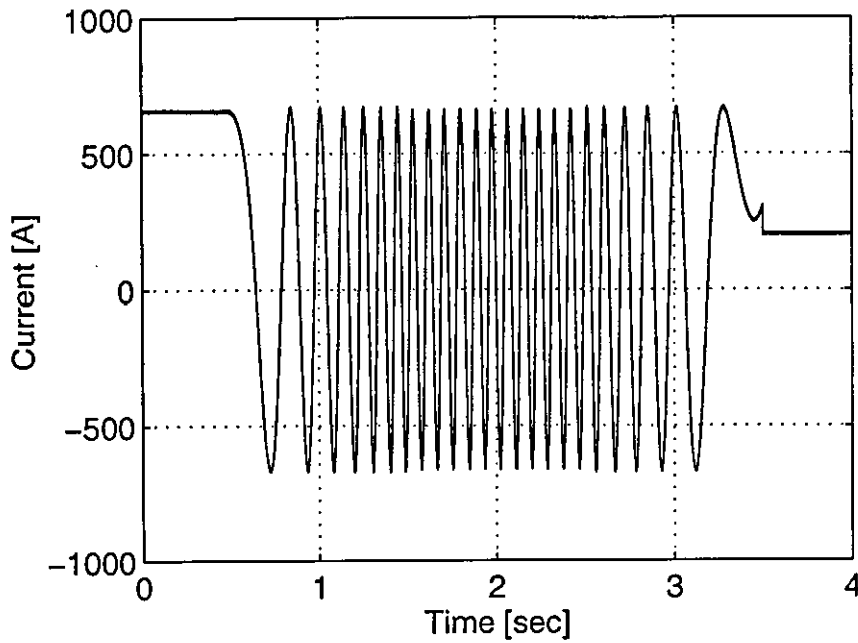


Figure 7-19 Computed results - Stator phase current characteristic for indirect field-oriented control of a LIM at moderate speed

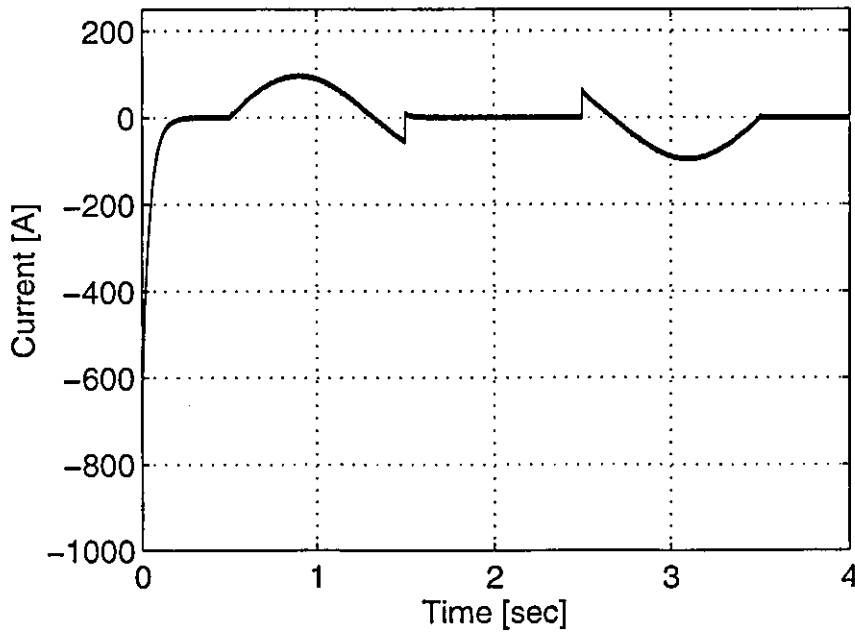


Figure 7-20 Computed results - Rotor phase current characteristic for indirect field-oriented control of a LIM at moderate speed

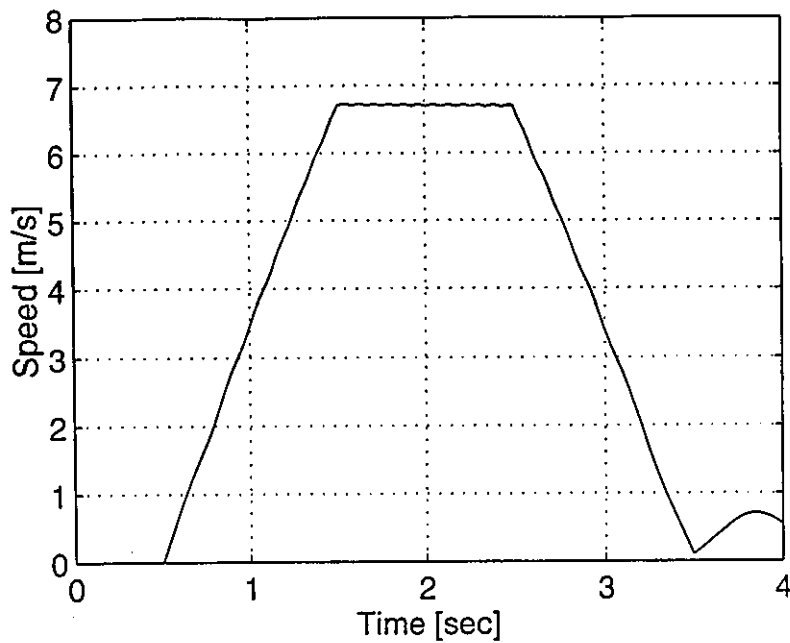


Figure 7-21 Computed results - Speed characteristic for direct field-oriented control of a LIM at moderate speed

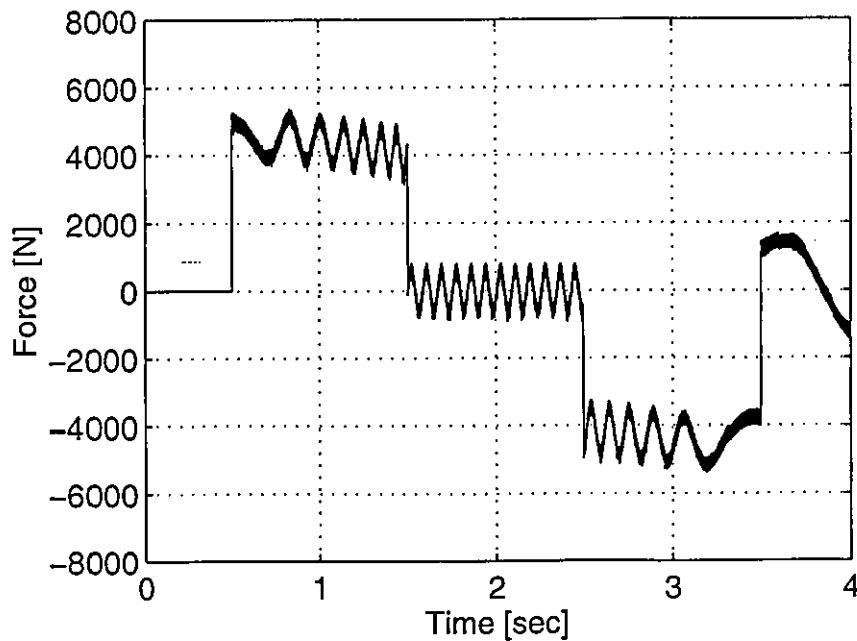


Figure 7-22 Computed results - Thrust characteristic for direct field-oriented control of a LIM

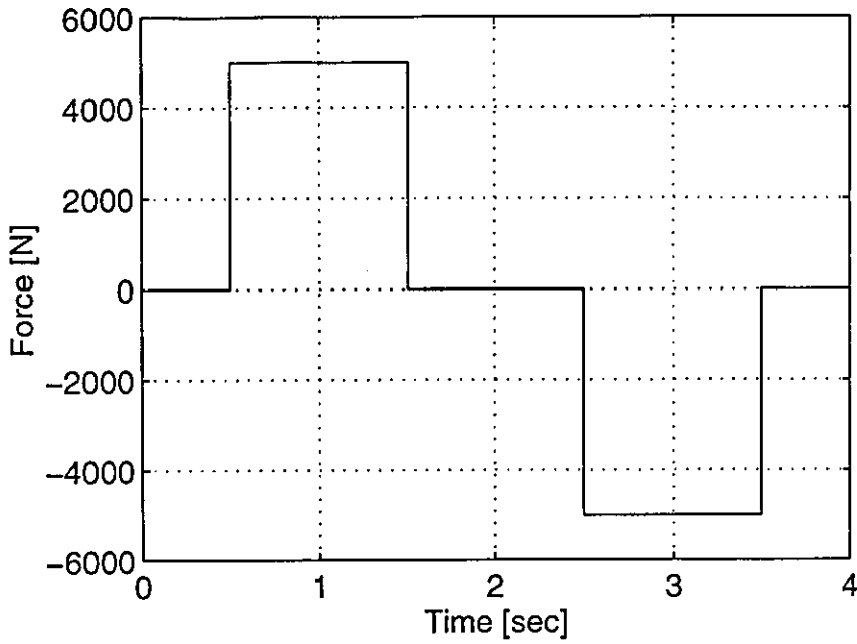


Figure 7-23 Computed results - Thrust demand characteristic for direct field-oriented control of a LIM

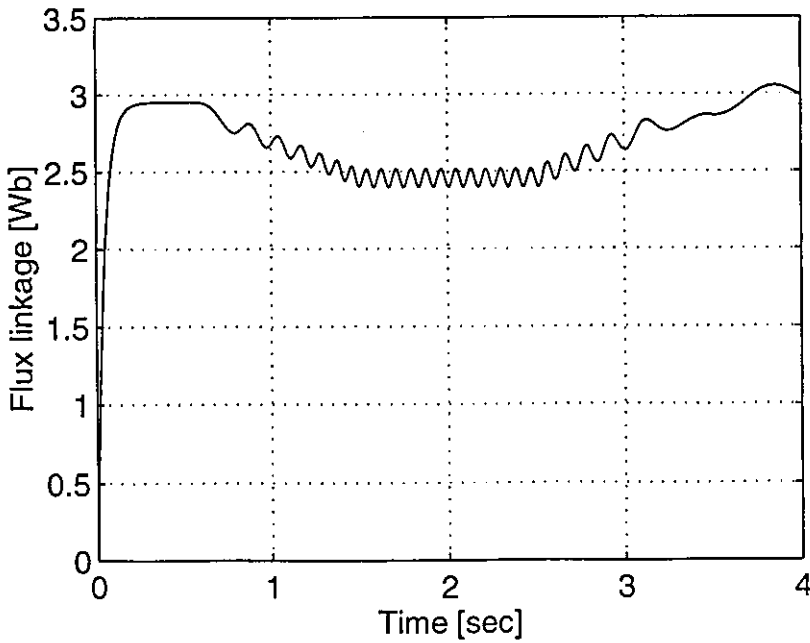


Figure 7-24 Computed results - Flux characteristic for direct field-oriented control of a LIM at moderate speed

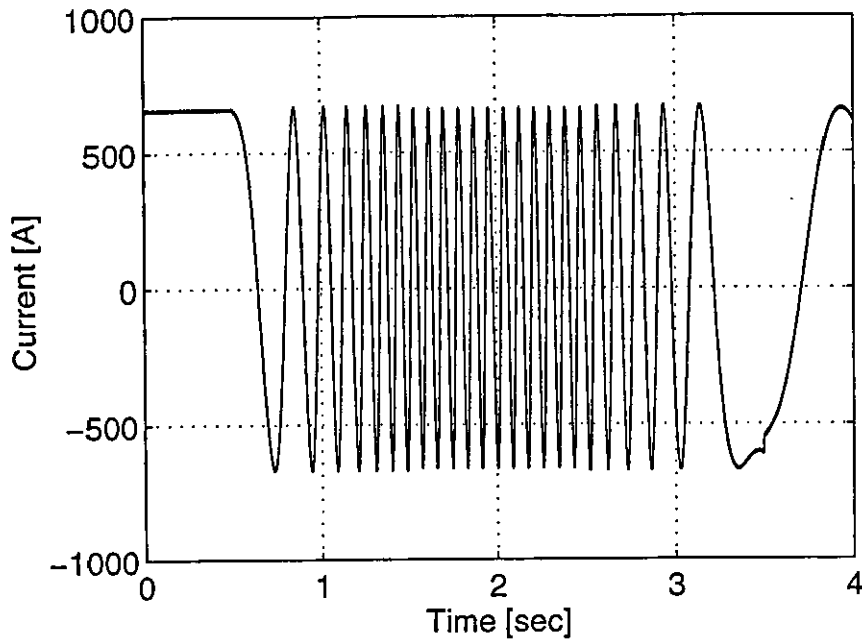


Figure 7-25 Computed results - Stator phase current characteristic for direct field-oriented control of a LIM at moderate speed

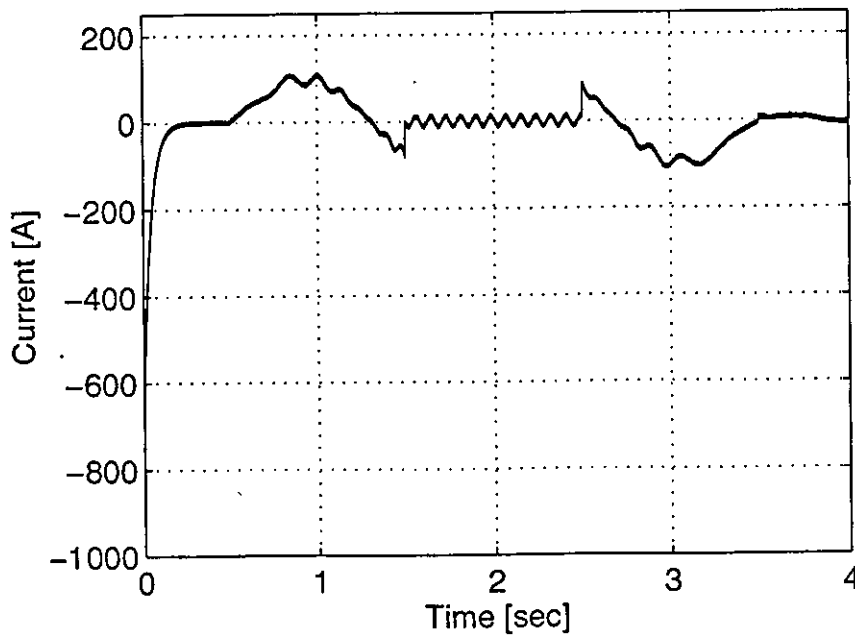


Figure 7-26 Computed results - Rotor phase current characteristic for direct field-oriented control of a LIM at moderate speed

PROGRAM DESCRIPTION

Simulating complex drive systems with many switching elements on a digital computer is complicated, because the system differential equations are often non-linear. In addition, frequent discontinuities in the values of the device parameters are introduced by the switching or control algorithms.

8.1 Numerical methods in electrical engineering

Existing simulation packages like *ACSL* and *ESL* are general purpose packages, which require the system equations to be entered in the form of differential equations or differential algebraic equations. However application-specific packages like *SPICE2* and *EMTP* are specifically for the simulation of electrical or electronic circuits, and provide convenient ready-to-use modules for typical components.

It was decided to simulate the inverter-fed induction motor drive with its vector control system in *FORTRAN77*. This allowed the program to be easily tailored to the needs of the simulation. All floating-point computations are done in double precision to ensure maximum accuracy.

8.2 Discrete events

The program written is able to handle efficiently discrete event discontinuities. It will treat these events according to their type - scheduled or conditional.

8.2.1 Scheduled

For a scheduled event like a known change in the input demand, the integration process is carried out to the instant where the scheduled event occurs, since this instant is known in advance.

8.2.2 Conditional

For a conditional event like a change in the conduction state of a device, the integration step may go beyond the instant where the event occurs, since this instant is not known in advance. Accurate breakpoint detection is needed to locate the instant of the conditional event, and the system equations then re-integrated to that point (refer to section 8.4). Although several devices can change state within any time step, the integration is carried out to the nearest event of all conditional events detected.

8.3 Simulation of switches

Most difficulties that arise in simulation programs are due to the different ways in which switches are modelled [55]. Diodes have their on and off states controlled by the power circuit. On the other hand, devices such as bipolar junction transistors, MOS field effect transistors, gate-turn-off thyristors and insulated gate bipolar transistors are turned on and off by control signals applied to their control terminal, and are therefore termed controllable switches.

In this simulation, diodes are considered to be semi-ideal switches, having a low resistance in the on-state and an infinite resistance in the off-state. Although, a small leakage current flows through the device when reverse biased, and it conducts with a small forward voltage drop, these values are normally negligibly small compared to the operating voltages and currents of the circuit.

An ideal controllable switch will block large forward and reverse voltages with zero current flow when off, conduct large currents with zero voltage drop when on, and switch between states instantaneously when triggered. Using the same arguments as for diodes, the switch is treated as a combination of an ideal and a two-valued resistor switch, with a low-resistance in its on-state and as an open circuit in the off-state.

The device switching times are short in comparison with the period of the operating frequency, and the switch action can be assumed to be instantaneous.

8.4 Breakpoint detection

To avoid any discontinuities, such as the introduction of a time-delay during switch operation due to a change in the state of the switch that could inadvertently effect the overall accuracy of the simulation, accurate breakpoint detection is required. In other words, the instant where the criteria for turn-on and turn-off are satisfied has to be accurately determined. Clearly, this instant will be a function of time itself, and also dependant on the current/voltage in the circuit.

8.4.1 Criteria for device turn-on and turn-off

The bias states of the devices is easily obtained from the branch voltage tensor $[V_B]$ of Eq.(4-6). However, their resistance has initially been set to the forward resistance values in the resistance tensor $[R_p]$, and the voltages are therefore only valid when these devices are conducting.

The conditions for device turn-on and turn-off are

- *Turn-on:* The device is forward biased (and gate-triggered).
- *Turn-off:* The device is turned-off as soon as its anode current attempts to go negative, or there is a change in switching conditions.

8.4.2 Iterative linear interpolation

Various different breakpoint detection methods have been highlighted [55]. In this simulation, breakpoint detection is carried out through the use of an iterative linear interpolation method in which the breakpoint is passed before it is detected. Once detected, the breakpoint is interpolated to evaluate a new integration step-length, and the system equations are re-integrated to that point. This process is repeated twice to ensure that sufficient accuracy is achieved in the breakpoint detection. The step-length is then reset to its initial value, to avoid small time steps before breakpoints and therefore to reduce the overall simulation time.

The required control signals are generated by tolerance band control and if, at the end of an integration step, there is a change in switching conditions, linear interpolation is implemented to evaluate the time instant when the current reached the upper or lower limit.

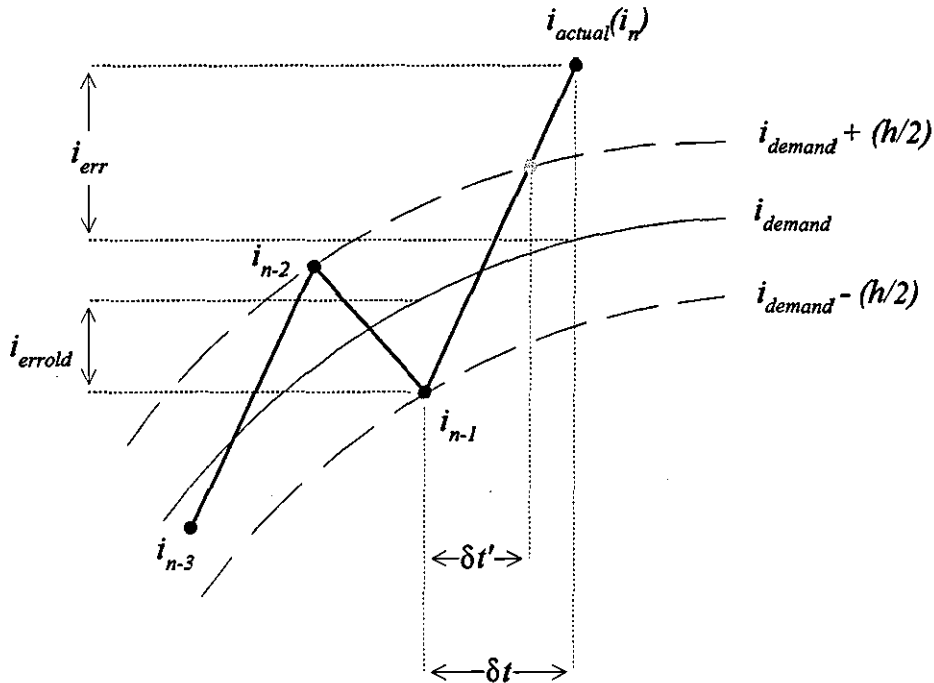


Figure 8-1 Linear interpolation

From Fig. 8-1,

$$\delta t' = \frac{(h / 2) - i_{errold}}{i_{err} - i_{errold}} \cdot \delta t$$

where, $\delta t'$ is the time from the start of the previous step to the instant at which current reaches the upper or lower limit,
 h is the specified tolerance band,
 i_{errold} is the error at the end of the previous step, and
 i_{err} is the error at the end of the present step.

The system equations are then re-integrated from the start of the previous step up to t' . The system topology is updated and the analysis proceeds as before.

Similarly, the current through each device is given by the first six components of the primitive current tensor $[I_p]$, which is updated at the end of every integration step. If the current through the device is negative at the end of an integration step, the time at which it went negative is evaluated from

$$\delta t' = \frac{i_{\text{previous}}}{i_{\text{previous}} - i_{\text{current}}} \delta t$$

where, $\delta t'$ is the time from the start of the previous step to the instant at which the device current is zero,

i_{previous} is the current at the end of the previous step, and

i_{current} is the current at the end of the present step.

The system equations are then re-integrated from the start of the previous step up to t' . The device states are updated, and the analysis proceeds as before.

8.5 Main program description

Outline flow charts for the program structure of each of the models described previously are given in Appendix E. Both the flowcharts and the documented-listings should be consulted in conjunction with the following program description.

For the complete inverter-motor system,

- The motor and inverter parameters, and also the integration step length and length of run, are read in from a file called "linmot.dat". A listing of this can be found in Appendix D.
- The initial conditions of the state variables and device states are defined.
- The phase equivalent circuit parameters of the induction motor are obtained from the per-phase equivalent circuit, with the initial quantities expressed in per-unit form.

- The inductance and rate-of-change of inductance terms that are functions of the rotor position are evaluated for the present rotor displacement x .
- The primitive tensor equations are initially constructed, followed by tensor transformations to produce the equations relevant to a particular inverter topology. The transformation tensor linking the basic network with the reduced network is dependant on the conduction state of the devices.
- All matrix operations such as multiplication, subtraction and matrix inversion are performed by the respective subroutines.
- The equations are arranged in a form suitable for numerical integration, and a step-by-step solution is performed using the *Runge-Kutta* subroutine to evaluate the new independent currents.
- The primitive current tensor is evaluated to provide the new stator and rotor currents and from these, the motor thrust F_x is calculated.
- The mechanical equation is integrated to give the rotor velocity v , and the displacement x of the rotor, which are used in the inductance calculations for the next integration step.
- The current derivative tensors and branch voltage tensors are determined to give the motor phase voltages.
- The control algorithms are implemented that generate the three-phase reference currents mutually displaced by 120° .
- The required control signals for the inverter switches are generated by tolerance band control.
- If there is a change in switching conditions, or the devices conduction state, the system equations are re-integrated using a reduced time step t' . The new circuit topology is evaluated, and the integration allowed to resume.
- The results are send to a plot-file, and the next integration step is performed.

8.5.1 Subroutines

Hysteresis - This subroutine generates the required drive signals for the inverter switches by tolerance band control. The dummy arguments for the subroutine are

ierra, ierrb, ierrc: the current error for phases *a*, *b* and *c* respectively.

h: the specified tolerance band.

lega, legb, legc: switching functions for branches *a*, *b* and *c* respectively.

A value of '1' denotes a switch in the top of the inverter leg, and a '-1' a switch in the bottom of the leg. It is assumed that only one switch in a leg is conducting at any time.

Turn_On - This subroutine determines the conduction state of the inverter switches and diodes. The dummy variables for the subroutine are

Trans, Diode: determines the device to be turned on.

lega, legb, legc: switching functions for phases *a*, *b* and *c* (see *Hysteresis* subroutine).

Ip: the primitive current tensor.

On, Don: an array holding the conduction state of the inverter switches and diodes respectively. A value of '1' indicates that device is conducting, and '0' non-conducting.

RungeKutta - This subroutine performs numerical integration on the system equations using a Runge-Kutta 4th-order method. The equations have to be arranged in the form suitable for numerical integration,

$$\frac{d}{dt} [i_{n+1}] = [Y][i_n] + [Const]$$

The dummy variables for the subroutine are

Noequ: the number of equations to be solved.

Firstt: the present simulation time.

Deltat: the integration step-length.

Init: a vector holding the initial conditions.

Const: a vector holding the constants of the differential equations.

Y: a square matrix containing the coefficients of the state-variables.

MatT - This subroutine takes the transpose of a matrix, where the dummy arguments are

Rows, Cols: the order of the matrix.

Mat: the matrix to be transposed.

Prod: the transposed matrix.

MatPreMul - This subroutine multiplies a matrix by a constant. The dummy arguments of the subroutine are

Rows, Cols: the order of the matrix.

Mat: the matrix to be multiplied.

Value: the multiplication constant.

Prod: the resultant matrix.

MatInv - This subroutine determines the inverse of a square matrix by the gaussian elimination method. The dummy variables are

N: the order of the square matrix.

AugN: the matrix to be inverted.

X: the inverted matrix.

If the determinant of the matrix to be inverted is zero, then the program flow is halted and the appropriate error message displayed.

MatMul - This subroutine multiplies two matrices together, where the dummy arguments are

Rows1, Cols1: the order of the first matrix.

Rows2, Cols2: the order of the second matrix.

Mat1: the first matrix.

Mat2: the second matrix.

Prod: the product matrix.

MatSub - This subroutine subtracts one matrix from another. The dummy arguments are

Rows, Cols: the order of the two matrices.

Mat1: the first matrix.

Mat2: the second matrix.

Prod: the resultant matrix.

MatAdd - This subroutine performs the addition of two matrices. The dummy arguments of the subroutine are

Rows, Cols: the order of the two matrices.

Mat1: the first matrix.

Mat2: the second matrix.

Prod: the resultant matrix.

8.6 Input data file structure

The input parameters are listed as they appear in the data file i.e. in a sequential order, and are categorised under subheadings.

8.6.1 Voltage-fed induction motor model

Simulation parameters

1. Startt - integration start-time (s)
2. Endt - integration end-time (s)
3. Deltat - integration step-length (s)
4. Dispint - sampling interval for results (s)

Motor specific-parameters

5. Rs - stator phase resistance (Ω)
6. L12 - stator phase leakage inductance (H)
7. Rr - rotor phase resistance (Ω)

8. L21 - rotor phase leakage inductance (H)
9. Lm - magnetizing inductance (H)
10. Poles - number of poles
11. Inertia - moment of inertia ($\text{kg}\cdot\text{m}^2$)
12. kf - rotor friction coefficient ($\text{Nm}\cdot\text{rad}^{-1}\cdot\text{s}^{-1}$)
13. Tl - load torque (Nm)

Voltage-source parameters

14. Vmax - peak amplitude of phase voltage (V)
15. Fs - supply frequency (Hz)
16. Pdif - displacement angle between stator phases ($^\circ$)

8.6.2 Quasi-square wave / Sinusoidal PWM inverter with inductive loading

Simulation parameters

1. Startt - integration start-time (s)
2. Endt - integration end-time (s)
3. Deltat - integration step-length (s)
4. Dispint - sampling interval for results (s)

Inverter parameters

5. Rf - supply resistance (Ω)
6. Rd - filter resistance (Ω)
7. Rt - switch/diode operational resistance (Ω)
8. Lf - supply inductance (H)
9. Cd - filter capacitance (F)
10. Vdc - supply voltage (V)

Load parameters

11. Rs - phase resistance (Ω)
12. Ls - phase self-inductance (Ω)

Quasi-square wave / Sinusoidal PWM parameters

- 13. Amd - peak amplitude of modulation waveform
- 14. Bmd - peak amplitude of carrier waveform
- 15. Fs - switching (modulation) frequency (Hz)
- 16. Pdif - displacement angle between phases ($^{\circ}$)

Linear interpolation parameters

- 17. Maxiter- maximum number of iterations

8.6.3 Quasi-square wave / Sinusoidal PWM inverter-fed induction motor*Simulation parameters*

- 1. Startt - integration start-time (s)
- 2. Endt - integration end-time (s)
- 3. Deltat - integration step-length (s)
- 4. Dispint - sampling interval for results (s)

Motor parameters

- 5. Rs - stator phase resistance (Ω)
- 6. L12 - stator phase leakage inductance (H)
- 7. Rr - rotor phase resistance (Ω)
- 8. L21 - rotor phase leakage inductance (H)
- 9. Lm - magnetizing inductance (H)
- 10. Poles - number of poles
- 11. Inertia - moment of inertia ($\text{kg}\cdot\text{m}^2$)
- 12. kf - rotor friction coefficient ($\text{Nm}\cdot\text{rad}^{-1}\cdot\text{s}^{-1}$)
- 13. Tl - load torque (Nm)

Inverter parameters

- 14. Rf - supply resistance (Ω)
- 15. Rd - filter resistance (Ω)

- 16. Rt - switch/diode operational resistance (Ω)
- 17. Lf - supply inductance (H)
- 18. Cd - filter capacitance (F)
- 19. Vdc - supply voltage (V)

Quasi-square wave / Sinusoidal PWM parameters

- 20. Amd - peak amplitude of modulation waveform
- 21. Bmd - peak amplitude of carrier waveform
- 22. Fs - switching (modulation) frequency (Hz)
- 23. Pdif - displacement angle between phases ($^\circ$)

Linear interpolation parameters

- 24. Maxiter- maximum number of iterations

8.6.4 Current-regulated PWM inverter-fed linear induction motor

Simulation parameters

- 1. Startt - integration start-time (s)
- 2. Endt - integration end-time (s)
- 3. Deltat - integration step-length (s)
- 4. Dispint- sampling interval for results (s)

Linear induction motor parameters

- 5. Rs - primary phase resistance (Ω)
- 6. L12 - primary phase leakage inductance (H)
- 7. Rr - secondary phase resistance (Ω)
- 8. L21 - secondary phase leakage inductance (H)
- 9. Lm - magnetizing inductance (H)
- 10. L - effective machine length (m)
- 11. Poles - number of poles
- 12. Ppitch - pole-pitch (m)
- 13. Mass - weight of moving member (kg)

- 14. kf2 - friction coefficient ($\text{N}\cdot\text{kg}^{-1}$)
- 15. Fl - load force (N)

Inverter parameters

- 16. Rf - supply resistance (Ω)
- 17. Rd - filter resistance (Ω)
- 18. Rt - switch/diode operational resistance (Ω)
- 19. Lf - supply inductance (H)
- 20. Cd - filter capacitance (F)
- 21. Vdc - supply voltage (V)

Current-regulated PWM parameters

- 22. Ismax - peak amplitude of primary phase current (A)
- 23. Fs - supply frequency (Hz)
- 24. h - tolerance band (A)
- 25. Pdif - displacement angle between phases ($^\circ$)

Linear interpolation parameters

- 26. Maxiter- maximum number of iterations

8.6.5 Vector control of a linear induction motor

Simulation parameters

- 1. Startt - integration start-time (s)
- 2. Endt - integration end-time (s)
- 3. Deltat - integration step-length (s)
- 4. Dispint - sampling interval for results (s)

Linear induction motor parameters

- 5. Rs - primary phase resistance (Ω)
- 6. L12 - primary phase leakage inductance (H)

7. R_r - secondary phase resistance (Ω)
8. L_{21} - secondary phase leakage inductance (H)
9. L_m - magnetizing inductance (H)
10. L - effective machine length (m)
11. Poles - number of poles
12. P_{pitch} - pole-pitch (m)
13. Mass - weight of moving member (kg)
14. k_f - friction coefficient ($N \cdot kg^{-1}$)
15. F_l - load force (N)

Inverter parameters

16. R_f - supply resistance (Ω)
17. R_d - filter resistance (Ω)
18. R_t - switch/diode operational resistance (Ω)
19. L_f - supply inductance (H)
20. C_d - filter capacitance (F)
21. V_{dc} - supply voltage (V)

Current-regulated PWM parameters

22. h - tolerance band (A)
23. P_{dif} - displacement angle between phases ($^\circ$)

Vector control parameters

24. F_{com} - force demand (N)
25. I_{mr} - magnetizing current (A)

Linear interpolation parameters

26. $Maxiter$ - maximum number of iterations

**CHAPTER
NINE
CONCLUSION**

This thesis describes a Fortran program, developed to model the transient and steady-state performance of a current-regulated PWM inverter-fed induction motor. The implementation of a field-oriented control strategy is also examined.

A direct-phase model for the induction motor was chosen in preference to the simplified two-axis d-q model, as it allowed the machine phase variables to be directly monitored and therefore, a wider range of operating conditions to be more conveniently studied. The computed results of the transient and steady-state characteristics of a voltage-fed induction motor were compared with experimental results obtained from the literature, and these were in very close agreement.

The tensor approach was used in the analysis of the inverter system, as it deals very efficiently with the changing topology of the inverter. The analysis was easily extended to include the motor equations, to provide a model of the overall system. Since a field-oriented controller requires instantaneous control of the phase currents, this was achieved using tolerance band control, so as to provide the necessary switching waveforms to drive the inverter switches.

For a low-speed LIM, it may be concluded, that the equivalent circuit of the conventional induction motor may be used, with the appropriate modifications made to the parameter values to take into account the so called 'end-effect'. The performance of a current-regulated PWM inverter-fed LIM drive was analysed and compared with experimental results obtained from published literature, and these were in close agreement.

The performance of the inverter-motor drive was greatly improved with the use of a closed-loop control strategy. The direct and indirect methods of vector control, and the Natural Field Orientation control principle, which is based on the indirect measurement of the air-gap voltage, were investigated. With the latter control scheme it was not necessary to evaluate the rotor flux, and the system was not dependant on the rotor parameters. The former schemes are adapted and applied to the control of a LIM, to give a decoupled control of the thrust and flux.

Simulated results for the performance of the LIM drive under constant flux operation for the direct and indirect schemes are obtained. Both the systems were shown to have a good thrust response at low speed, down to zero speed, and it is hoped that further research will show that the system will give good all-round performance.

FURTHER WORK

A complete mathematical model of the inverter-motor drive has been developed and this can be used to study the transient and steady-state performance characteristics of the overall system.

- Having implemented a vector-control scheme for the inverter-motor system, the next step will be to analyse the all-round performance of the system, and to build an experimental rig to validate the system thoroughly.
- Natural Field Orientation offers an alternative method of field-oriented control, with its inherent simplicity and distinct advantages over the direct and indirect methods of vector control. The next step will be to investigate the performance of the natural field-oriented control system when applied to the control of a linear induction motor, and to validate these results experimentally.

REFERENCES

- [1] Al-Nimma, D.A., "Digital computer analysis of variable-frequency inverter-fed induction motor drive system", Ph.D. Thesis, Loughborough University of Technology, England, 1979
- [2] Duncan, J., "Linear induction motor-equivalent-circuit model", *IEE Proc.*, Vol. 130, Pt. B, No. 1, January 1983, pp. 51-57
- [3] Kron, G., *Equivalent Circuits of Electric Machinery*, Dover, 1967
- [4] Adkins, B., *The General Theory of Electrical Machines*, Chapman and Hall, London, 1957
- [5] Blease, I., Bhatia, R., and Pai, R.M., "Applying linear motors in material handling", *Maschine Design*, Vol. 61, No. 1, January 1989, pp. 91-96
- [6] Abdon, G.H., and Sherif, S.A., "Theoretical and experimental design of linear induction motors in automated manufacturing systems", *IEEE Trans. on Industry Applications*, Vol. IA-27, No. 2, March/April 1991, pp. 286-293
- [7] McLean, G.W., "Review of recent progress in linear motors", *IEE Proc.*, Vol. 135, Pt. B, No. 6, November 1988, pp. 380-416
- [8] Laithwaite, E.R., *Induction Machines for Special Purposes*, George Newnes Ltd, London, 1966
- [9] Boldea, I., and Nasar, S.A., *Optimum Goodness Criterion for Linear Induction Motor Design*, 1976, pp. 89-92
- [10] Russell, R.L., and Norsworthy, K.H., "Eddy currents and wall losses in screened-rotor induction motors", *IEE Proc.*, Vol. 105, Pt. A, 1968, pp. 163-175

-
- [11] Bolopion, A., Poloujadoff, M., and Findlay, R.D., "Models for balanced voltage operation of linear induction motors", *IEEE Trans. on Energy Conversion*, Vol. EC-1, No. 3, September 1986, pp. 118-122
- [12] Eastham, A.R., and Katz, R.M., "The operation of a single-sided linear induction motor with squirrel-cage and solid-steel reaction rails", *IEEE Trans. on Magnetics*, Vol. MAG-16, No. 5, September 1980, pp. 722-724
- [13] Poloujadoff, M., *The Theory of Linear Induction Machinery*, Oxford University Press, 1980
- [14] Yamamura, S., Itoh, H., and Ishikawa, Y., "Theories of the linear induction motor and compensated linear induction motor", *IEEE Trans. on Power Apparatus and Systems*, Vol. PAS-91, No. 1, January/February 1972, pp. 1700-1710
- [15] Iwamoto, M., Sakabe, S., Itani, K., Kitagawa, K., and Utsumi, G., "Experimental and theoretical study of high-speed single-sided linear induction motors", *IEE Proc.*, Vol. 128, Pt. B, No. 6, November 1981, pp. 306-312
- [16] Gieras, J.F., "Simplified theory of double-sided linear induction motor with squirrel-cage elastic secondary", *IEE Proc.*, Vol. 130, Pt. B, No. 6, November 1983, pp. 424-430
- [17] Gieras, J. F., Dawson, G. E., and Eastham, A.R., "A new longitudinal end effect factor for linear induction motors", *IEEE Trans. on Energy Conversion*, Vol. EC-2, No. 1, March 1987, pp. 152-159
- [18] Pai, R.M., Boldea, I., "A complete equivalent circuit of a linear induction motor with sheet secondary", *IEEE Trans. on Magnetics*, Vol. MAG-24, No.1, January 1988, pp. 639-652
- [19] Gieras, J.F., Dawson, G.E., and Eastham, A.R., "Performance calculation for single-sided linear induction motors with a double-layer reaction rail under constant current excitation", *IEEE Trans. on Magnetics*, Vol. MAG-22, No. 1, January 1986, pp. 54-62
-

-
- [20] Boldea, I., and Nasar, S.A., *Linear Electric Motors: Theory, Design, and Practical Applications*, Prentice-Hall, London, 1987.
- [21] Laithwaite, E.R., *Propulsion without Wheels*, The English Universities Press, 1970
- [22] Luda, G., *Drehstrom-Asynchron-Linearantriebe*, Vogel-Verlag, Wuerzburg, 1981
- [23] Gibbs, W.J., *Conformal Transformations in Electrical Engineering*, Chapman and Hall, London, 1958
- [24] Ooi, B.T., "A generalized machine theory of the linear induction motor", *IEEE Trans. on Power Apparatus and Systems*, Vol. PAS-92, No. 1, January 1973, pp. 1252-1259
- [25] Ooi, B.T., and White, D.C., "Traction and normal forces in the linear induction motor", *IEEE Trans. on Power Apparatus and Systems*, Vol. PAS-89, No. 4, April 1970, pp. 638-645
- [26] Wu, B., Dewan, S.B., and Slemon, G.R., "PWM-CSI inverter for induction motor drives", *IEEE Trans. on Industry Applications*, Vol. IA-28, No. 1, January/February 1992, pp. 64-71
- [27] Jarc, D.A., Connors, D.P., "Variable frequency drives and power factor", *IEEE Trans. on Industry Applications*, Vol. IA-21, No. 4, May/June 1985, pp. 771-779
- [28] Kron, G., *Tensors for Circuits*, Dover, 1959
- [29] Dirker, U., "AC-flux-vector control improves induction motor performance", *Powerconversion and Intelligent Motion*, Vol. 21, No. 6, June 1995, pp. 52, 55-59
- [30] Detering, R.L., "Flux vector control for AC motors", *Machine Design*, Vol. 61, No. 9, September 1989, pp. 176-178
-

- [31] Ogino, Y., Murakami, Y., Ohishi, K., and Nakaoka, M., "High performance ultra-low speed control of an inverter-fed linear induction motor using vector control scheme", *Proc. of the Fifth European Conference on Power Electronics and Applications*, Brighton, England, Vol. 5, September 1993, pp. 464-467
- [32] Aaltonen, M., Tiitinen, P., Lalu, J., and Heikkila, S., "Direct torque control of AC motor drives", *ABB Review*, No. 3, 1995, pp. 19-24
- [33] Pohjalainen, P., Tiitinen, P., and Lalu, J., "The next generation motor control method - Direct Torque Control, DTC", *Proc. European Power Electronics Chapter Symposium. Electric Drive Design and Applications*, Lausanne, Switzerland, October 1994, pp. 115-120
- [34] Brandstetter, P., "Control methods for induction motor drives with high dynamic performance", *Proc. European Power Electronics Chapter Symposium. Electric Drive Design and Applications*, Lausanne, Switzerland, October 1994, pp. 337-342
- [35] Zhong, H.Y., Messinger, H.P., and Rashad, M.H., "A new microcomputer based direct torque control system for three phase induction motor", *IEEE Trans. on Industry Applications*, Vol. IA-27, No. 2, March/April 1991, pp. 294-298
- [36] Bausch, H., "Flux-estimation of a PWM inverter-fed torque-controlled induction machine based on terminal quantities", *Proc. International Conference on Electrical Machines*, September 1992, pp. 833-837
- [37] Akin, E., "Vector control of induction motor through rotor flux orientation with stator flux components as reference", *Proc. International Conference on Electrical Machines*, September 1992, pp. 853-857
- [38] Kreindler, L., Moreira, J.C., Testa, A., and Lipo, T.A., "Direct field orientation controller using the stator phase voltage third harmonic", *IEEE Trans. on Industry Applications*, Vol. IA-30, No. 2, March/April 1994, pp. 441-447
-

- [39] Lipo, T.A., "Flux sensing and control of static ac drives by the use of flux coils", *IEEE Trans. on Magnetics*, Vol. **MAG-13**, No. 5, September 1977, pp. 1403-1408
- [40] Ohtani, T., Takada, N., and Tanaka, K., "Vector control of induction motor without shaft encoder", *IEEE Trans. on Industry Applications*, Vol. **IA-28**, No. 1, January/February 1992, pp.
- [41] Yang, G., and Chin, T. H., "Adaptive-speed identification scheme for a vector controlled speed sensorless inverter-induction motor drive", *IEEE Trans. on Industry Applications*, Vol. **IA-29**, No. 4, July/August 1993, pp. 820-824
- [42] Kubota, H., "Speed sensorless field-oriented control of induction motor with rotor resistance adaptation", *IEEE Trans. on Industry Applications*, Vol. **IA-30**, No. 5, September/October 1994, pp. 1219-1224
- [43] Joensson, R., "Natural field orientation - a new voltage control system for the AC induction motor", *Proc. of the Sixteenth International Intelligent Motion (Motor-Con) Conference*, Long Beach, USA, Vol. **16**, October 1989, pp. 140-155
- [44] Joensson, R., "Measurements on a new AC induction motor control system", *Proc. of the Third European Conference on Power Electronics and Applications*, Aachen, West Germany, Vol. **3**, October 1989, pp. 17-22
- [45] Joensson, R., "Natural field orientation (induction motor control)", *Proc. of the Eighteenth International Intelligent Motion Conference*, Philadelphia, USA, Vol. **18**, October 1990, pp. 141-55
- [46] Joensson, R., "Improved natural field orientation control of an AC induction motor", *Powerconversion and Intelligent Motion*, Vol. **17**, No. 3, March 1991, pp. 22-29
-

- [47] Joensson, R., "Natural field orientation (NFO) provides sensorless control of AC induction servo motors", *Powerconversion and Intelligent Motion*, Vol. 21, No. 6, June 1995, pp. 44-51
- [48] "Self tuning drives: the next technology step ?", *Drives and Control*, Vol. 10, No. 1, January 1994, p. 29
- [49] Khambadkone, A.M., and Holtz, J., "Vector controlled induction motor drive with a self-commissioning scheme", *IEEE Trans. on Industrial Electronics*, Vol. IA-38, No. 5, October 1991, pp. 322-327
- [50] Rubin, N.P., Harley, R.G., and Rashad, M.H., "Evaluation of various slip estimation techniques for an induction machine operating under field-oriented control conditions", *IEEE Trans. on Industry Applications*, Vol. IA-28, No. 6, November/December 1992, pp. 1367-1375
- [51] De Doncker, R.W., and Novotny, D.W., "The Universal Field Oriented Controller", *Proc. of the Twenty-Third IEEE-IAS Annual Meeting Conference*, Pittsburgh, USA, Vol. 23, October 1988, pp. 450-456
- [52] Profumo, F., Griva, G., Pastorelli, M., Moreira, J., and De Doncker, R.W., "Universal Field Oriented Controller based on air gap flux sensing via third harmonic stator voltage", *IEEE Trans. on Industry Applications*, Vol. 30, No. 2, March/April 1994, pp. 448-455
- [53] Piana, G., and Harley, R.G., "An aid for teaching field oriented control applied to induction machines", *IEEE Trans. on Power Systems*, Vol. 4, No. 3, August 1989, pp. 1258-1262
- [54] Ogasawara, S., Akagi, H., and Nabae, A., "The generalized theory of indirect vector control for AC machines", *IEEE Trans. on Industry Applications*, Vol. IA-24, No. 3, May/June 1988, pp. 470-478
- [55] Mohan, N., Robbins, W.P., and Undeland, T.M., "Simulation of power electronic and motion control systems - an overview", *Proc. of the IEEE*, Vol. 82, No. 8, August 1994, pp. 1287-1302
-

BIBLIOGRAPHY

Bishop, R.H., *Modern Control Systems Analysis and Design Using MATLAB*, Addison-Wesley, Workingham, 1993

Dyck, V.A., *FORTRAN 77 - An Introduction to Structured Problem Solving*, Preston Publishing Co., 1984.

Edwards, J.D., *Electrical Machines and Drives*, Macmillan, Basingstoke, 1991.

Edwards, J.D., *Electrical Machines*, International Textbook Co. Ltd, Aylesbury, 1973.

Fransua, A. and Magureanu, R., *Electrical Machines and Drive*, Technical Press Oxford, Oxford, 1984.

Gerald, C.F., *Applied Numerical Analysis - 2nd ed.*, Addison-Wesley, London, 1978.

Gibbs, W.J., *Tensors in Electrical Machine Theory*, Chapman and Hall, London, 1952

Gibbs, W.J., *Electrical Machine Analysis using Tensors*, Pitman, 1967

Griffiths, D.V., *Numerical Methods for Engineers*, Blackwell Scientific Publications, Oxford, 1991.

Laithwaite, E.R., *Linear Electric Motors*, Mills and Boon, 1971.

Lander, C.W., *Power Electronics - 3rd ed.*, McGraw-Hill International Editions, 1993.

Mohan, N., Undeland, T.M. & Robbins, W.P. *Power Electronics : Converters, Applications, and Design*, Wiley, New York, 1989.

Monro, D.M., *A Crash Course in Fortran 77*, Edward Arnold, London, 1989.

Robert, S., *Electric Power System Components*, Van Nostrand Reinhold, London, 1979.

Jones, C.V., *Unified Theory of Electrical Machines*, Butterworths, 1967.

Lee, R., and Wilson, L., *Electronic Transformers And Circuits - 3rd ed.*, Wiley, New York, 1988.

Slemon, G.R., and Straughen, A., *Electric Machines*, Addison-Wesley, London, October 1982.

De Vahl Davis, G., *Numerical Methods in Engineering & Science*, Chapman and Hall, London, 1986.

Yamamura, S., *Theory of Linear Induction Motors*, Wiley, New York, 1972.

**DERIVATION OF THE PHASE PARAMETERS FROM THE PER-PHASE
EQUIVALENT CIRCUIT**

The following transformations convert the per-unit equivalent circuit parameters of the induction motor shown in Fig.2-1, into the phase parameters expressed in Ohms and Henrys.

$$\text{Base impedance } Z_b = \frac{\text{rated phase voltage}}{\text{rated phase current}}$$

The supply angular frequency is given by $\omega = 2\pi f_s$,
where f_s is the supply frequency.

$$L_s = \frac{Z_b}{\omega} \left(X_{ls} + \frac{2}{3} X_m \right)$$

$$M_s = \frac{Z_b X_m}{3\omega}$$

$$L_r = \frac{Z_b}{\omega} \left(X_{lr} + \frac{2}{3} X_m \right)$$

$$M_r = \frac{Z_b X_m}{3\omega}$$

$$M_{sr} = \frac{2}{3} Z_b X_m$$

$$R_s = Z_b R_s$$

$$R_r = Z_b R_r$$

FLUX DENSITY CALCULATIONS

The peak value of magnetic flux density in the air-gap of a single-sided LIM, neglecting saturation effects, is [22, 23]

$$B_s = \frac{E}{4\sigma_k \alpha_i N k_w f_s \tau 2a}$$

where

$$\alpha_i \approx \frac{2}{\pi}$$

$$\sigma_k \approx \frac{\pi\sqrt{2}}{4}$$

The air-gap voltage E is evaluated from the modified equivalent circuit of the LIM shown in Fig.3-3, which takes longitudinal end-effects into account by modifying the emf across the mutual impedance [2]. Alternatively, the air-gap flux density can be expressed in terms of the magnetizing current and branch impedance as

$$B_s = \frac{L'_m i_{mr}}{N k_w \tau 2a}$$

where L'_m is the modified value of the magnetizing inductance given by Eq.(3-21).

At synchronous speed, no current is induced in the rotor conductors and the air-gap magnetic field is therefore entirely due to the magnetization currents flowing in the stator windings. Hence, the calculated value of peak flux density in the air-gap of the test LIM, for an input current $i_s = 465$ A rms and frequency 10Hz, at slip $s = 0$, is

$$B_s = \frac{0.00388 \times \sqrt{2} \times 465}{96 \times 0.958 \times 0.287 \times 0.216}$$

$$= \underline{\underline{0.45 \text{ T}}}$$

SYSTEM PARAMETERS

C.1 Induction motor parameters*Nameplate details*

Power rating	= 0.75kW
Line voltage (delta-connected stator)	= 220V, 50Hz
Number of pole pairs, p	= 3
Motor inertia, J	= 0.045kgm ²

Equivalent circuit and phase parameters

Stator and rotor resistance, R_s, R_r	= 5.09 Ω
Leakage inductances of stator and rotor windings, L_{ls}, L_{lr}	= 0.034H
Excitation inductance, L_m	= 0.697H
Self-inductances of stator and rotor windings, L_s, L_r	= 0.499H
Mutual inductances between stator phases and between rotor phases, M_s, M_r	= 0.233H
Maximum mutual inductance between 3-phase stator and rotor circuits, M_{sr}	= 0.465H

Induction motor performance parameters

Rated torque	= 7.0Nm
Steady-state torque on no-load	= 2.09Nm

C.2 Linear induction motor parameters

These parameters are for a large single-sided linear induction motor with a double layer secondary i.e. aluminium and steel, developed for an urban transit system using steel wheels on rail suspension [2]. The secondary iron is laminated to avoid saturation over the range of interest, and to ensure that the equivalent circuit constants were not significantly influenced by frequency.

Core construction

Active length, L	= 1.896m
Active width, $2a$	= 0.216m
Active depth, h	= 0.099m

Winding details

Number of phases, m	= 3
Number of poles, $2p$	= 6
Pole pitch, τ	= 0.2868m
Connection	= Wye
Series turns / phase, N	= 96
Slots / pole / phase, q	= 4

Reaction rail

Aluminium cap width, $2c$	= 0.3m
Aluminium cap thickness, d	= 0.0045m
Back iron width, w	= 0.240m
Back iron thickness, h_{sec}	= 0.0375m

Operating conditions

Nominal air-gap, g	= 8 - 11mm
Primary weight, $mass$	= 640kg
Nominal supply voltage, V_{dc}	= 600V dc
Nominal supply current, i	= 465A

Equivalent circuit parameters

Primary resistance, R_s	= 0.038 Ω
Primary leakage inductance, L_{ls}	= 0.00104H
Secondary resistance referred to primary, R_r	= 0.109 Ω
Secondary leakage inductance referred to primary, L_{lr}	= 0.0002H
Magnetizing inductance, L_m	= 0.00449H

C.3 Inverter parameters*Filter branch*Smoothing capacitor, C_d = 5000 μ FResistance, R_d = 0.05 Ω *Source impedance*Resistance, R_f = 0.5 Ω Inductance, L_f = 0.02H*Switch/diode operational resistance*Resistance, R_s = 0.001 Ω *Inverter supply voltage*Inverter supply voltage, V_{dc} = 380V dc

APPENDIX D

SIMULATION DATA FOR A VECTOR-CONTROLLED LIM DRIVE

0.0d0 1.0d0 0.00001d0 0.001d0 (simulation parameters)
0.038d0 0.00104d0 0.109d0 0.0002d0 0.00449d0
1.722d0 6 0.287d0 640.0d0 0.05d0 50.0d0 (LIM parameters)
0.5d0 0.05d0 0.001d0 0.02d0 5000d-6 380.0d0 (inverter parameters)
5.0d0 120.0d0 (current-regulated PWM parameters)
2500.0d0 657.0d0 (vector control parameters)
5 (interpolation parameters)

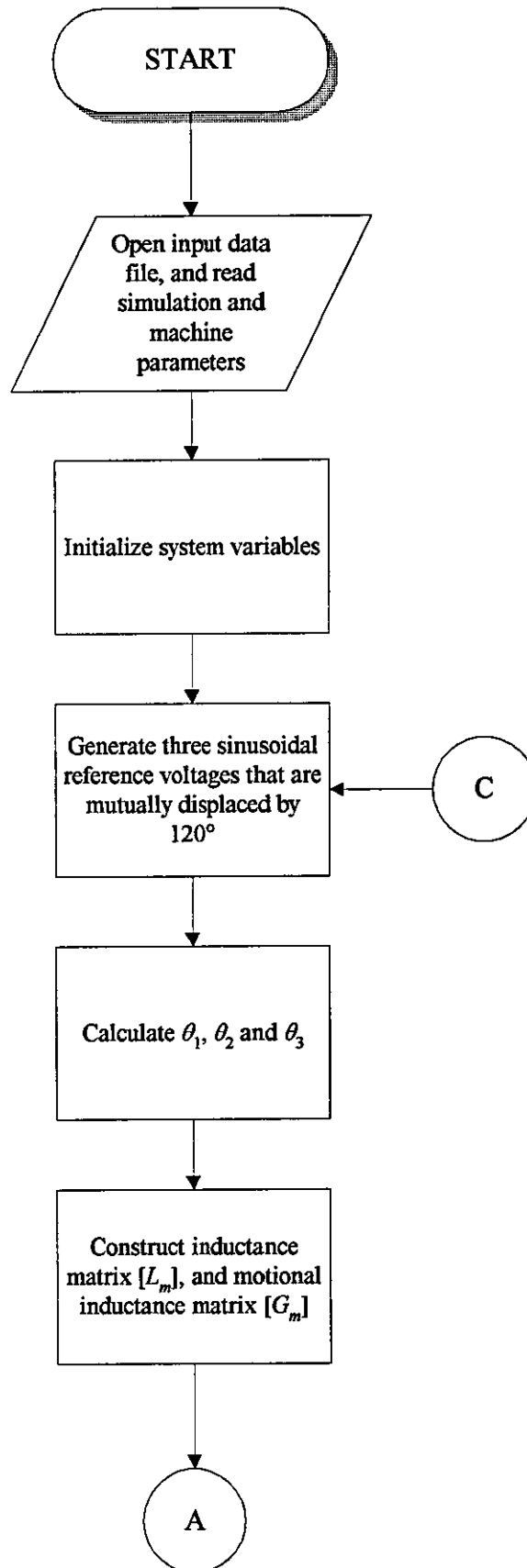
PROGRAM FLOWCHARTS

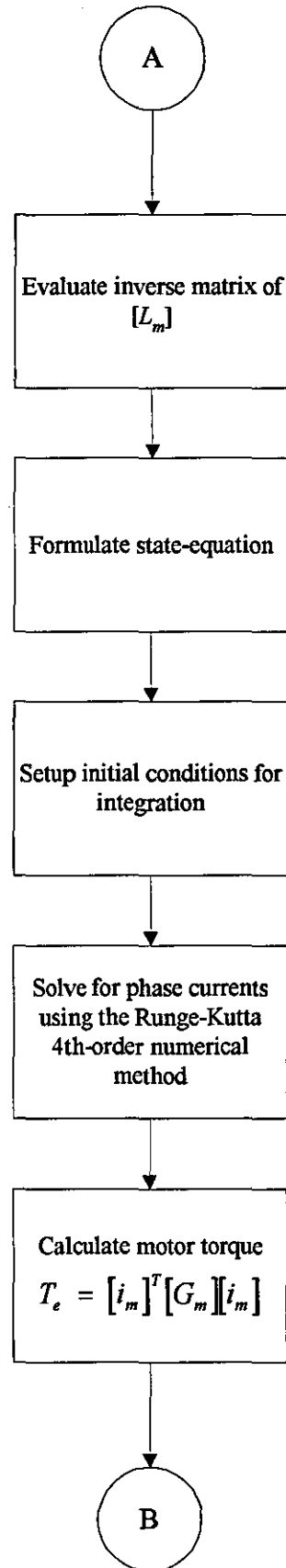
E.1 Voltage-fed induction motor..... 141

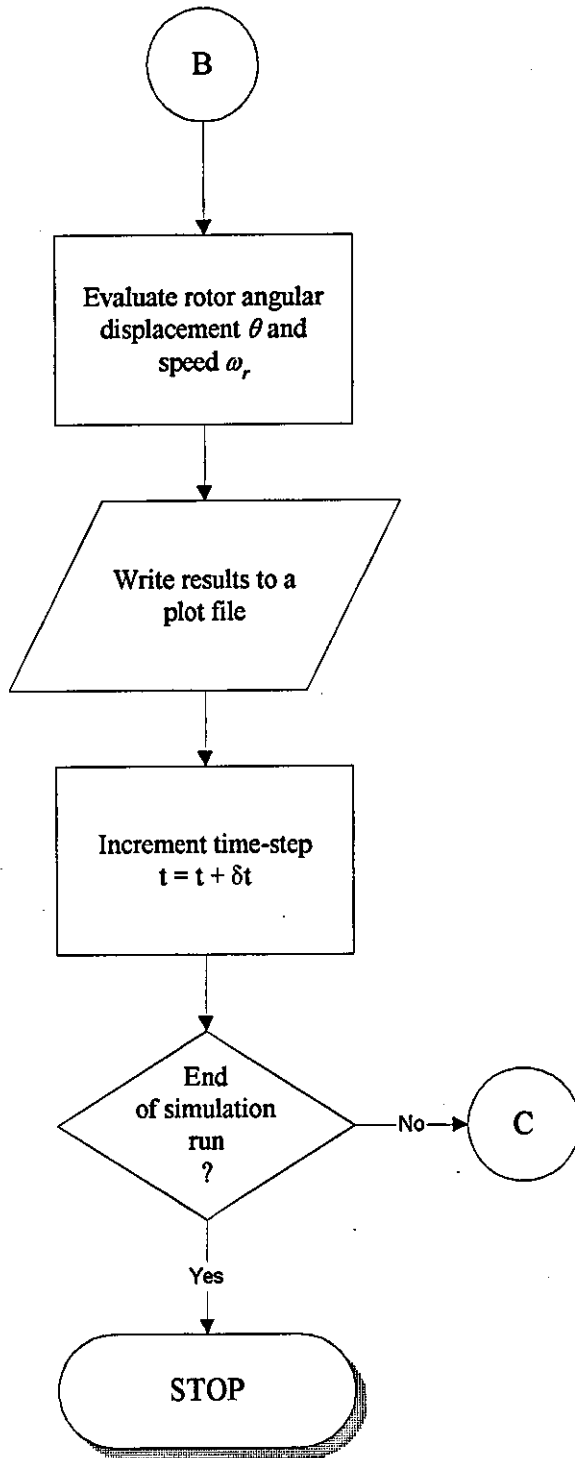
E.2 Inductively-loaded voltage-source inverter..... 144

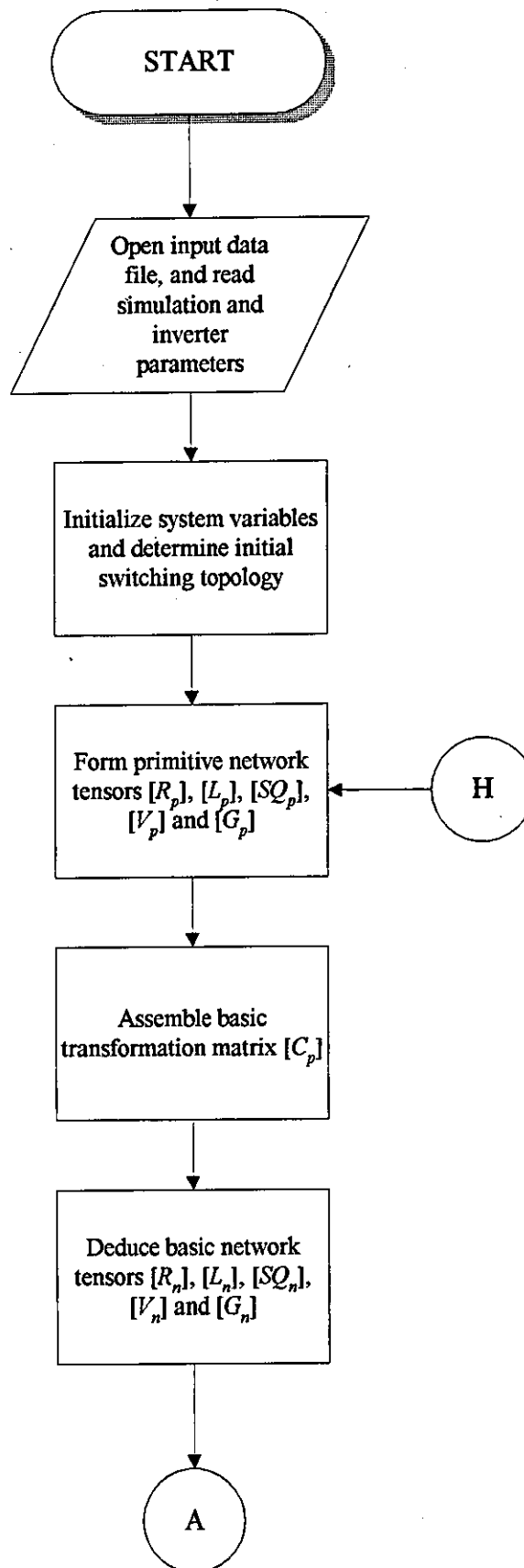
E.3 Linear induction motor drive under constant current excitation 149

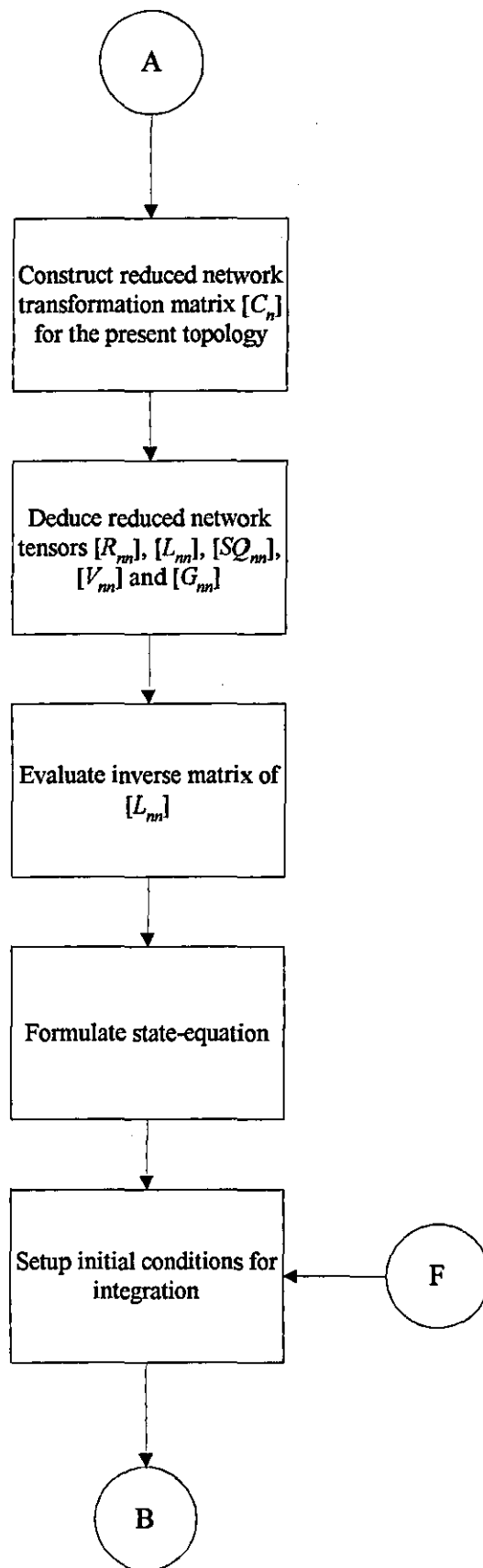
E.4 Vector-controlled linear induction motor drive..... 155

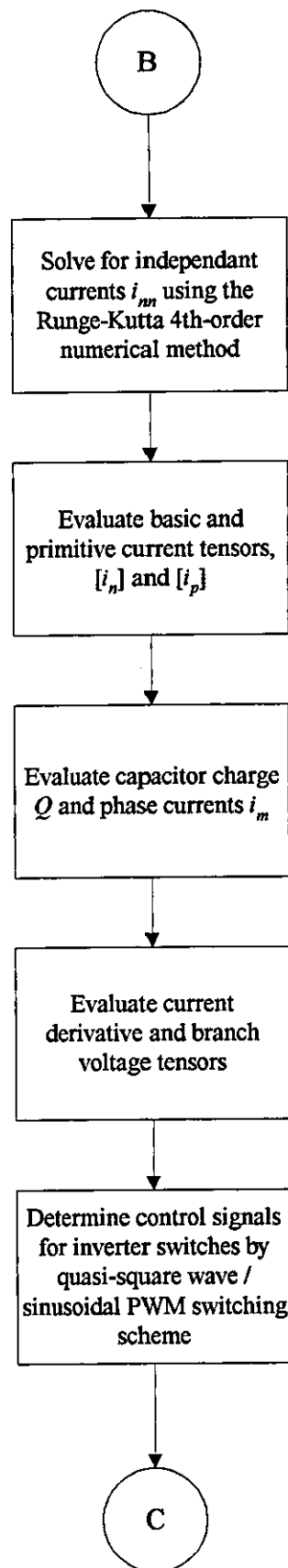


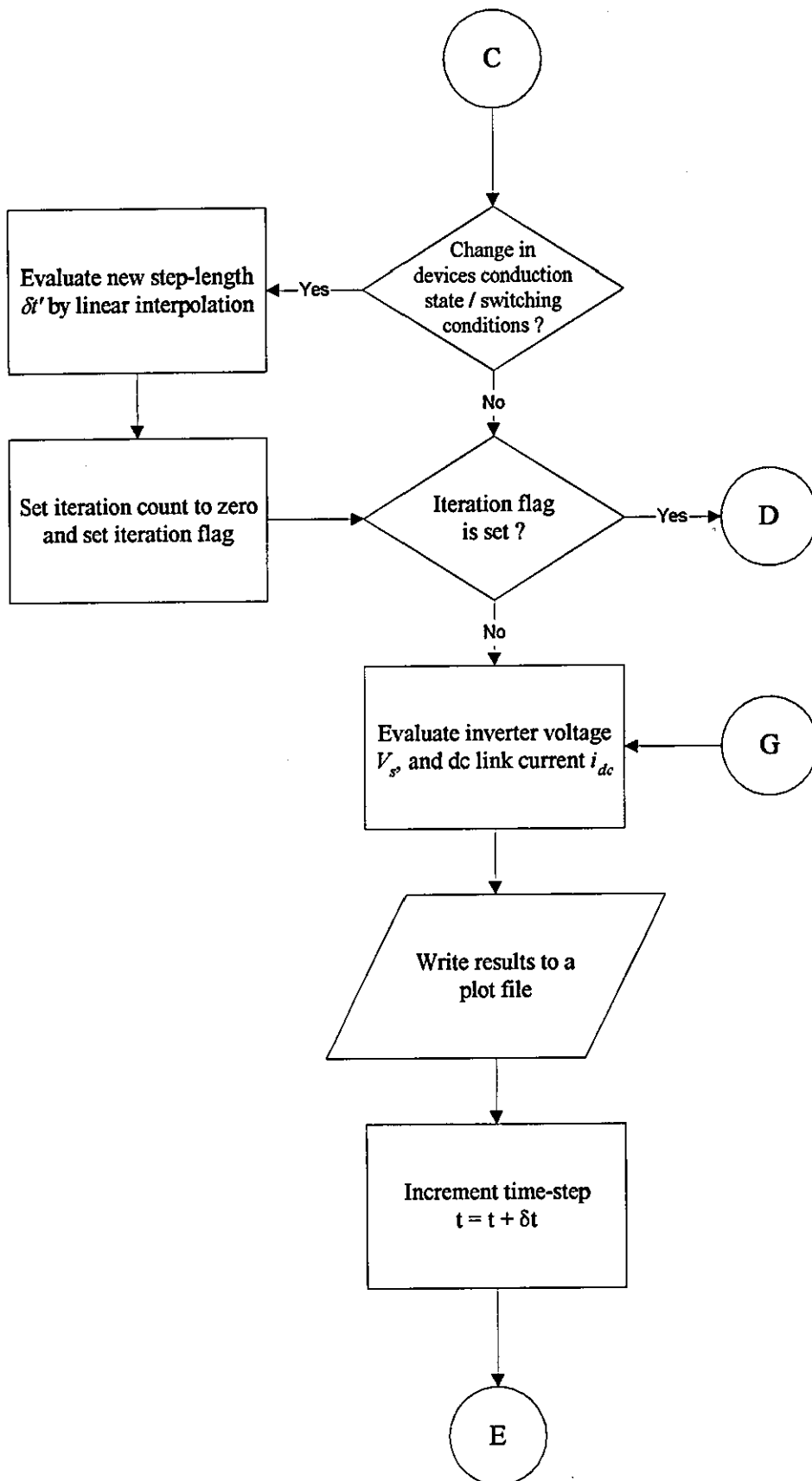


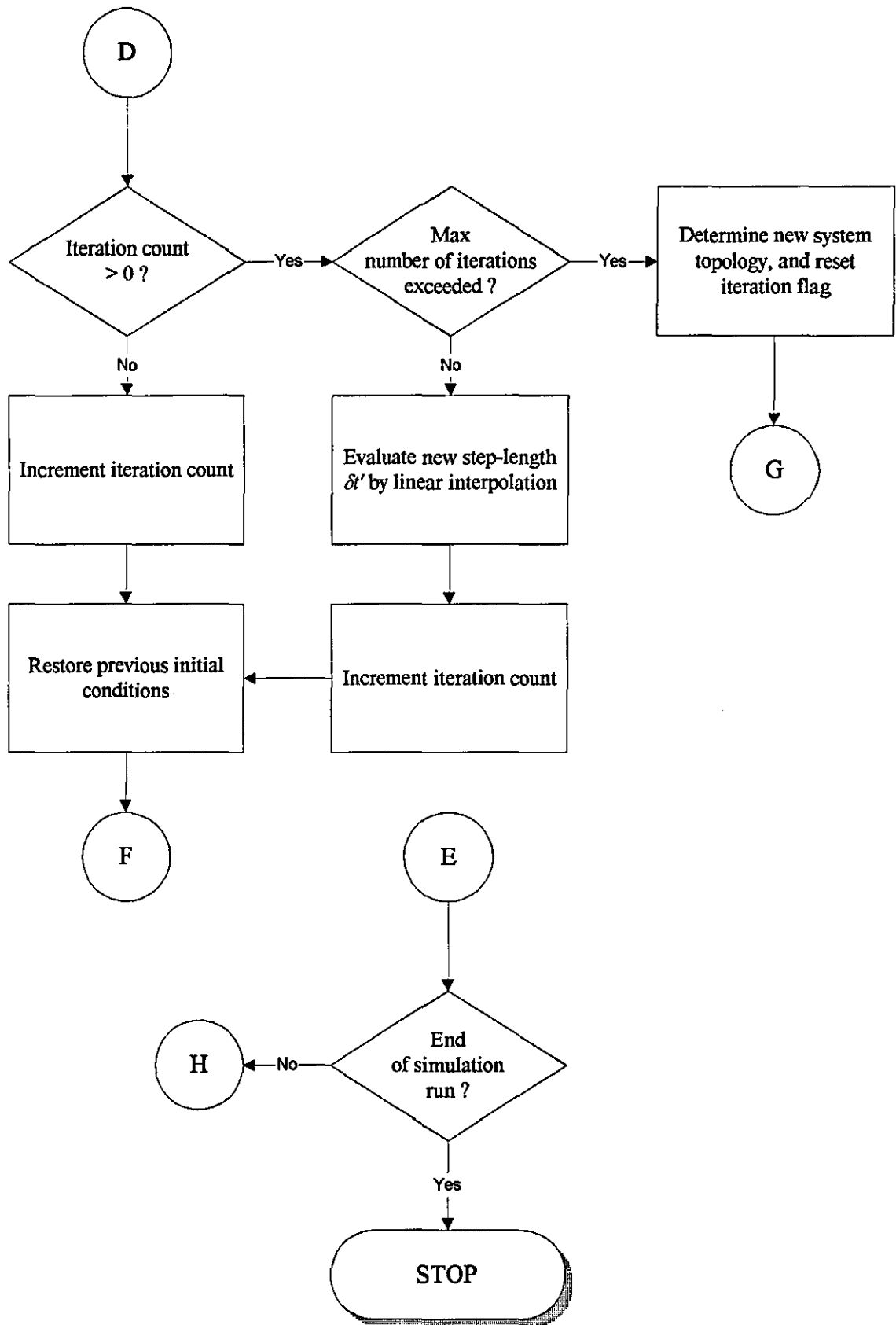


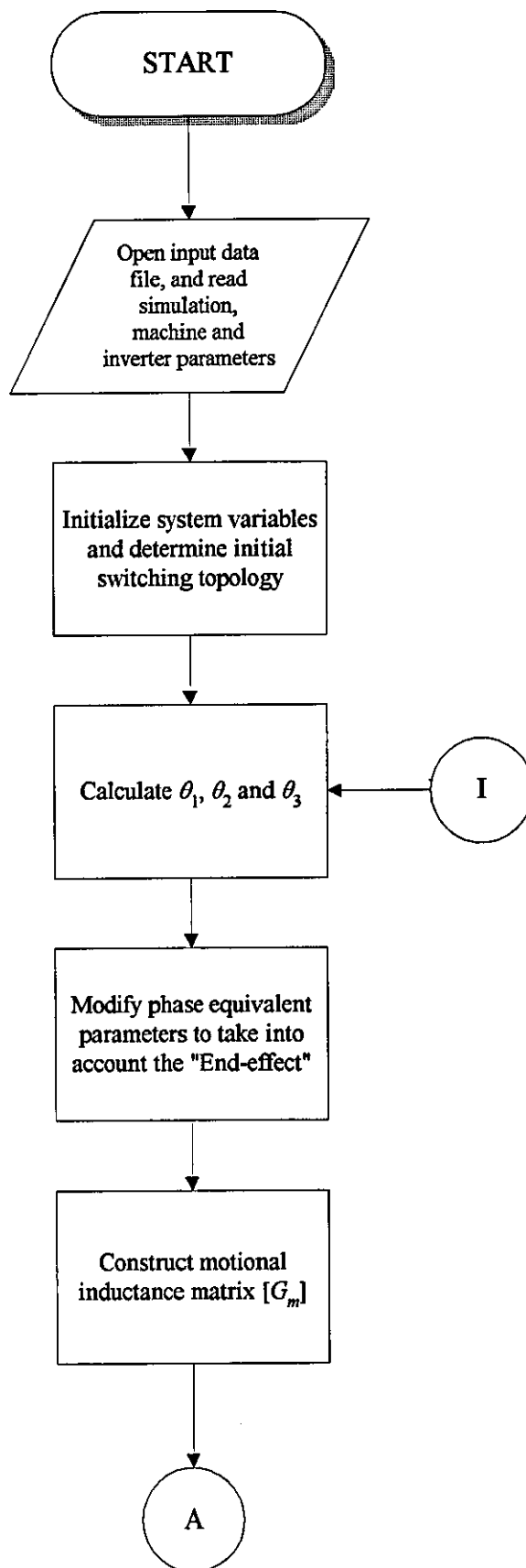


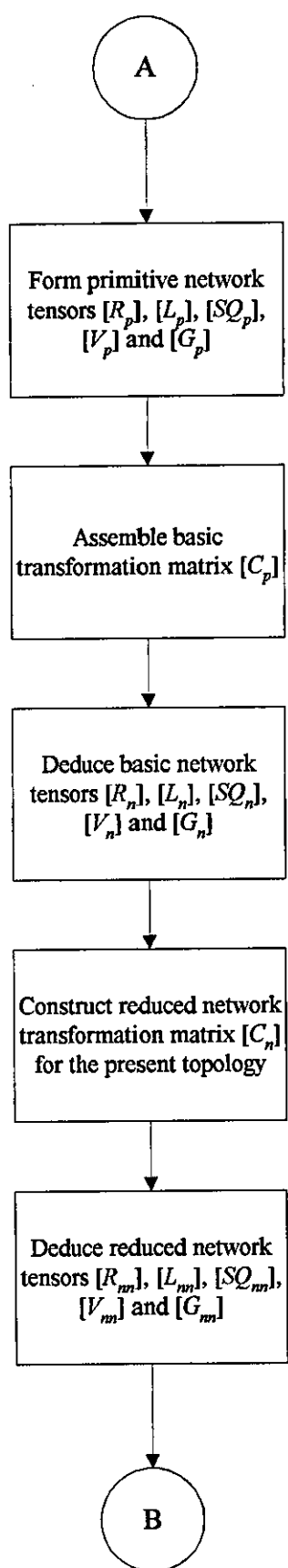


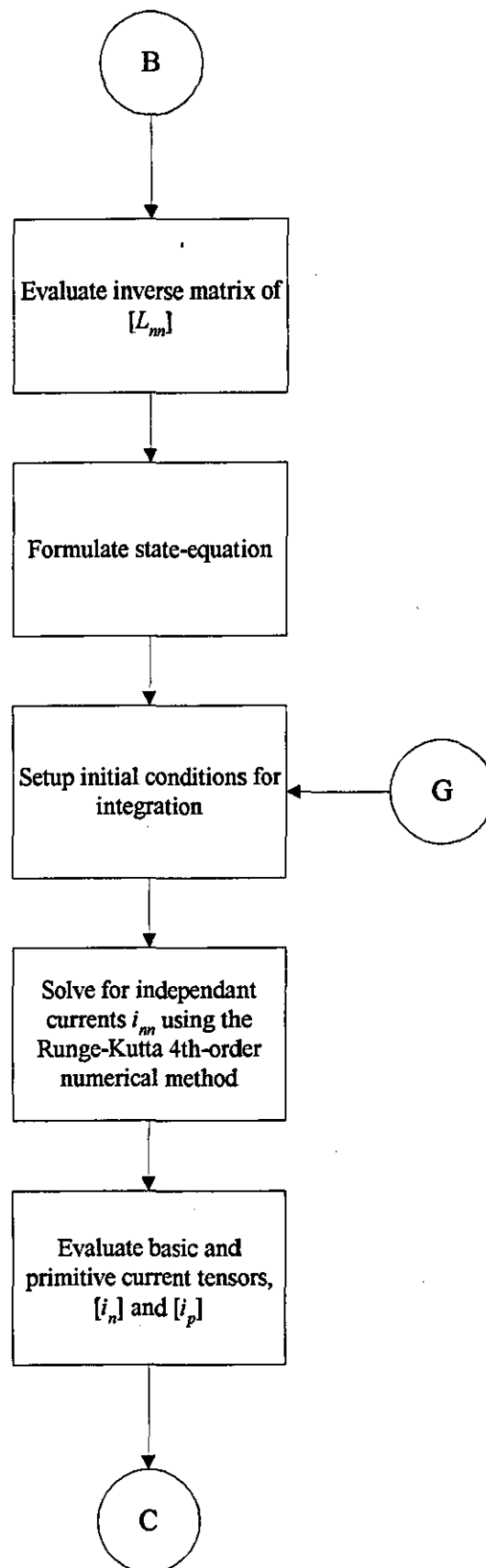


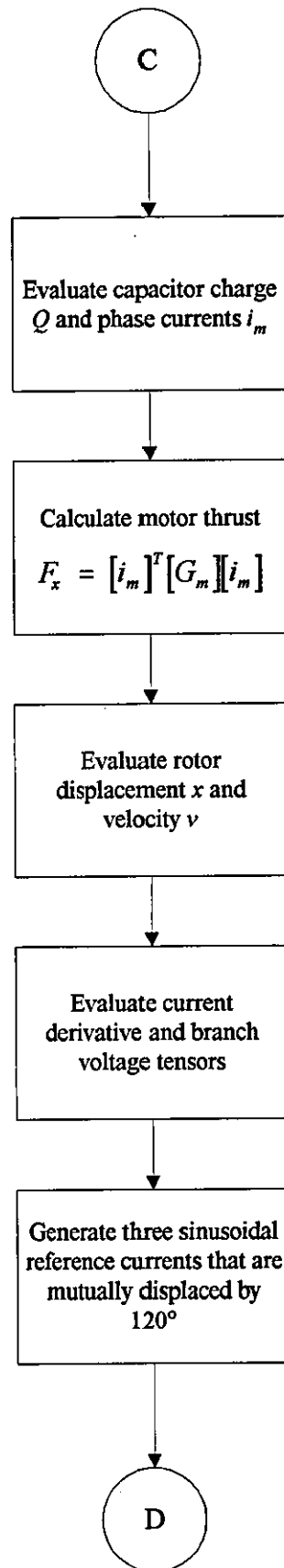


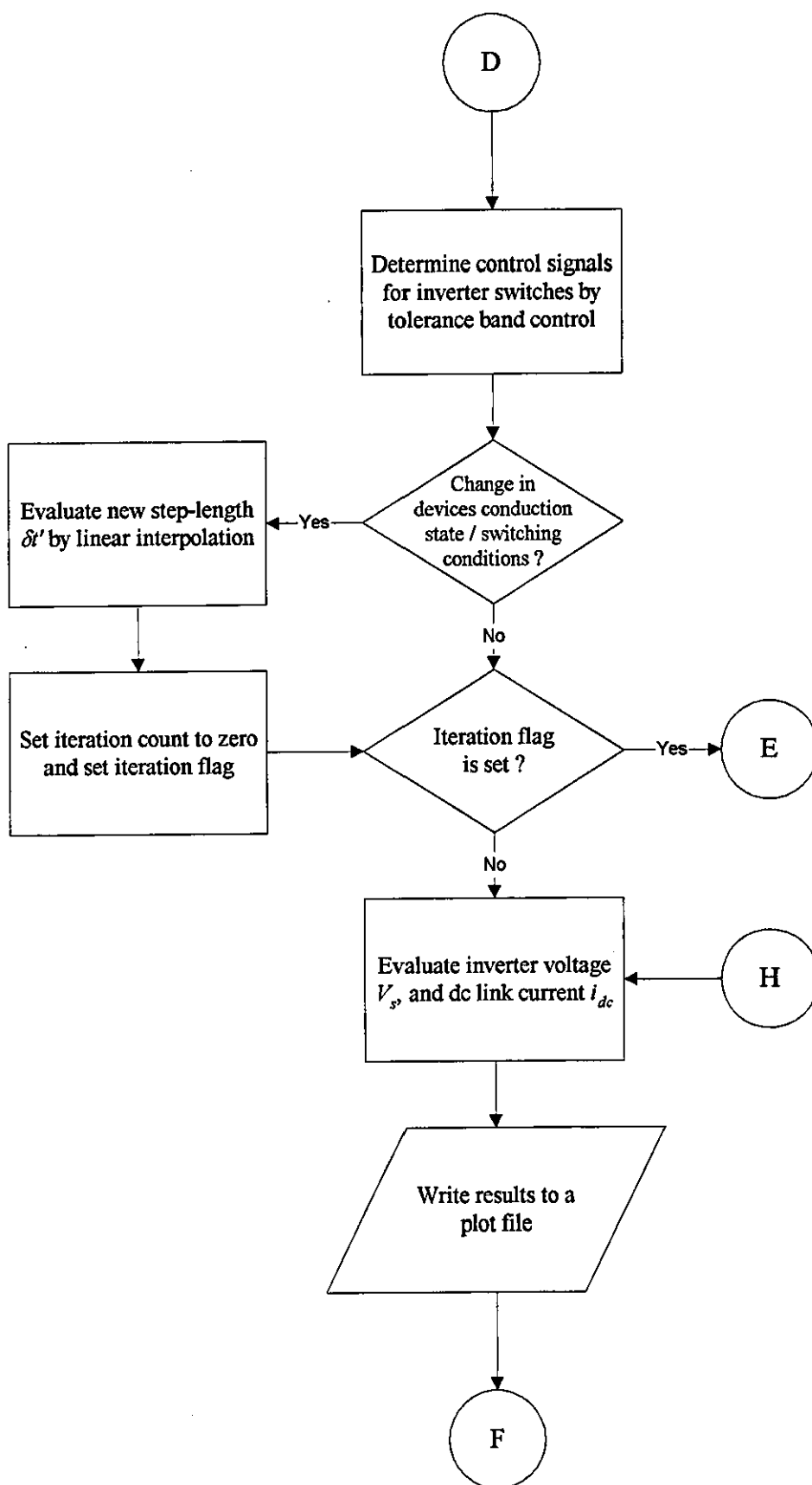


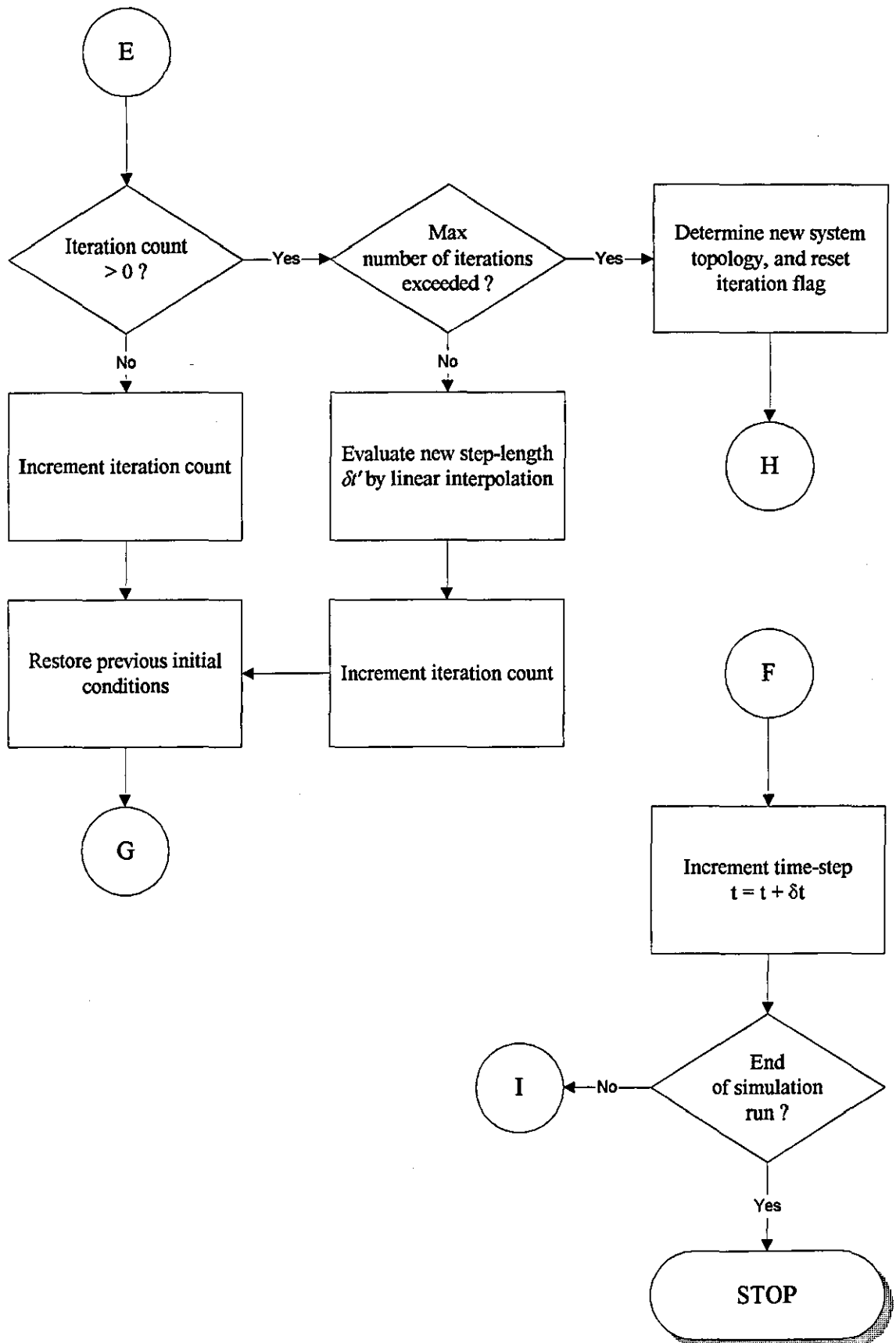


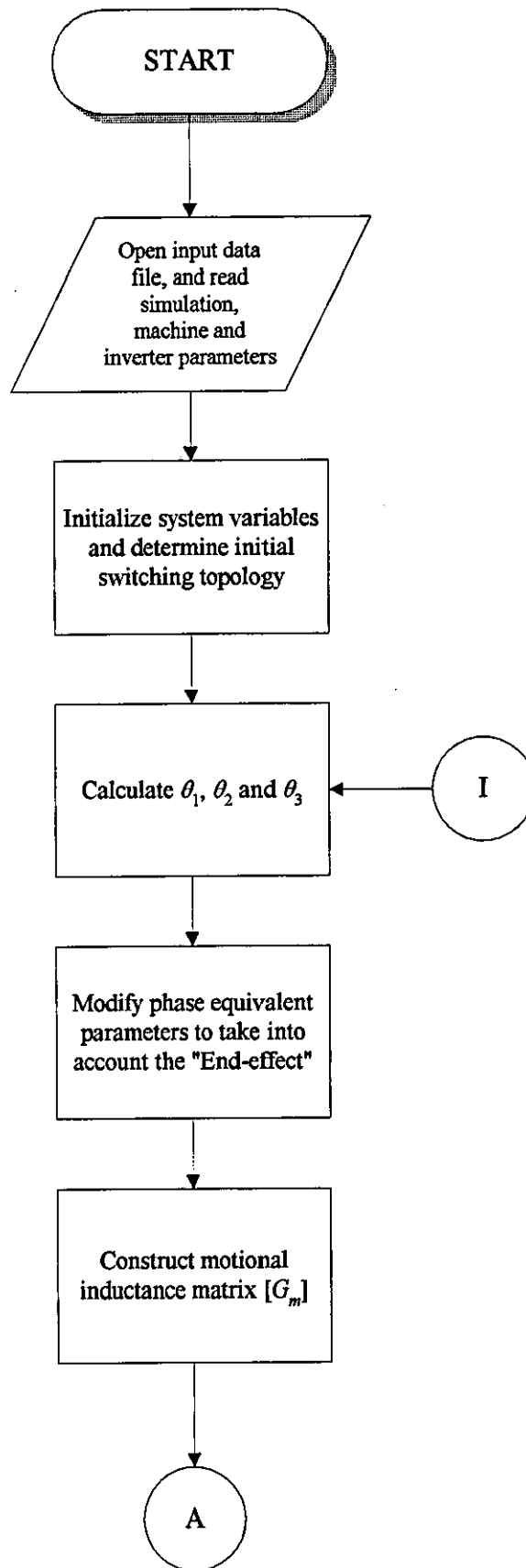


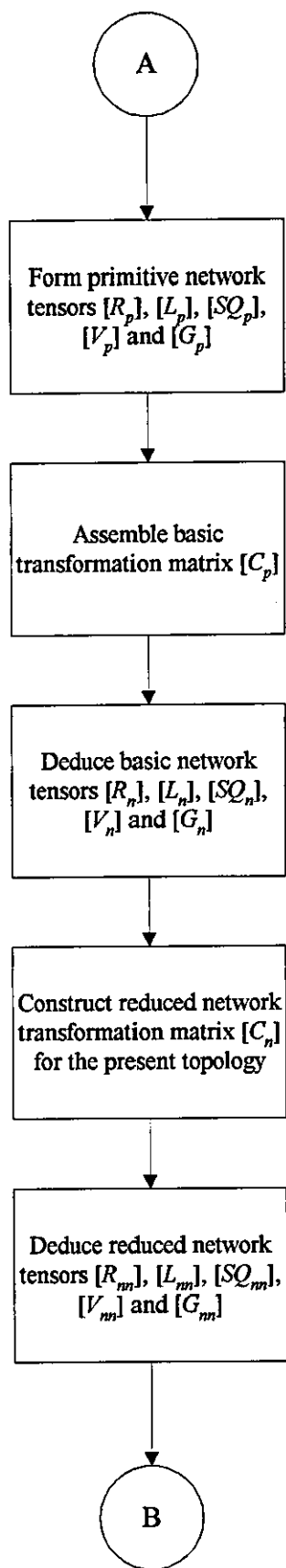


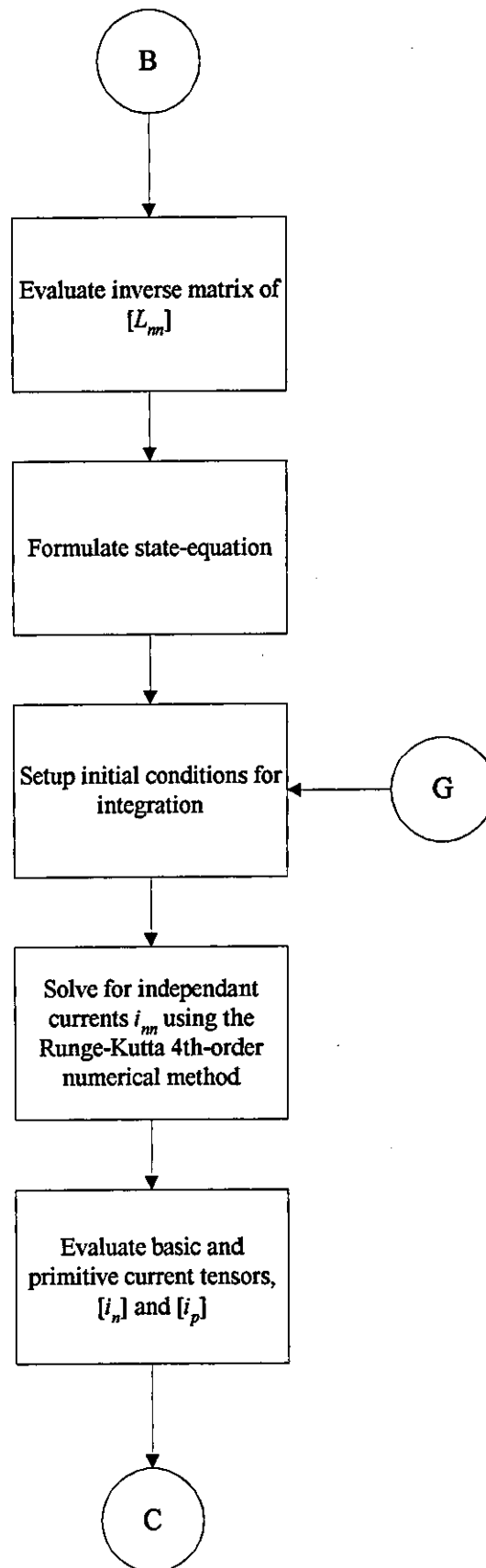




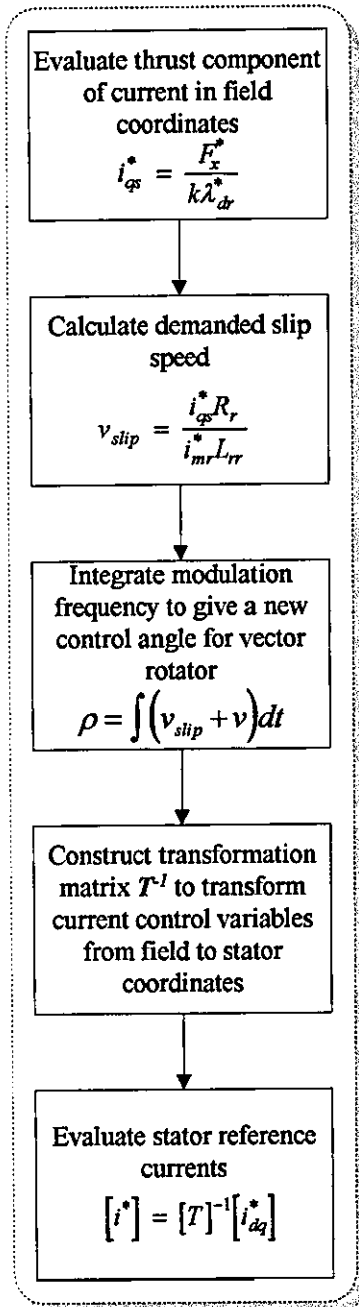




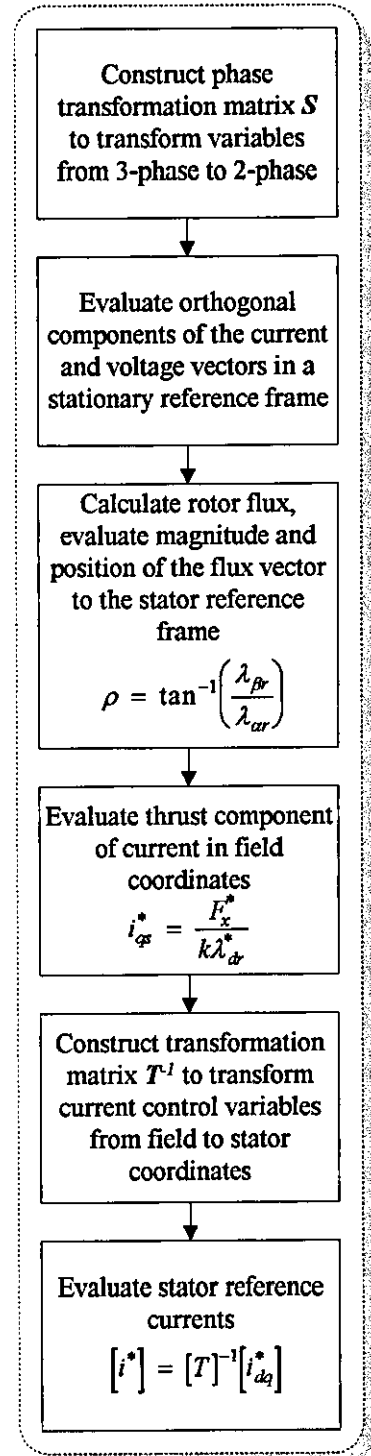


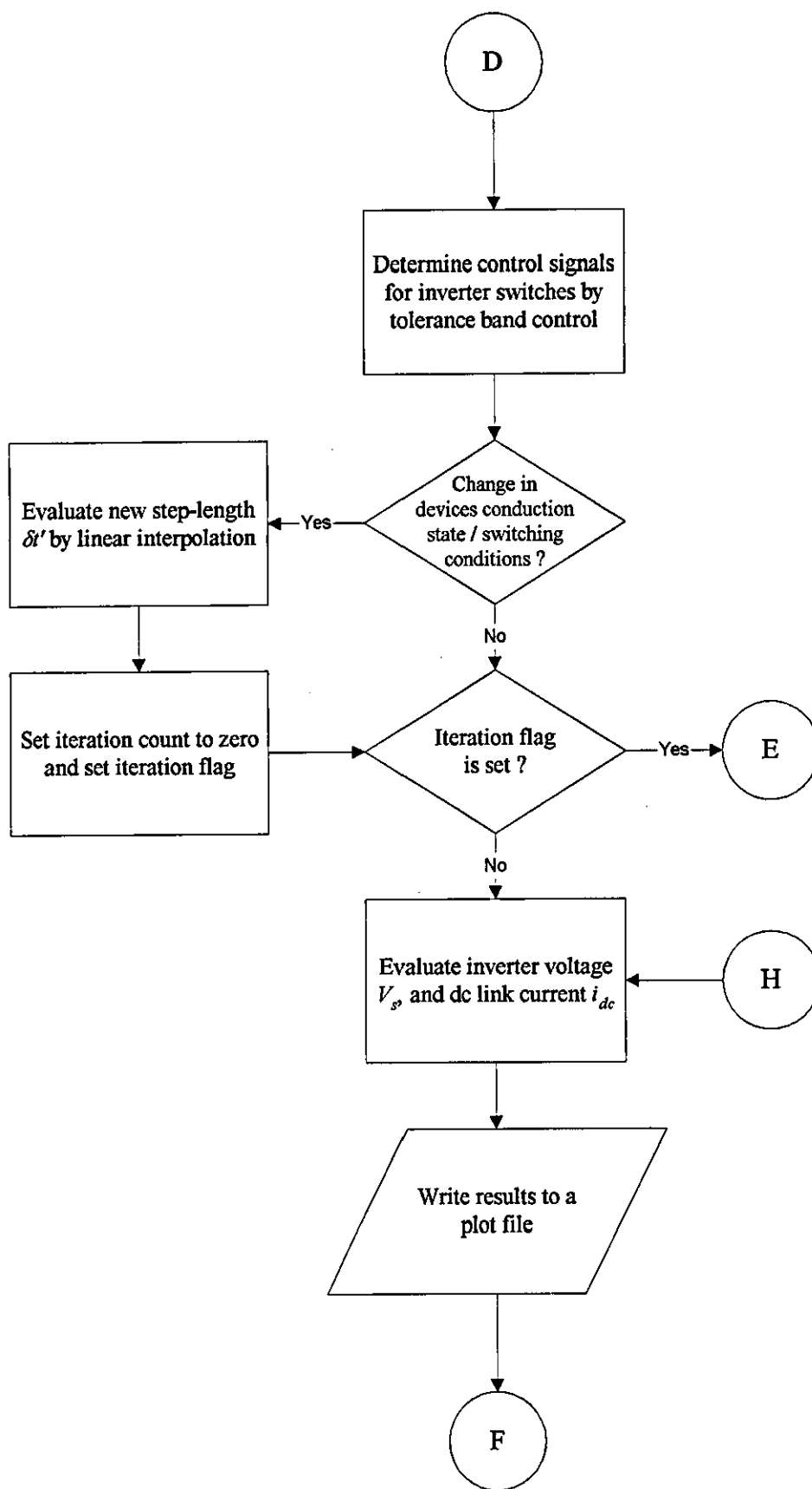


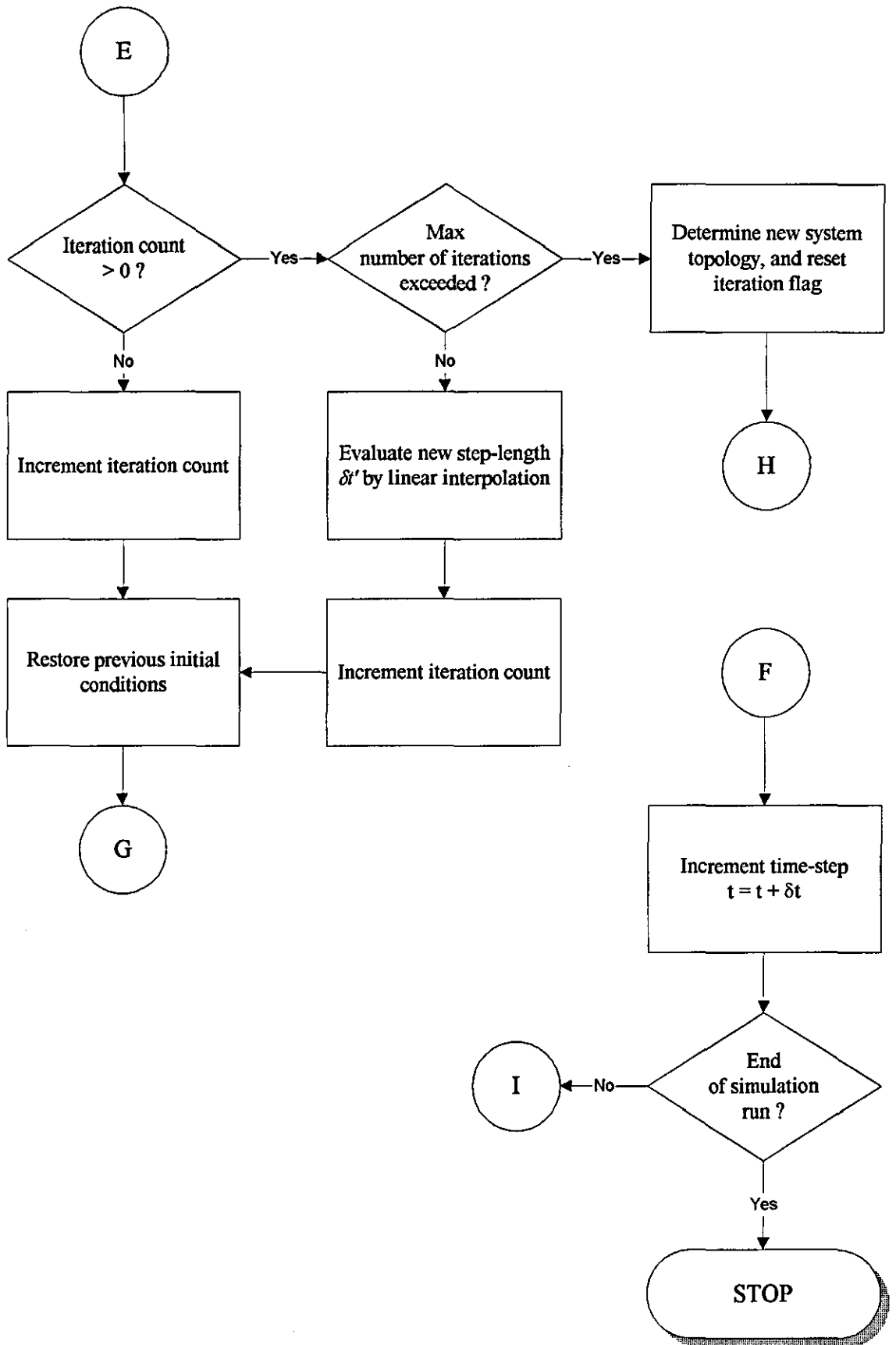
Indirect field-oriented control



Direct field-oriented control







MAIN PROGRAM
SIMM

```

% Transient analysis of a rotary Induction Motor
% in the time domain

% Load simulation and machine parameters

param

% Construct phase transformation matrix (2 - 3phase conversion)

alpha=0.0
S(1,1)=cos(alpha)
S(1,2)=-sin(alpha)
S(2,1)=cos(alpha-(2.0d0*pi/3.0d0))
S(2,2)=-sin(alpha-(2.0d0*pi/3.0d0))
S(3,1)=cos(alpha-(4.0d0*pi/3.0d0))
S(3,2)=-sin(alpha-(4.0d0*pi/3.0d0))

% Display simulation parameters

deltat
finish

% Start of main loop

time=start;
while time < finish;

t=[time:deltat:time+deltat]';

% Load Induction Motor State Model

statemodel

% Evaluate Vds and Vqs in a stationary reference frame

Vds=(Va*sin(2.0d0*pi*Fs*t)*2/3)-(Vb*sin(2.0d0*pi*Fs*t-(240*pi/360))/3)-
(Vc*sin(2.0d0*pi*Fs*t+(240*pi/360))/3);
Vqs=(Vb*sin(2.0d0*pi*Fs*t-(240*pi/360))*sqrt(3)/3)-
(Vc*sin(2.0d0*pi*Fs*t+(240*pi/360))*sqrt(3)/3);

% Evaluate stator phase currents

u=[Vds Vqs];
[y,x]=lsim(A,B,D,H,u,t,x0);
x0=x(2,:);
Current=[S]*[y(2,:)]';

% Evaluate rate of change

delta=[A11 A12]*x(1,:)' + B11*[Vds(1,1);Vqs(1,1)];

% Evaluate stator air-gap flux

```

```

OldEd=Ed;
OldEq=Eq;
Ed=Vds(1,1)-Rs*y(2,1)-(Ls-M)*delta(1,1);
Eq=Vqs(1,1)-Rs*y(2,2)-(Ls-M)*delta(2,1);
A=[0 0;0 0];
B=[1 0;0 1];
D=[1 0;0 1];
H=[0 0;0 0];

u=[OldEd OldEq;Ed Eq];
[y3,x3]=lsim(A,B,D,H,u,t,x30);
x30=x3(2,:);
fluxd=y3(2,1);
fluxq=y3(2,2);

% Evaluate electromechanical torque

PTorque=Torque;
Tem=(3/2)*ppairs*(fluxd*y(2,2)-fluxq*y(2,1));

% Evaluate rotor angular speed

A=[-ppairs*friction/Inertia];
B=[ppairs/Inertia];
D=[1];
H=[0];

Torque=Tem-Tl;
u2=[PTorque;Torque];
[y2,x2]=lsim(A,B,D,H,u2,t,x20);
x20=x2(2,:);
wr=y2(2,1);

% Store results

count=count+1;
result(count,:)=['time,Current',Tem,wr];

% End of main loop

time=time+deltat;
end

% Display results
results;

```

**SUBROUTINE TO CONSTRUCT A STATE MODEL FOR THE INDUCTION
MOTOR**

STATE.M

```
% Define a state model for the rotary induction machine
```

```
% Construct state model
% Rs = stator resistance
% Rr = rotor resistance
% Ls = stator self-inductance
% Lr = rotor self-inductance
% M = mutual inductance
% ro = leakage coefficient
% Tr = rotor time constant
% wr = motor angular velocity
```

```
I = [1 0;
      0 1];
```

```
J = [0 -1;
      1 0];
```

```
A11=- (Rs/(ro*Ls)+(1-ro)/(ro*Tr))*I;
A12=M/(ro*Ls*Lr)*((1/Tr)*I-wr*J);
A21=(M/Tr)*I;
A22=- (1/Tr)*I+wr*J;
A=[A11 A12;A21 A22];
```

```
B11=1/(ro*Ls)*I;
B21=[0 0;
      0 0];
B=[B11;B21];
```

```
D12=[0 0;
      0 0];
D=[I D12];
H=[0 0;
   0 0];
```

MACHINE AND SIMULATION PARAMETERS

PARAM.M

```
% Remove all previously defined variables  
clear
```

```
% Simulation (input) parameters
```

```
Va=-380;  
Vb=-380;  
Vc=-380;  
Fs=50;  
x0=[0 0 0 0];  
x20=[0];  
x30=[0 0];  
start=0.0;  
finish=0.4;  
deltat=0.00001;  
fluxq=0;  
fluxd=0;  
Eq=0;  
Ed=0;  
count =0;
```

```
% Machine parameters
```

```
Rs = 5.09  
Rr = 5.09  
Ls = 0.732  
Lr = 0.732  
M = 0.699  
ro = 1-M^2/(Ls*Lr)  
Tr =Lr/Rr  
wr = 0.0  
ppairs = 3.0  
inertia=0.045  
friction=6.33e-3  
Tl=0.0  
Torque=0.0
```

SUBROUTINE TO DISPLAY RESULTS
RESULTS.M

```
% View results in the form of graphical plots

% Display stator phase currents

subplot(221);
plot(result(:,1),result(:,2:4));
grid;
xlabel('Time [sec]');
ylabel('Current [A]');
title('Stator phase currents');

% Display electromechanical torque

subplot(222);
plot(result(:,1),result(:,5));
grid;
xlabel('Time [sec]');
ylabel('Torque [Nm]');
title('Machine Torque');

% Display rotor angular speed

subplot(223);
plot(result(:,1),result(:,6));
grid;
xlabel('Time [sec]');
ylabel('Rotor speed [Rad/s]');
title('Machine Speed');

% Display stator phase-A current

subplot(224);
plot(result(1:(0.1/deltat),1),result(1:(0.1/deltat),2));
grid;
xlabel('Time [sec]');
ylabel('Current [A]');
title('Stator phase current');
```

